ELSEVIER

Coordination Chemistry Reviews
172 (1998) 3–97

COORDINATION CHEMISTRY REVIEWS

Iron 1995

Ebbe Nordlander *, Anders Thapper, Jason King, Christian Lorber, Håkan Carlsson, Fabio Prestopino, Nicola Focci

Inorganic Chemistry 1, Chemical Centre, Lund University, Box 124, S-221 00 Lund, Sweden

Contents

* Corresponding author.

PII S0010-8545(98)00090-3

1. Introduction

This review covers the coordination chemistry of iron for 1995. The following journals have been covered by a combination of searching in Chemical Abstracts and independent searches in the following journals: Acta Chemica Scandinavica; Acta Crystallographica Sect. C; Angewandte Chemie International Edition in English; Bulletin of the Chemical Society of Japan; Bulletin des Sociétés Chimiques Belges, Chemistry: A European Journal; Helvetica Chimica Acta; Inorganic Chemistry; Inorganica Chimica Acta; Journal of the American Chemical Society; Journal of the Chemical Society, Chemical Communications; Journal of the Chemical Society, Dalton Transactions; Journal of the Chemical Society, Perkin Transactions 2; Journal of Coordination Chemistry; New Journal of Chemistry; Polyhedron.

Carbonyl compounds have been classified as organometallic compounds and are not included. Most iron–heterometal complexes have been excluded. This review does not aim to be fully comprehensive; omissions or errors are entirely the fault of the authors.

2. Complexes with hydride ligands

The stabilities of classical and non-classical isomers of $Fe(PH_3)_3H_4$ have been studied using a non-local quasi-relativistic density functional method [1]. The non-classical hydride (**1**), rather than the classical hydride (**2**), was found to be most stable. The structure for the Fe hydride complex was in good agreement with the previously determined structure.

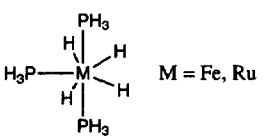

M = Fe, Ru

(1)

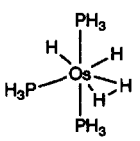

(2)

3. Complexes with halide ligands

The interaction of iron(III) halides with 18-crown-6 and 15-crown-5 generates a number of products. The structures of two of these, $[FeCl_3(H_2O)_2]$(15-crown-5) (**3**)

and $H(FeBr_4)(15\text{-crown-5})\cdot(H_2O)_2$ (**4**) have been determined by X-ray crystallography [2]. Complex (**3**) features trigonal-pyramidal $FeCl_3$ moieties which are hydrogen-bonded to a 15-crown-5 ligand and thus form a polymeric chain. In complex (**4**) the crown ether acts simply as a dielectric medium to separate tetrahedral $FeBr_4^-$ ions which have no bonding interactions with the crown ether. Thermal decomposition of the complexes by thermogravimetric analysis yields water, acetaldehyde, dioxane, Cl_2, Br_2, CO, CO_2 and hydrated Fe(II) halides and oxides, as determined by IR and Mössbauer spectroscopy. The reduction of $FeBr_2$ and $FeBr_3$ in both water and diglyme by $NaBH_4$ has been investigated [3]. In dry diglyme, the reduction yields stable iron borohydride coordination compounds, probably $(diglyme)_nFe(BH_4)_2$ and $(diglyme)_nFe(BH_4)_3$ for iron(II) and iron(III) respectively. When the compounds are heated, iron(II) gives nanoscale Fe_2B and iron(III) gives nanoscale FeB, which have been identified by Mössbauer spectroscopy. Treating the iron borohydride compounds with water causes precipitation of Fe_2B in both cases; Fe_2B has been identified by Mössbauer spectroscopy and X-ray powder diffraction. Reduction of $FeBr_2$ and $FeBr_3$ in water yields non-crystalline nanoscale Fe(s).

4. Complexes with cyanide or isocyanides

The reaction of $[Fe(CN)_5(H_2O)]^{3-}$ and 2-nitroso-1-naphthol (**5**) has been studied [4]. In a first step, the aquo ligand is replaced by (**5**) to give $[Fe(CN)_5(\mathbf{5})]^-$. In a second step, catalysed by mercury(II) ions, $[\{Fe(CN)_5\}\text{-}(\mu\text{-}CN)\text{-}\{Fe(CN)_3(\mathbf{5})\}]^{6-}$ (**6**) is formed, where (**5**) now acts as a didentate ligand. Complex (**6**) has been characterized by analytical, IR and UV–VIS spectral data. These data indicate that the ligand has predominately the quinone oximic structure. The preparation of $Fe[Fe(\mathbf{5})_3]_2$ is also reported.

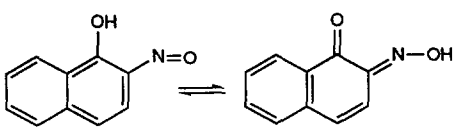

(5)

The coordination of nitriles [5] or amines [6] to $[Fe(CN)_5(H_2O)]^{3-}$ (**7**) has also been investigated. The equilibrium constants for the nitriles were determined indirectly using the complex $[Fe(CN)_5(MeCN)]^{3-}$ obtained from (**7**) in an acetonitrile–water solution. Values of $\log K$ for the ligand substitution in (**7**) were determined for PhCN (3.5), $NCCH_2NH_3^+$ (3.3), $NCCH_2COO^-$ (2.5), and $NCNH_2$ (2.3); there is little dependence on the nitrile basicity. For amines (e.g. $NH_2SO_3^-$, $NH_2NH_3^+$, $NH_2CH_2CF_3$, NH_2CH_3), substituting H_2O in (**7**), the values of $\log K$ were shown to obey the linear free-energy relation $\log K = 0.05pK + 3.75$ over a range of 11 pK units, thus showing almost no dependence on pK. Proton nuclear magnetic resonance spectroscopy has been used to determine the solution

structure of $[Fe(CN)_4(7)]^{2-}$ and $[Fe(CN)_4(7)]^{-}$ [7]. Ligand (7) is chelating to make a five-membered ring and the conformation of the methyl group (CH_3CH_2N–) is preferably anti with respect to the iron atom when looking down the CH_2–N bond.

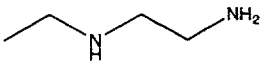

(7)

A spectrophotometric study of the reaction of cyanide ions and pentacyanoferrate(II) complexes, $[Fe(CN)_5L]^{3-}$, in aqueous solution and water–mono-alcohol mixtures suggest that, with excess CN^-, first-order kinetic behaviour is exhibited between 1 bar and 1 kbar at 298.2 K [8]. There is little change in the value of the rate constant (approximately one-half of one order of magnitude) for L being a range of positively charged and neutral pyridine ligands. However, thiourea and quinoxaline are much more labile, with rate constants ten and 300 times greater respectively, than those for the pyridine ligands. Addition of 40% MeOH has only a very small effect on the rate constant. For reactions in aqueous solution, the volumes of activation are all positive, confirming the expected bond extension of the leaving group in a dissociative mechanism.

5. Complexes with *N*-donor ligands

5.1. Complexes with N-heterocyclic ligands

5.1.1. Complexes with pyridine and polypyridine ligands

Gas-phase ion–molecule reactions have been studied for a number of monopositive metal ions, including Fe^+, with heteroatomic ligands [9]. The ligands were py, bpy, 4,4′-bipyridine, phen, tpy, and pyrene. The iron ions were produced by laser desorption in a quadrupole ion trap mass spectrometer and made to react with the ligands. The products detected were of the form $(FeL)^+$, $(FeL_2)^+$, $(FeL_3)^+$, and $(FeLH_2O)^+$. Only phen and bpy formed the trimers. Pyrene probably from sandwich-type complexes via π-bonding. The hydration phenomenon was only observed for the monomer complexes and after a longer reaction time. The ligand with the largest propensity for hydration was 4,4′-bipyridine, explained by its large polarizability and the fact that it can only attach to the metal with one atom. 1,10-Phenanthroline has the largest binding affinity, followed by tpy, bpy, 4,4′-bipyridine and pyridine.

The strongly coloured complexes $[Fe(X)_2]^{2+}$ (X=(**8**–**10**)) have been prepared [10]. The colour has been assigned to MLCT bands. Cyclic voltammetry and bulk electrolysis experiments have been carried out, showing that each complex displays a combination of the redox processes expected for the $Fe(tpy)_2^{2+}$ core and for the two 4′ groups. The process $[Fe(\mathbf{9})_2]^{2+} \leftrightarrow [Fe(\mathbf{10})]^{2+} + 4H^+ + 4e^-$ is found to be chemically reversible under protic conditions.

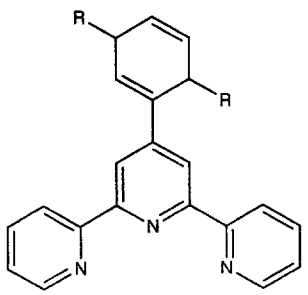

(8) : R=OMe
(9) : R=OH

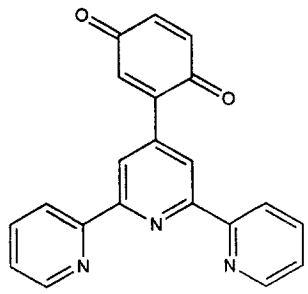

(10)

Molecular mechanics calculations on the complexes (**11**–**17**) have been performed [11]. The calculated structures of complexes (**11**) and (**12**) where compared with the known structure of (**11**) and the preliminary structure of (**12**) respectively, both determined by X-ray crystallography. The comparison shows that the calculated and experimental structures were virtually superimposable. This implies that the calculated structures for complexes (**11**–**17**) are good representations for the structures of the complexes. All eight complexes have almost the same metal–metal separation and ligand orientation; only the bridging linkages differ [12]. The electrochemical behaviour of (**11**), (**12**) and (**15**) has been studied. The complexes display four apparent redox process: one (metal-based) at potentials higher than 0 V (vs SCE) and three (ligand-based) at potentials below 0 V. Each redox process is, in fact, a pair of overlapping one-electron waves. The metal-based redox processes correspond to the $6^+/5^+$ ($Fe(III)_2/Fe(III),Fe(II)$) and $5^+/4^+$ ($Fe(III),Fe(II)/Fe(II)_2$) one-electron redox couples; similarly, there are ligand-based 4^+–2^+, 2^+–0 and 0–2^- waves, each of which consist of one-electron processes. The potentials of each one-electron process have been resolved by analysis of Osteryoung square wave voltammetry data.

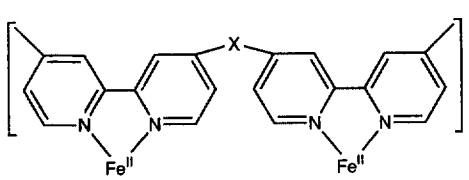

(**11**) X = $(CH_2)_2$
(**12**) X = $(CH_2)_3$
(**13**) X = CH_2-S-CH_2
(**14**) X = CH_2-O-CH_2
(**15**) X = $(CH_2)_4$
(**16**) X = $(CH_2)_5$
(**17**) X =

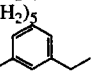

The complexes $[Fe(tpa)(S\text{–}Ar)]^+$ (Ar = C_6H_2-2,4,6-Me_3 (**18**), C_6H_4-4-Me (**19**), C_6H_5 (**20**) and C_6H_4-4-Cl (**21**)) have been proposed as models for the isopenicillin N synthase enzyme substrate complex [13]. Reaction of (**18**–**21**) or the dinuclear complex $Fe_2(O_2CCH_3)_2(tpa)_2](BPh_4)_2$ (**22**) with NO at −80 °C leads to the formation of NO adducts. The NO adducts exhibit charge transfer bands in the visible region which cannot be detected for the adduct of (**22**). This observation indicates that the thiol ligands are still bound in the NO adducts of (**18**–**21**). The EPR

spectra of the adducts of (**18–22**) indicate that the ground state for all systems is $S=\frac{3}{2}$. The EPR spectrum of (**21**) is consistent with the formation of $[Fe(tpa)(O_2CCH_3)(NO)]^+$. The EPR spectra of the adducts of (**18–21**) show greater rhombicity than those of (**22**); this is attributed to the presence of the thiolate ligand. Reaction of (**18–21**) with dioxygen at low temperature results in the formation of transient blue–green species; it is proposed that an auto-oxidation reaction (Scheme 1, L = tpa) takes place. On warming to room temperature, the transient intermediates are converted to μ-oxo–diiron complexes.

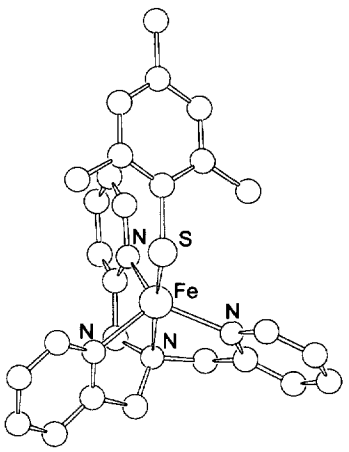

(**18**)

The dinuclear oxalate-bridged complexes $[Fe_2(C_2O_4)(X)_2](ClO_4)_2 \cdot yH_2O$ (X = (**24**), $y=0$; X = (**25**), $y=0.5$; X = (**26**), $y=1$) have been prepared [14]. Variable-temperature magnetic susceptibility measurements of these complexes reveal that there are weak antiferromagnetic interactions between the complexes. The magnetic exchange is mediated by interactions between the metal $d_{x^2-y^2}$ orbitals and the oxalate σ orbitals.

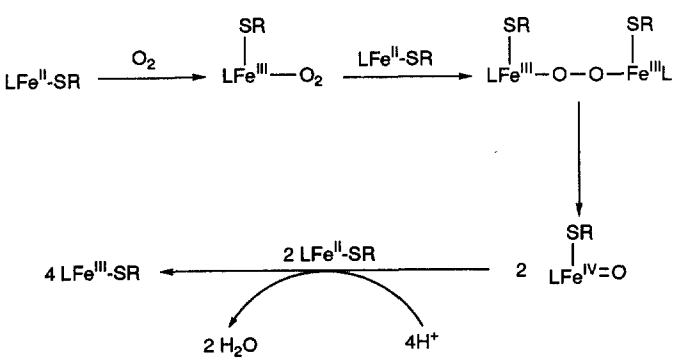

Scheme 1.

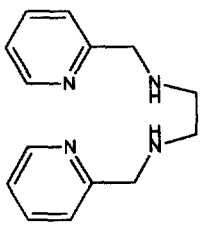

(24)

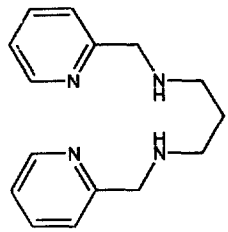

(25)

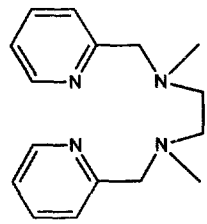

(26)

A new pentadentate ligand (**27**) and complexes of (**27**) and iron(II) have been synthesized [15]. The X-ray structure of the complex $[Fe(NCMe)(\mathbf{27})](ClO_4)_2$ (**28**) has been determined. The iron atom is octahedrally coordinated by N atoms. The four pyridine N atoms occupy the equatorial positions with the pyridine rings perpendicular to plane. The short Fe–N bond lengths indicate a low-spin iron(II) complex. Cyclic voltammetry of (**28**) shows a reversible oxidation at 990 mV vs NHE. Reaction of (**28**) with a large excess of H_2O_2 in acetone gives a purple species assigned as $[Fe(OOH)(\mathbf{27})]^{2+}$ (**29**) by its EPR spectrum and its electrospray mass spectrum. Complex (**29**) is able to oxidize alkanes with an activity comparable with the best non-haem iron oxidation catalysts.

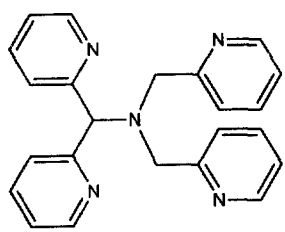

(27)

Iron(II) complexes of the pentadentate ligand (**30**) and the potentially hexadentate ligand (**31**) have been isolated [16]. Both ligands behave as pentadentate ligands in their iron(II) complexes of the general formulation $[FeL(X)]^{n+}$ (L=(**30**) or (**31**), $n=1$ or 2) with the sixth coordination site (X) occupied by an auxiliary ligand, e.g. H_2O, Cl, SCN or CN. The crystal structure of $[Fe(\mathbf{30})(H_2O)][PF_6]_2 \cdot H_2O$ shows that the nitrogen atom of one of the 6-methyl-2-pyridylmethyl groups of the formally hexadentate ligand is not coordinated to the iron atom. Instead a water molecule occupies the sixth coordination position. The complexes show peroxidase activity. The availability of a labile site on the relatively stable iron(II) complexes, along with no apparent tendency to form oxo-bridged diiron(III) species, are likely to be important factors in the mechanism of the oxidation reactions.

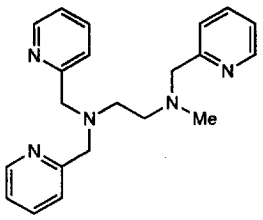

(30)

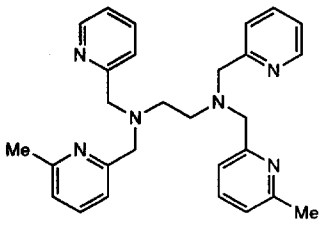

(31)

Several iron(II) complexes have been synthesized in order to model the structures and reactions of α-keto acid-dependent non-haem iron enzymes [17]. The complexes are [Fe(II)(6-Me–tpa)(X–bf)](ClO_4) (X=H (**33**), *m*-NO_2, *p*-F, *p*-CH_3, *p*-OCH_3; bf=benzoylformate), [Fe(II)(6-Me–tpa)(**34**)](ClO_4), [Fe(II)(5-Me–tpa)(bf)](BPH_4) and [Fe(II)(tpa)(bf)(MeOH)](ClO_4) (**35**). The crystal structures of two of the complexes, (**33**) and (**35**)·2MeOH were also determined. In complex (**33**) the bf ligand chelates to the iron through the oxygen atoms, whereas only the carboxylate oxygen is bound to the iron in complex (**35**) and a methanol molecule occupies the other position. Both complexes (**33**) and (**35**) react with substrates 2,4-di-*tert*-butylphenol and triphenylphosphine in the presence of oxygen to give 4,4′, 6,6′-tetra-*tert*-butyl-2,2′-biphenol and $OPPh_3$ respectively. Kinetic studies on the complexes with substituted benzoylformate ligands indicated a nucleophilic mechanism. The proposed mechanism involves an iron(III)-superoxide species, formed by dioxygen binding to the iron(II) centre, that attacks the benzoylformate keto carbon. Subsequent oxidative decarboxylation affords the oxidizing species [Fe(II)(6-Me–tpa)(Obz)]$^+$ and [$Fe(III)_2O(tpa)_2(Obz)_2$]$^{2+}$ for complexes (**33**) and (**35**) respectively.

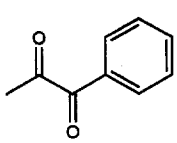

(33)

5.1.2. Complexes with other N-heterocyclic ligands

The kinetics of outer-sphere electron transfer between [$Fe(\mathbf{36})_3$]$^{2+}$ and substitutionally labile Fe^{3+} introduced as [FeL_6]$^{3+}$ (L=dimethylacetamide (**37**) or acetamide (**38**)) in acetonitrile has been studied at 25 °C [18]. Perchlorate was used as counterion for both complexes. Both reactions can be described by one mechanism, suggesting that the acidic hydrogen atoms of (**38**) do not affect the mechanism. Three rapid solvation pre-equilibria [FeL_6]$^{3+}$=[FeL_3]$^{3+}$+3L (coordinated MeCN is omitted) have to be invoked to accommodate the variations in the redox rate constants. For driving-force reasons, only [FeL_6]$^{3+}$ and [FeL_3]$^{3+}$ are redox-active.

For the solvate species, the overall reaction rates are controlled by both the reactivities of the reacting species and their availabilities. The redox constants of (**38**) are larger than those of the corresponding (**37**) species. This may be attributed to (**37**) being the stronger Lewis base. On the other hand, the availabilities of the reacting species are higher in the case of (**37**). The stabilities of the $[FeL_6]^{3+}$ solvate species are suggested not to be a function of the donor strength of L, but rather of its size, tentatively expressed by the effective molecular hard-sphere diameter.

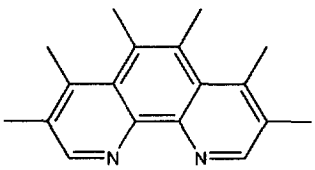

(**36**)

A detailed X-ray absorption study of the iron K and $L_{2,3}$ edges in $Fe(II)(phen)_2(NCS)_2$ (**39**) has been performed [19]. Complex (**39**) is a pseudo-octahedral spin transition complex and the XANES features at the two edges are very sensitive to the spin state. Calculations of the X-ray absorption cross-sections at both edges were made to evaluate the origins of these perturbations. The changes in the XANES spectra at the iron K edge spectra of the two states were due to the structural changes around the iron, whereas the changes in the iron $L_{2,3}$ edge spectra originated from changes in the occupancy of the 3d levels split by the pseudo-octahedral crystal field.

Ligand (**40**) forms a high-spin complex with iron(II), $[Fe(\mathbf{40})_2](ClO_4)_2$ (**41**) [20]. Titration of (**41**) with base stepwise deprotonates the imino-hydrogen of the benzimidazole groups. This enhances the σ donation from ligand to metal ion and the back donation ($t_{2g} \rightarrow \pi^*$) assisting a high-spin to low-spin transition in (**41**). The transition is reversible: the high-spin state is formed when acid is added to the low-spin complex.

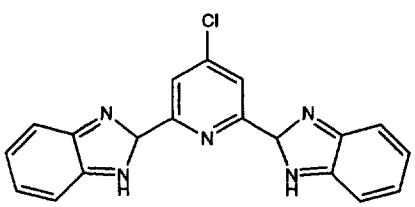

(**40**)

The complexes $[Fe\{H_2\text{–}(\mathbf{42})\}_2(MeOH)_2](OAc)_2$ (**43**), $[Fe\{H_2\text{–}(\mathbf{42})\}_3]CO_3$ (**44**), $[Fe\{H\text{–}(\mathbf{42})\}_2]_n$ (**45**) and $\{Fe(\mathbf{42})\}_n$ (**46**) (H_2–(**42**)=2,2′-biimidazole) have been prepared and the crystal structures of (**43–45**) have been determined [21]. In the solid state structure of (**43**), the $[Fe\{H_2\text{–}(\mathbf{42})\}_2(MeOH)_2]^{2+}$ molecules are linked via a hydrogen bonding network involving the acetate counterions. Similarly, the

crystal structure of (**44**) reveals that $[Fe\{H_2–(\mathbf{42})\}_3]^{2+}$ molecules of (**44**) are linked through the carbonate anions in a hydrogen bonding network. The $[Fe\{H–(\mathbf{42})\}_2]$ in (**45**) are also linked via hydrogen bonding, whereas (**46**) is proposed to be an extended network of hexa-coordinate $Fe(\mathbf{42})_3$ complexes that are interlinked via the ligands. Mössbauer spectroscopy indicates the presence of high-spin ferrous ions in distorted octahedral fields of all four complexes. Variable-temperature magnetic measurements indicate the virtual absence of any magnetic interactions in compounds (**43–45**). Compound (**46**) undergoes a magnetic phase transition to a paramagnetic state (a weak ferromagnetic ground state) at 25 K.

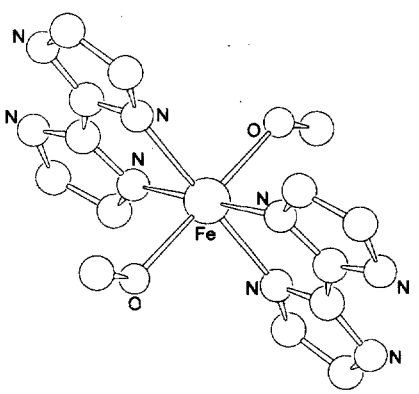

(43)

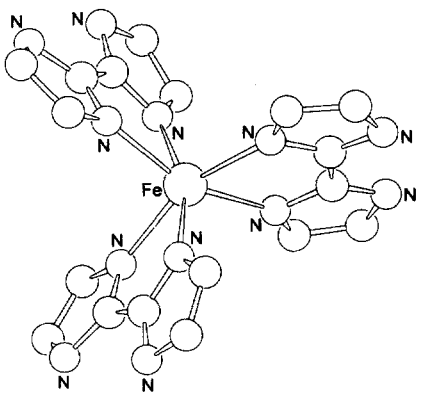

(44)

Thermal reaction of $K[H_2B(pz)_2]$ and pz*H affords $K[HB(pz)_2(pz^*)]$ which on reaction with $FeCl_2$ gives the iron(II) pyrazolylborate complex, $[Fe(HB(pz)_2(pz^*))_2]$ (**47**), whereas $[Fe(HB(pz)(pz^*)_2)_2]$ (**48**) can be synthesized by reaction of $K[H_2B(pz^*)_2]$, pyrazole and $FeCl_2$ [22]. Optical spectroscopy and magnetic susceptibility measurements of (**47**) and (**48**) reveal that thermal spin crossover is exhibited in toluene solution. Comparison with the published behaviour of $[Fe(HB)(pz^*)_3)_2]$ and $[Fe(HB(pz)_3)_2]$ shows that the high-spin state is favoured by an increasing number of methyl substituents.

The crystal structures of low-spin $[\{B(Pz)_4\}_2Fe]$ (**49**) and $[\{PhB(pz)_3\}_2Fe]$ (**50**) have been determined [23]. Comparison of the structures of the low-spin $[\{HB(pz)_3\}_2Fe]$ (**51**) and $[\{HB(3,5\text{-}Me_2\text{–}pz)_3\}_2Fe]$ (**52**) indicate that the steric effects of ligand substituents may influence the electron configurations of the Fe–pyrazolyl–borate complexes. Although (**49**) and (**50**) are usually low-spin complexes, (**52**) is a high-spin complex and complex (**51**) undergoes spin crossover around room temperature. It is suggested that intraligand contact between the phenyl and pyrazolyl groups in complex (**50**) (or the non-bonded and the bonded pyrazolyl groups in complex (**49**)) prevents the iron from achieving an ideal octahedral coordination sphere and, therefore, favours the low-spin state for this complex. Furthermore, it is argued that interligand contacts between the methyl groups in 3-position in complex (**52**) hinder the complex from assuming a low-spin state.

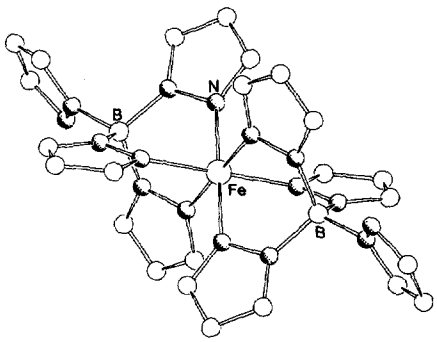

(49)

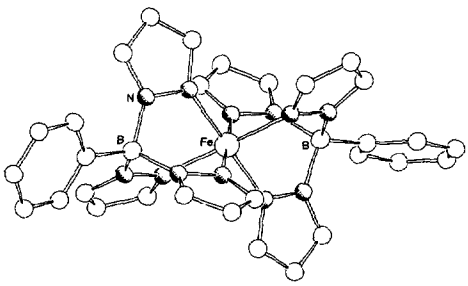

(50)

The complex [Fe(II)(**53**){HB(3,5-$Me_2pz)_3$}] (**54**), a model for the active site(s) in α-ketoglutarate-dependent dioxygenases, has been prepared [24]. Exposure of an acetonitrile solution of (**54**) to air, followed by the addition of a small amount of HCl, leads to the formation of benzoic acid. Similar reactions in the presence of excess cyclohexene or *cis*- or *trans*-stilbene led to the formation of epoxides, as well as ketones and alcohols. Oxidation of cyclohexene in the presence of the free radical scavenger tributyltin hydride resulted in formation of the corresponding epoxide but not the ketone or alcohol. Proposed reaction mechanisms that are consistent with these results are shown in Scheme 2.

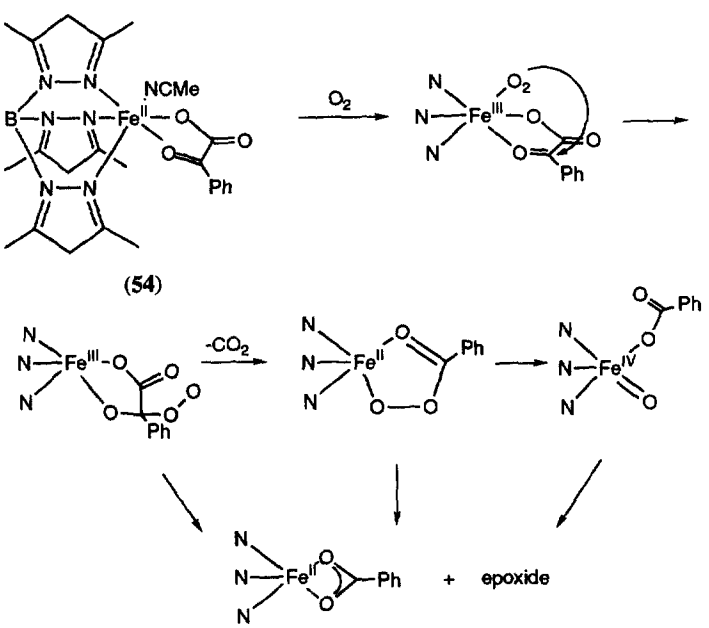

Scheme 2.

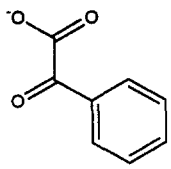

(53)

Transition metal halide complexes with 1,2,4-triazole (**55**) as a ligand have been studied [25]. The iron(II) complex [$FeCl_2$(**55**)] was studied by electronic absorbance and values of D_q and B were obtained. These values and the room-temperature magnetic moment were consistent with pseudo-octahedral coordination of the iron atom. The structure is suggested to be polymeric and a monodimensional chain bridged by both Cl and (**55**). Two iron(II) complexes with iodine, thiocyanate, and 4-amino-1,2,4-triazole (**56**) have been found to possess reversible thermochromism (colour change from white to pink) [26].

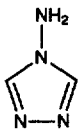

(56)

The thermochromism originates from the spin state of the complex. The complexes were Fe(**56**)I_2 (**57**) and Fe(**56**)$_{2.5}$$(NCS)_2 \cdot H_2O$ ((**58**)$\cdot H_2O$). Both (**57**) and (**58**) have a dependence of μ_{eff} on T with a spin transition $^5T_2 \leftrightarrow {}^1A_1$; complex (**58**) shows a smooth dependence, whereas (**57**) has a sharp dependence with hysteresis. The Mössbauer spectra at 295 K and 75 K of (**57**) and (**58**) show that the complexes are in high-spin and low-spin states respectively at the two temperatures. Mössbauer and IR data, together with comparison of known Fe–triazole complexes, suggests an FeN_6 core for (**57**) with a polynuclear unlimited chain structure. Complex (**58**) is also suggested to have FeN_6 cores, but to exist as a dimer with three 1,2-bridging triazoles, two terminal triazoles and four NCS ligands.

5.2. *Complexes with imines and oximes*

The N_4 tetradentate Schiff base ligand H_2(**59**)

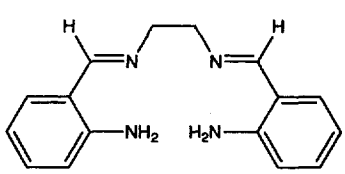

H_2-(**59**)

which is synthesized by condensation of 2-aminobenzaldehyde and ethylenediamine, has been reacted with iron(III) halides in acetone [27]. Two of the product complexes, Fe(**59**)Cl and Fe(**59**)Br · H_2O, exhibit spin crossover between the ^2T and ^6A states. This has been demonstrated by magnetic susceptibility measurements, variable temperature ^{57}Fe Mössbauer spectroscopy and ESR at 77 K. Work carried out on the related complex, Fe(salen)(ImH)X (X = ClO_4, PF_6, BF_4), correlated the adopted spin-state with the size of the dihedral angle between the phenyl rings of the ligand. Structural investigation of complexes of copper and nickel with (**59**) reveals a large dihedral angle between the phenyl rings of the ligand which may be related to the observation of spin crossover in the Fe(III) complex.

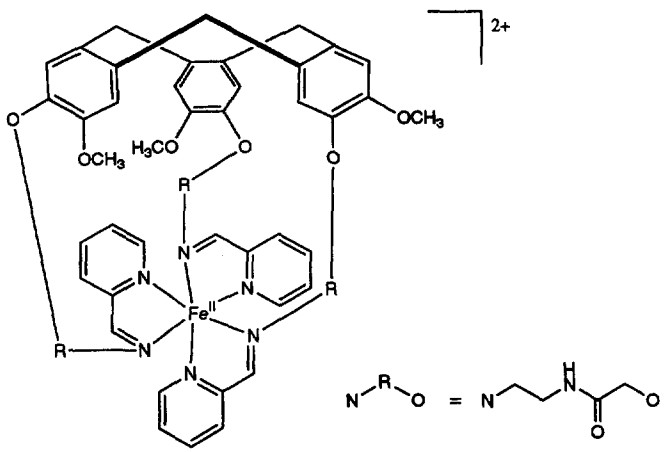

[Fe(**60**)]$^{2+}$

By reacting $FeCl_2$ with a C_3-cycloveratrylene ligand with three spacers ending with iminopyridine groups (**60**), a complex with an unusual spin state transformation was obtained [28]. The complex [Fe(**60**)]$(PF_6)_2$ (**61**) was structurally characterized by X-ray crystallography. The iron is distorted octahedrally coordinated by six N atoms. The magnetic moment of (**61**) has a very weak temperature dependence (6–300 K), suggesting a coexistence of low- and high-spin forms. The high spin fraction was estimated to 15–20% from magnetic measurements and the Mössbauer spectra at 78 and 300 K. The anion plays a role in this behaviour since [Fe(**60**)]$(ClO_4)_2$ shows a clear low-spin behaviour. Magnetic measurements show that introducing a methyl group at the 6-position of the pyridine ring gives a high-spin complex which is explained by the increased $Fe–N_{py}$ distance. In aqueous solution, the complex $[Fe(\mathbf{62})(MeIm)_2]^+$ undergoes aquation producing $[Fe(\mathbf{62})(MeIm)(H_2O)]^+$ (**63**) [29]. One-electron oxidation of (**63**) affords a mixed-valence (III/II) bridged dinuclear complex. The formation constant for this reaction was determined: $K_{dim} = 1.0 \times 10^4$. The nature of the bridging group is not clear, but it is proposed to be a μ-hydroxo group.

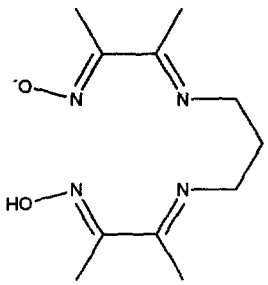

(62)

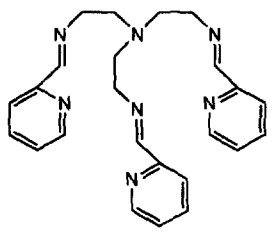

(64)

The crystal structure of [Fe(**64**)]$(PF_6)_2$ (**65**) has been determined [30]. The coordination geometry around the iron(II) ion is a trigonal antiprism, twisted by 6°. The three pyridine N atoms make out one of the coordination triangles and the three imino N atoms the other. The average $Fe–N_{pyridine}$ bond length is 1.981 Å and the average $Fe–N_{imino}$ bond length is 1.950 Å. The $Fe\cdots N_{amine}$ distance is 3.427 Å, i.e. too long for any bonding interaction.

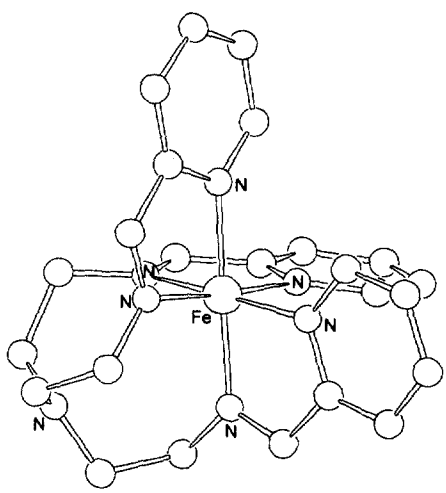

(65)

5.3. Complexes with macrocyclic ligands

Complexes of iron(II) [31] and iron(III) [32] and the hexadentate ligand (**66**) have been reported. The iron(II) complex was made by the reaction of (**66**) and $Fe(ClO_4)_2 \cdot 6H_2O$ and gave [Fe(**66**)]$(ClO_4)_2$. Effective magnetic moments at room temperature suggest that the iron(II) complex has a d^6 high-spin configuration. Comparison of powder X-ray diffraction measurements implies that $[Fe(\mathbf{66})]^{2+}$ has

the same C_1-symmetric structure as $[Zn(\mathbf{66})]^{2+}$, for which the single-crystal X-ray structure has been determined. In the structure, two of the six-membered pendant arm chelate rings adopt a boat conformation and the third has a twist-boat conformation. The MN_6 polyhedron is distorted trigonal prismatic. Air oxidation of $[Fe(\mathbf{66})](ClO_4)_2$ in the presence of NEt_3 gives microcrystals of [Fe(III)(**67**)], where (**67**) is the triply deprotonated (**66**). If the deep blue crystals are dissolved in MeCN that is made acidic with $HClO_4$ the solution turns pale green as the ligand is protonated. This reaction is completely reversible. Magnetic susceptibility measurements indicate a high-spin d^5 configuration of the iron(III) in [Fe(III)(**67**)], showing that the three anilido groups are strong π-donors generating a weak ligand field. The structure of [Fe(III)(**67**)] is assumed to be identical with that of [Mn(IV)(**67**)] having a C_3 symmetry with three six-membered anilido rings.

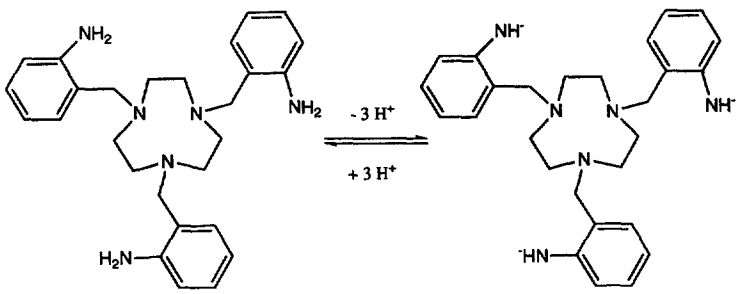

(66) (67)

Iron complexes with ligands based on Me_3–tacn have been synthesized and their reactions with DNA have been investigated [33]. The complexes were (Me_3–tacn)$FeCl_3$ (**68**) and (ps–Me_2–tacn)$FeCl_3$ (**69**)–(**71**), where ps–Me_2–tacn is the ligand with a psoralen (a DNA photo-cross-linking agent) moiety attached. By attaching the intercalator psoralen with a hydrocarbon chain to the ligand, the metal complex is brought closer to the DNA. The complexes induce cleavage of single-stranded DNA in the presence of dioxygen. Irradiation further increases the efficiency of the psoralen complexes. The cleavage has low sequence specificity and the reaction is suggested to be a cationic iron species binding to the phosphate backbone of DNA. The crystal structure of (**68**) has also been determined. The geometry about the iron is a trigonally distorted octahedron with the N–Fe–N angles constrained by the ligand and the Cl–Fe–Cl angles expanded.

As a model of the coordination of NO to non-haem ferrous enzymes, two model compounds have been studied [34]. The nitrosyl coordination can reveal details about intermediates in the chemistry with dioxygen of these enzymes. The complexes [Fe(Me_3–tacn)(NO)(N_3)$_2$] and [Fe(edta)(NO)] were studied using X-ray absorption, resonance Raman, absorption, magnetic circular dichroism (MCD) and EPR spectroscopies. Spin-restricted and spin-unrestricted SCF–Xα–SW electronic structure calculations have also been made. The calculations and spectroscopic results suggest a high spin Fe^{3+} antiferromagnetically coupled to NO^- with NO^- involved

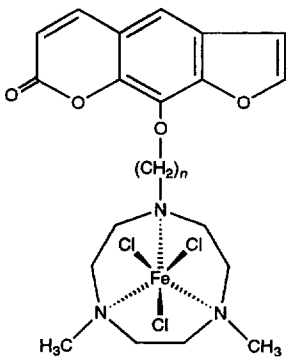

(**69**) n=3
(**70**) n=4
(**71**) n=6

in a strong donor bonding interaction to the Fe^{3+} in both complexes. The Fe–NO bond is bent in the complexes studied and the calculations and resonance Raman results show that this derives from an in-plane bonding interaction of the NO^- π^* orbital and the d_{xz} orbital on the iron atom. The calculations were extended to involve possible oxygen intermediates. The description of the intermediates is parallel to the Fe^{3+}–NO^- complexes with a superoxide antiferromegnetically coupled to a high spin ferric centre.

5.4. Miscellaneous N-donor complexes

Reaction of $FeSO_4$ with $Na_2H_2edta \cdot 2H_2O$ yields the complexes $[Fe(H_2O)_4][Fe(edtaH)(H_2O)]_2 \cdot 4H_2O$ (**72**) and $[Fe(edtaH_2)(H_2O)] \cdot 2H_2O$ (**73**) [35]. Structural characterization reveals that the mono-anion in (**72**) is a pentagonal bipyramid in which the edtaH ligand is hexadentate. The Fe(II)$(edtaH_2)(H_2O)$ unit in (**73**) also contains seven-coordinate pentagonal bipyramidal iron. The two protonated equatorial glycine arms remain uncoordinated with C=O bond lengths of 1.31 Å compared with 1.24 Å for the axial C=O groups.

EPR spectroscopic observation of the titration of NO–Fe(II)Blm (Blm = bleomycin) with DNA indicates that the metal domain undergoes a change in environment as the (DNA base pair):(drug) ratio increases to 50:1 [36]. For NO–Fe(II)Blm, $\nu(^{15}N–O)$ occurs at 1589 cm^{-1}, which is similar to the value reported for NO–haemoglobin and NO–myoglobin. When DNA is added (3bp per drug molecule) the absorption is broadened. Injection of dioxygen into a solution of ON–Fe(II)BlmDNA leads to a low-spin Fe(III)BlmDNA complex, as determined by ESR spectroscopy. The NO is largely oxidized to NO_2^-. It is suggested that the initial reaction of ON–Fe(II)Blm with O_2 generates Fe(III)Blm and peroxynitrite $OONO^-$. If $OONO^-$ is formed, it does not appear to cause detectable DNA damage.

The iron(II) complexes of bleomycin and its model compound (**75**) were studied focusing on geometric and electronic structure [37]. MCD spectra, X-ray absorption spectroscopy (XAS) and EXAFS analysis on solid $[Fe(II)(\mathbf{75})]^+$ revealed a five-coordinated iron centre with a square pyramidal geometry with one short Fe–N bond. In solution $[Fe(II)(\mathbf{75})]^+$ has a distorted octahedral geometry with a solvent molecule on the sixth position; it maintains its short Fe–N bond. The complex [Fe(II)(**74**)] has similar spectral features, suggesting a six-coordinate iron centre with similar ligation, including the short Fe–N bond. Unusual moderately intense low-energy iron(II)→pyrimidine MLCT transitions were found in the low-temperature optical absorption and MCD spectra of [Fe(II)(**74**)] and $[Fe(II)(\mathbf{75})]^+$. This pyrimidine π-backbonding mediates the electron density on the Fe(II) centre which contributes in giving the complex an ability to bind π-acceptor exogenous ligands converting the complex to a low-spin state.

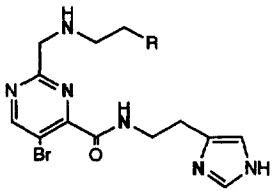

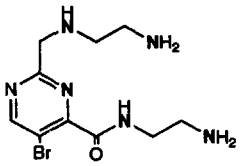

Coordinated nitrogens are in **bold type**

(**75**) R=NH_2
(**76**) R=$NHCH_3$
(**77**) R=$N(CH_3)_2$

(**78**)

Model studies of activation of the ferrous complexes of (**75–78**) $[Fe(II)(\mathbf{75–78})]^+$) investigated what structural features of the iron site in the bleomycin complex controlled oxygen binding [38]. The complexes $[Fe(II)(\mathbf{75})]^+$ and $[Fe(II)(\mathbf{76})]^+$ bind CO, NO and coordinate O_2 at the sixth site and give EPR spectra similar to activated bleomycin, whereas $[Fe(II)(\mathbf{78})]^+$ is unable to bind CO and NO and does not give the characteristic EPR spectrum. Therefore, it was suggested that the trans disposition of the pyrimidine and imadazole groups (the latter missing in $[Fe(II)(\mathbf{78})]^+$) in the basal plane of Fe(II) is essential for O_2 activation. The coordination of the primary NH_2 group is also essential, since $[Fe(II)(\mathbf{77})]^+$, in which the amine is not coordinated, was unable to bind CO and O_2. As a mimic of the metal binding part of bleomycin, the complexes $[Fe(\mathbf{75})]^{n+}$ ($n=1,2$) (**79**, **80**) have been synthesized and lipid peroxidation with these complexes in the presence of O_2 or H_2O_2 has been studied [39]. The iron(II) complex (**79**) reacts with oxygen to give $[(\mathbf{75})Fe(III)–O–OH]^+$ as an active intermediate, identified by its EPR spectrum. Complex (**80**) gives the same intermediate in its reaction with H_2O_2. The intermediate hydroperoxo complex then reacts through H atom abstraction with linoleic acid and arachidonic acid affording mainly the 13-OOH and the 15-OOH positional isomers respectively. It is suggested that a similar intermediate exists in the peroxidation reactions of Fe–blm.

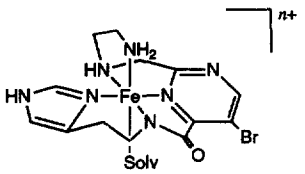

(79) n=1
(80) n=2

A five-coordinate iron complex (**81**) with an N_4-ligand and an axial aqua ligand have been synthesized and structurally characterized [40]. Complex (**81**) is made by oxidation of (**82**) by Ag(I) salts or $Ce(NH_4)_2(NO_3)_6$. Complex (**82**) has a reversible oxidation wave at +0.46 V (vs SCE). The X-ray single crystal structure of (**81**) shows that the N atoms are nearly planar with the Fe atom 0.362 Å above the N_4 plane. Compounds (**81**) and (**82**) were investigated by zero-field and high-field Mössbauer spectroscopy; they give spectra with similar fine and hyperfine structures and identical δ_{Fe} values (0.14(1) mm s^{-1} and 0.14(2) mm s^{-1} respectively) indicating that the oxidation of (**82**) is essentially ligand based. The C_φ–N distances in (**81**) are also shorter than expected for an Fe(IV) complex and more consistent with a semiquinone-like ligand and an Fe(III) atom.

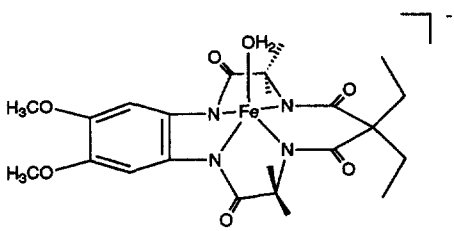

(82)

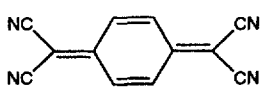

(83)

The iron(II) complex $[Fe(CH_3OH)_4(\mathbf{83})_2](\mathbf{83})\cdot 2CH_3CN$ (**84**) has been prepared [41]. The crystal structure of (**84**) shows that the iron atom has a slightly elongated octahedral N_2O_4 coordination sphere with two molecules of (**83**) occupying the axial positions and four methanol molecules in the equatorial positions. There are two forms of (**83**) in the crystal structure: one monoanionic, coordinated to the iron atom, and one neutral. They are stacked in columns (···BAAB···) linked by the coordination to iron.

6. Complexes with tetrapyrrole macrocycles

6.1. Complexes with phthalocyanines

Absorption and MCD spectra have been reported for $Na[(CN)_2Fe(III)(pc)]$ [42]. Analysis of the low temperature variable field MCD spectra allowed the assignment

of the ground spin state to ^2E_g for the complex, which represents the first open shell metallophthalocyanine with an orbitally degenerate ground state to be submitted to comprehensive spectra analysis.

Metal complexes of hexadecachlorophthalocyanine H_2(**85**) have gained interest as substances in photoreceptors and optical recording substrates. The formation of such an iron(II) complex, $[Fe(II)(\mathbf{85})(CN)_2]^{2-}$, from $[Fe(\mathbf{85})(DMSO)_2]^{2-}$ in dimethyl sulfoxide has been studied [43]. The complex is highly soluble in dmf and dmso and has an ϵ_Q band of 92 000 and 110 000 $dm^3\ mol^{-1}\ cm^{-1}$ centred at 680 nm and 685 nm respectively. Only the formation of the dicyano complex could be followed spectroscopically, and a rate constant $k = 4.2 \times 10^{-3}\ dm^3\ mol^{-1}\ s^{-1}$ was determined. The equilibrium constant for the formation of $[Fe(II)(\mathbf{85})(CN)_2]^{2-}$ was determined to be $K = 1.6 \times 10^3\ dm^3\ mol^{-1}$.

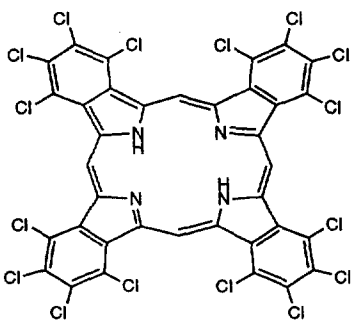

H_2(**85**)

The mixed-ligand dimetallic N-bridged species [(TPP)Fe–N–Fe(pc)] and the oxidation product formed by its reaction with I_2 have been studied [44]. The oxidized Fe–Fe compound (**86**) was characterized by X-ray crystallography and was found to be a monopositively charged Fe–Fe μ-nitrido dimer with I_5^- as counterion. The Fe–N–Fe bridge is nearly linear (179°) and octahedral coordination of the iron atoms is achieved by an H_2O and a THF molecule on the Fe(pc) and the Fe(TPP) respectively.

6.2. Complexes with porphyrins

6.2.1. Axially ligated porphyrin complexes

A new crystal form of $[Fe(TPP)(H_2O)_2]ClO_4$ (**87**) has been reported [45]. The crystal structure contains two independent molecules of (**87**). The Fe–N bond lengths are almost identical, whereas the Fe–O bond lengths differ slightly in the two unique molecules. The coordination geometry of this new form is very similar to an earlier report on the structure of (**87**) in a different crystal form, but it shows some interesting differences compared with the previously published structure of a tetrahydrofuran solvated form. The solvated form has a more expanded porphinato core

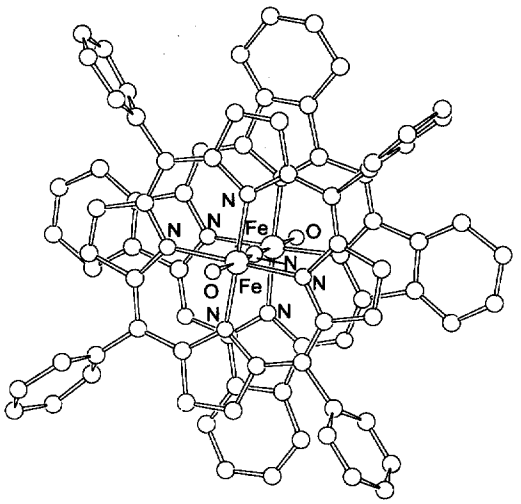

(86)

and shorter Fe–O bonds; both differences were suggested to originate from the more extensive hydrogen bonding in the solvated form.

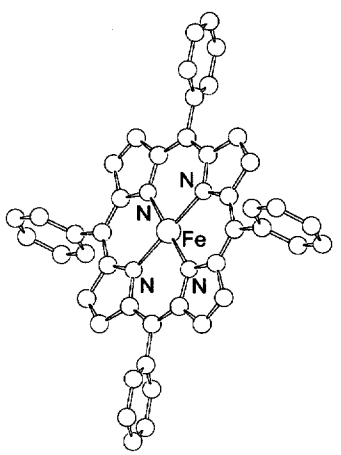

(87)

The crystal structure of [Fe(III)(TPP)($OCOCF_3$)] has been reported [46]. The iron(III) atom is displaced 0.48 Å out of the mean plane of the porphyrin. This, together with the Fe–N bond lengths (2.054 Å as a mean), is indicative of iron(III) in a high-spin state ($S=\frac{5}{2}$). Comparisons of structures of several [Fe(III)(TPP)(X)] ($X=OCH_3$, CO_2CH_3, $OCOCF_3$, SO_2C_6, OSO_3H, SO_3CF_3, $OClO_3$) crystal struc-

tures were made; these show a trend of increasing Fe–O bond lengths together with decreasing Fe–N bond lengths and out-of-plane displacement. The complexes with longest Fe–O bonds also showed most $S=\frac{3}{2}$ character.

Relaxation times for low-spin Fe(III)(TPP)(*N*-MeIm)$_2$ have been measured by spin–echo (10–25 K) and saturation recovery (10–28 K) experiments [47]. At low temperature, iron electron spin relaxation rates are slow with respect to electron–electron spin–spin splitting, but as the temperature is increased this relation is inverted. The measured relaxation times for the Fe(III) have been used to analyse the temperature-dependent changes in the spin–echo decays and the saturation recovery data using an interacting nitroxyl spin label and thus to determine that the interspin distance for these complexes is in the range 10.5–15 Å. There is good agreement between the results obtained by the two methods for this distance.

An iron(III) porphyrin bis-phosphonite complex can be synthesized using an intermediate with a weakly coordinating perchlorate ligand [48]. The complex [Fe(TPP){P(OMe)$_2$Ph}$_2$]ClO$_4$ (**88**) was made in this way, as well as its analogues, where the phenyl rings of the porphyrin were fully meta- or para-substituted. The proton NMR spectrum of (**88**) has an unusual pyrrole proton signal at δ 3.1 (25 °C) which has an anti-Curie behaviour in the temperature dependence of the isotropic shift indicative of a $(d_{xz},d_{yz})^4(d_{xy})^1$ ground state, usual for low-spin iron(III) atoms. The EPR spectrum is in agreement with a $(d_{xy})^1$ ground state for the complex. The proposed explanation is the stabilizing effect of the low-basicity phosphonites on the low-spin iron(III) state.

The ligand Ph[N$_2$O$_2$]$^-$ has successfully been coordinated to iron porphyrins [49]. It is the anion of cupferron and is related to the NO-releasing anion R$_2$N[N$_2$O$_2$]$^-$, which has been used in investigations of the role of nitric oxide as a bioregulatory agent. One of the iron porphyrin products [(TPP)Fe(η^2-ON(Ph)–NO)]·0.1CH$_2$Cl$_2$ was characterized by X-ray crystallography. The ligand showed binding to a formally six-coordinate Fe(III) centre in a didentate σ-O fashion.

A new molecular mechanics (MM) force field model has been used to investigate the planar and ruffled conformations of [Fe(TMP)(L)$_2$]$^+$, where L is a pyridine or imidazole derivative [50]. The example [Fe(TMP)(1,2-Me$_2$Im)$_2$]ClO$_4$ showed a strongly ruffled structure and the MM calculations indicated that this was due to the anisotropic distribution of steric bulk and the relative perpendicular orientation of the axial ligands. Furthermore, the *meso*-mesityl groups of the porphyrins investigated showed a slightly staggered minimum energy orientation, which was other evidence for important bonded interactions between ligands and the peripheral substituents in six-coordinate species. For four-coordinate [Fe(*meso*-tetraaryl-porphyrin)]$^+$ species, the primary determinant for the core conformation was the interaction between peripheral aryl groups and the porphyrin core. The ^{57}Fe chemical shifts have been determined for the ^{57}Fe-enriched model haem complexes with TPP, TMP and OEP in which at least one of the axial ligand is PMe$_3$ [51]. The shifts have been determined by recording the ^{31}P NMR spectrum using double resonance at the appropriate ^{57}Fe frequency. The variation of δ with substituent type, axial ligand electronic characteristics, steric crowding, solvent and temperature have been

investigated. Increasing the electron-donating nature of the substituents, for example, is found to increase the chemical shift. Structures have been determined for the complexes (p-OMe)$_4$(TPP)Fe(PMe$_3$)$_2$ and (OEP)Fe(PMe$_3$)$_2$. In both complexes the porphyrinate core is planar and the axial phosphines have methyl groups staggered.

Proton and deuterium NMR spectroscopy have been used to study the reactivity of the π-cation radical complexes [(TPP$^{\cdot}$)Fe(III)Cl][SbCl$_6$] and [(TPP$^{\cdot}$)Fe(III)(ClO$_4$)$_2$] with pyridine [52]. The addition of pyridine to either of the two iron complexes at −70 °C gives a stable complex, (**89**), that could be isolated on a synthetic scale as the (μ-oxo) bridged complex {[β-py–TPP)Fe(III)]$_2$O}(ClO$_4$)$_2$, and unstable (**90**) and (**91**). The ^{1}H NMR spectra of the high spin complex (**89**)–Cl$_2$ and the low spin complex [(**90**)–(py)$_2$]Cl$_2$ were presented and analysed.

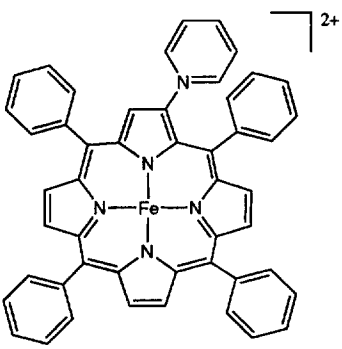

(89)

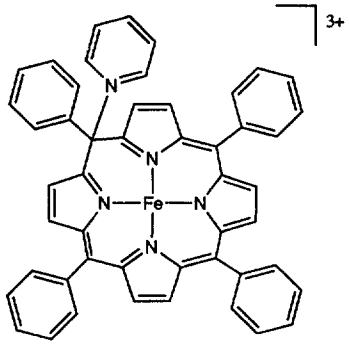

(90)

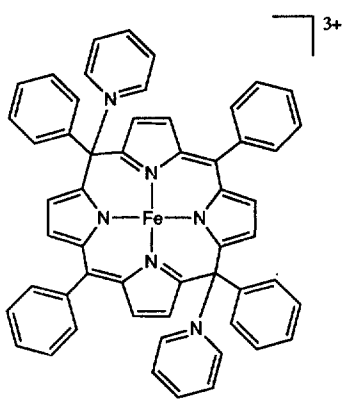

(91)

The compound [Fe(III)(TPP)(η^1-O–NC(CN)$_2$)] (**92**) has been prepared and characterized by single-crystal X-ray crystallography (TTPH$_2$=5,10,15,20-

tetratolylporphyrin) [53]. The ambidentate nature of the pseudohalide nitrosodicyanometanide ligand was shown by the preparation of $[Ir(I)(\eta^1\text{-}N(O)C(CN)_2)(CO)(PPh_3)_2]$, where the ligand binds through the nitrogen instead of the oxygen. Both compounds were characterized by a range of spectroscopic methods.

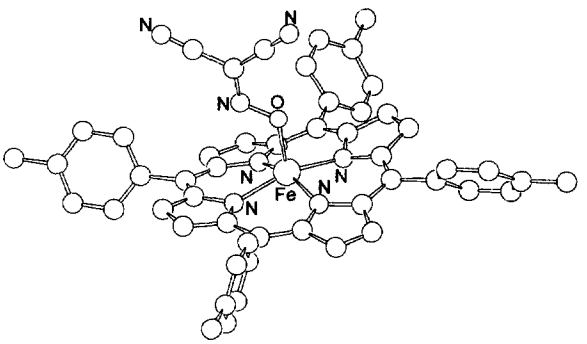

(92)

The magnetic properties of two iron(III) complexes of tailed porphyrins on the addition of pyridine have been investigated [54]. Adding pyridine to a solution of high-spin [Fe(III)(**93**)Cl] gave no EPR signal at 77 K of the low-spin complex with pyridine coordinated. When pyridine was added to a solution of [Fe(III)(**93**)Cl] the EPR signal at 77 K of the high-spin complex disappeared and two new signals appeared. The two new signals originated from two species with a different spin-state in equilibrium. One of the signals ($g_z=3.08$, $g_y=2.20$, $g_x=1.27$) is proposed to be the six-coordinate low-spin complex with the tailing imidazole and a pyridine molecule coordinated. The other signal ($g_\perp=4.26$, $g_\parallel=2.00$) could be the intermediate where the pyridine is coordinated but the imidazole is still uncoordinated. This would give rise to an intermediate spin-state.

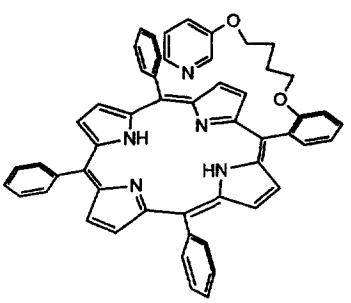

H_2(**93**)

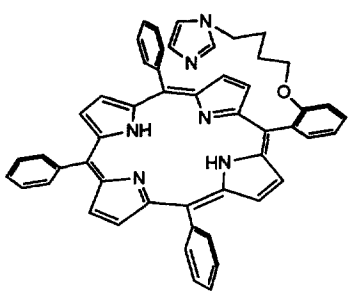

H_2(**94**)

The green reaction product of a coupled oxidation of iron(II)(OEP) in pyridine using dioxygen as oxidant and ascorbic acid as reductant has been structurally

characterized as (**95**)PF_6 [55]. The structure of the product, verdohaem, has two independent in-plane Fe–N distances of 1.977(6) and 1.966(5) Å. This is indicative of a low-spin iron(II) complex. In the crystal, the two pyridines lie parallel to each other. Electrochemical measurements made on (**95**) showed a one-electron reduction at −1.07 V in dmf–pyridine (vs Ag/Ag^+) and a quasi-reversible one-electron oxidation at 0.28 V in CH_2Cl_2–pyridine but the oxidation product is chemically unstable.

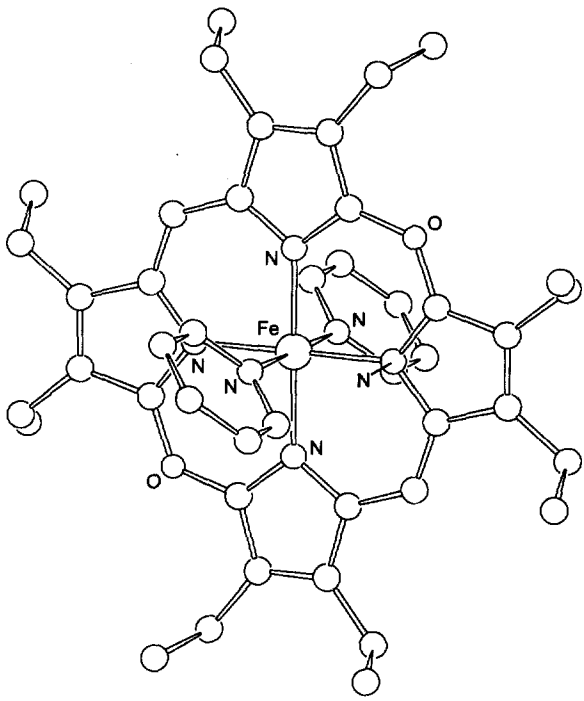

(95)

To improve and confirm the correlations between information from resonance Raman spectroscopy and structural features in β-pyrrole-substituted metalloporphyrins, three new octaethylporphyrin complexes have been synthesized [56]. The crystal structures of [Fe(OEP)(NCS)]·C_7H_8 (**96**), [Fe(OEP)(*N*-MeIm)$_2$][Ag(*N*-MeIm)$_2$][PF_6]$_2$ (**97**) and [Fe(OEP)(DMSO)$_2$](PF_6) (**98**) are reported; the core structures of these compounds represent a high-spin pentacoordinate, a low-spin hexacoordinate and a high-spin hexacoordinate porphyrin complex respectively. The resonance Raman spectroscopic properties of these three complexes and Fe(OEP) and Fe(OEC) have been correlated to the core size of the porphyrin (chlorin), i.e. the measure of the centre of the porphyrin to the pyrrole nitrogen atoms. It was found that the core-sensitive resonance Raman modes exhibit an inverse linear dependence on the porphyrin core size.

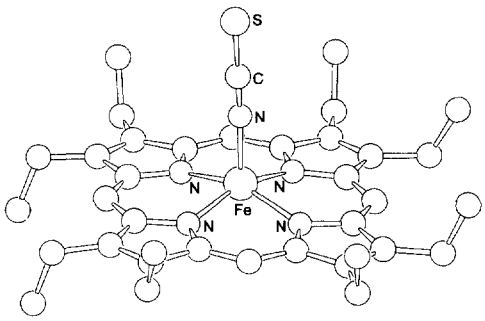

(96)

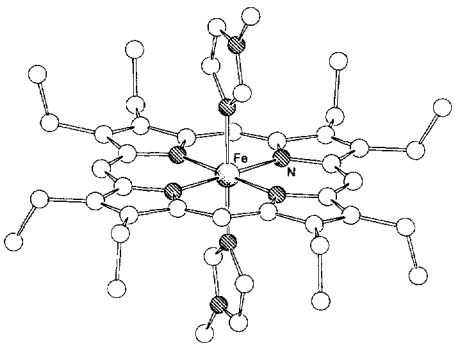

(97)

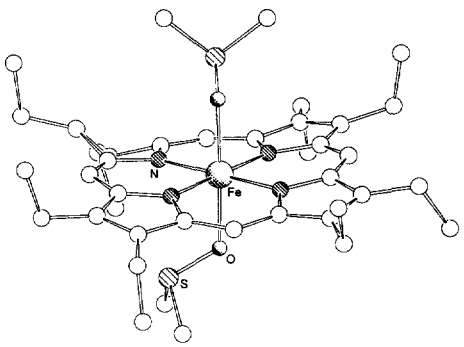

(98)

The electronic structure of the iron complex of *meso*-hydroxyporphyrin (**99**) was observed spectroscopically in a pyridine solution [57]. In pyridine, the hydroxyl group of (**99**) was deprotonated, resulting in the resonance structures (**100**) and (**101**). Different complexes, where L were substituted pyridine ligands, showed that the basicity of the axial substituents modulates the population of (**100**) and (**101**). The formation of π-radical character was essential in haem breakdown, since only (**101**) showed high reactivity towards O_2 to form verdohaem (**102**), a pathway with possible interesting extrapolations to biological systems.

Physical and kinetic data for six new Fe(porphyrin)(NO) complexes, prepared by reductive nitrosylation of the corresponding chloride with nitric oxide in the presence of excess methanol and 2,6-lutidine, have been presented [58]. The complexes were five-coordinate with nitric oxide in a bent geometry. The differences in rates of nitric oxide dissociation for the different compounds, when treated with coordinating ligands, were large. These results were proposed to have implications for mechanistic studies of, for example, the haem in soluble guanylyl cyclase.

Using $AgSbF_6$ as oxidant, the chemical one-electron oxidation of (OEP)Fe(II)(NO) (**103**) and complexes (**104**) and (**105**) have been studied in order to model a proposed $[Fe(NO)]^+$ reaction intermediated in the catalytic cycle of

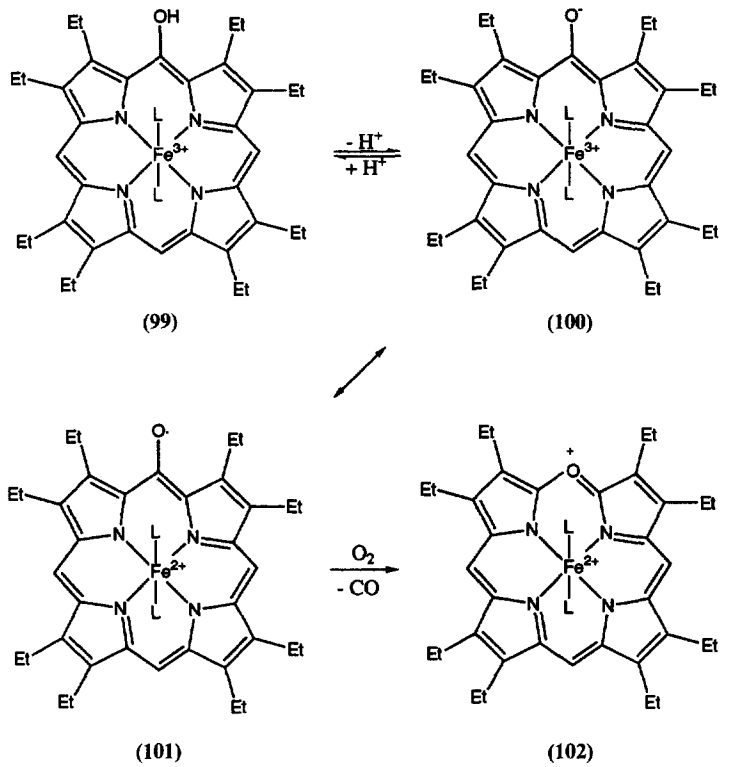

dissimilatory nitrate reductase [59]. In the case of (**103**) the corresponding ferric complex is formed. Oxidation of (**104**) and (**105**) led to ligand-based π-cation radical complexes, which have been characterized by UV–VIS, EPR, NMR and IR spectroscopy. The presence of NO in the π-cation radical complexes is confirmed by the detection of $\nu(^{15}N–O)$ bands in their IR spectra. Addition of 1 equiv. of *N*-methylimidazole leads to the formation of Fe(II)(NO^+)(*N*-MeIm) complexes in all three cases. When another equivalent of *N*-MeIm was added, the OEP complex shows relative stability, whereas the others release NO.

The first nitrosamine complex of a metalloporphyrin has been reported [60]. The X-ray crystal structure of $[(TPP)Fe(Et_2NNO)_2]ClO_4$ (**106**) was determined. The porphyrin core was expanded, indicative of a high-spin ferric complex; the nitrosamine ligands are bound in a σ-O fashion.

To model the active site of cytochrome P-450 a number of Fe(II) porphyrins (Fe(TPP), Fe(TPivPP), and (**107–109**)) have been synthesized having a thiolate group as the fifth axial ligand [61]. The association and dissociation constants for both CO and O_2 coordination have been determined using laser flash photolysis. The influence of the basicity of proximal ligands on the rate parameters have been studied for nitrogenous, thiolate and ethanolate ligands with a wide range of pK_a values. Increase of the pK_a value of the ligand decreases the association rates for

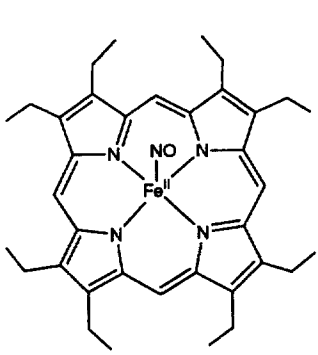

(103)

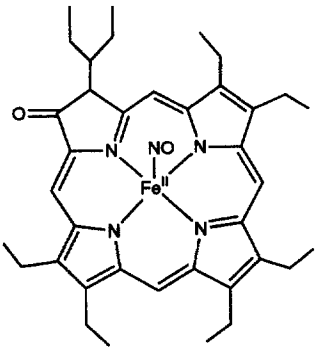

(104)

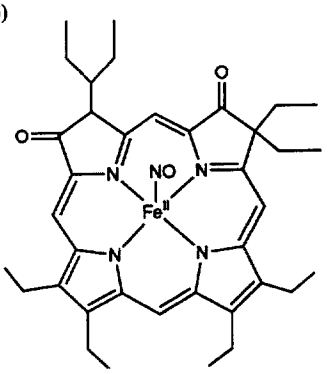

(105)

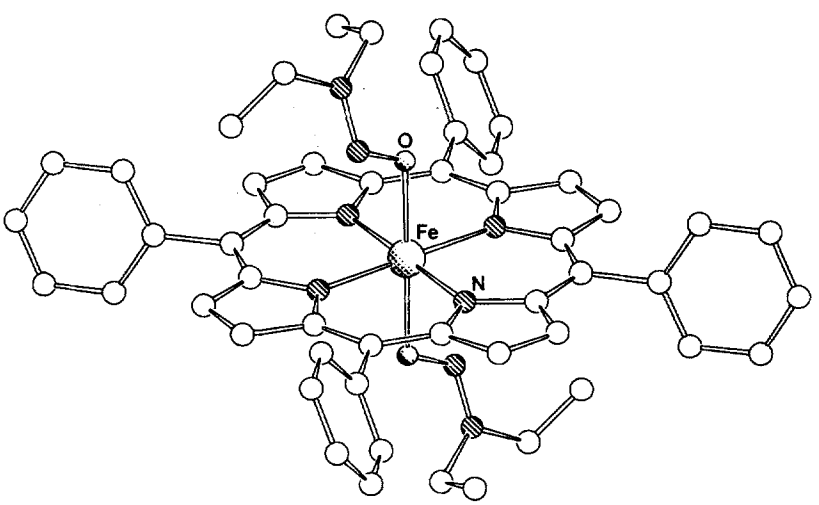

(106)

O_2 and CO, whereas the dissociation rate increases for CO and decreases for O_2. This gives a large decrease in the affinity ratio $M = K_{CO}/K_{O_2}$ going from nitrogen to thiolate coordination.

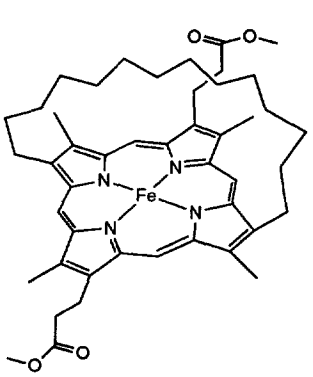

(107)

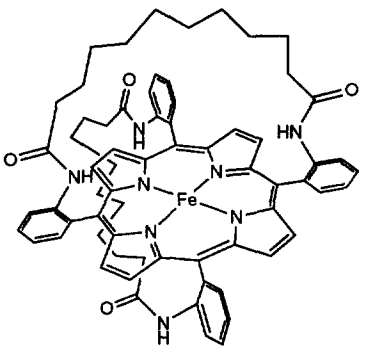

(108)

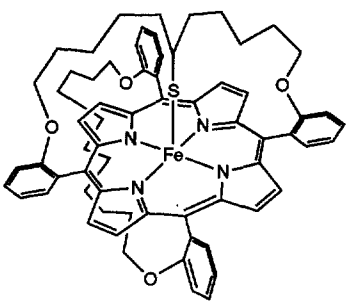

(109)

Resonance Raman studies of photo-reduced and chemically reduced iron-protoporphyrin-IX dimethyl ester chloride [Fe(III)(**110**)(Cl)] have been reported [62]. The studies were made in the presence of 1,2-dimethylimidazole (1,2-Me_2Im) or 2-methylimidazole in DMSO at temperatures down to 50 K. With room temperature laser irradiation in the Soret region complex with the imidazole axial ligand [Fe(III)(**110**)(1,2-Me_2Im)] only partial photoreduction is achieved owing to the fast diffusion of molecules which reduces the power density of the irradiation. When the temperature is lowered to 250 K the thermal motion is restricted and photoreduction becomes almost complete. Dissociated $(1,2\text{-}Me_2Im)^+$ can diffuse away and another molecule occupy the position to give [Fe(III)(**110**)(1,2-Me_2Im)]. In the temperature region between 200 and 150 K the DMSO matrix is solid which partly softens on laser irradiation, stabilizing the intermediate-spin reduced Fe(II)(**110**) species. At 50 K the DMSO matrix is a rigid solid, making dissociation impossible

and no photoreduction is observed. Chemical reduction at temperatures around 200 K gives the same product as the photoinduced reduction.

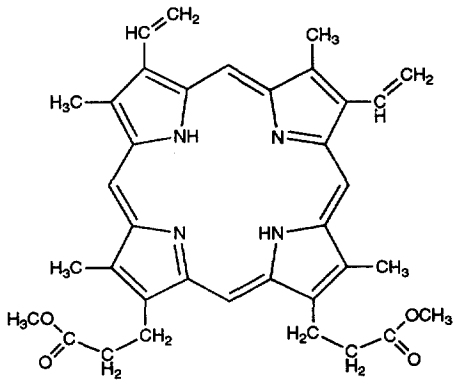

(110)

Steady state and transient absorption spectroscopies have been employed to study ligand photolysis and recombination associated with complexes LL'Fe(II)protoporphyrin IX (L=L'=DMSO (**111**); L=L'=ImH; L=DMSO, L'=*N*-MeIm (**112**) in DMSO [63]. The steady state optical absorption spectra indicate a low-spin six-coordinate haem iron. Photoexcitation of (**111**) leads to a transient species which contains five-coordinate high-spin haem iron. The transient difference spectrum has $abs_{min}=423$ nm and $abs_{max}=435$ nm. The transient species decays with $k_1=2.13+0.04\times10^6\ s^{-1}$. Photolysis of (**112**), however, gives a transient difference spectrum with $abs_{min}=423$ nm and $abs_{max}=439$ nm. Decay of this species follows biphasic kinetics.

Chelation of monochelated protohaem, protohaem monomethyl ester mono[3-(1-imidazoyl)propyl]amide (**113**), has been studied by measuring the rate of return following flash photolysis of CO–(**113**) samples in the presence of *N*-MeIm [64]. This allows measurement of both rate constants, K_B^C and K_{B}^{B} (Scheme 3), relative to the CO association rate by following the recombination for a period of minutes after photolysis. Results indicate that bound internal imidazole is displaced by *N*-MeIm at concentrations greater than 0.012 M. A base elimination mechanism is consistent with all the results obtained.

As a model system for cytochrome P-450, the iron(III)-porphyrin-catalysed epoxidation of terminal alkenes has been studied, focusing on the *N*-alkylhaemin formation [65]. The alkenes studied were allyltrimethylsilane, 4,4-dimethyl-1-pentene, norbornadiene, norbornene, styrene, and vinylcychlohexane. Apart from the well-documented primary *N*-alkylhaemin (**114**) a second *N*-alkyl species is detected. Both species have a characteristic band at 435 nm, but one of the products is unstable and decomposes to give the original iron porphyrin with a band at 410 nm. Both the species are also catalysts for the epoxidation of alkenes using pentafluoroiodobenzene as the oxygen donor. The proposal is that the unstable species is a secondary

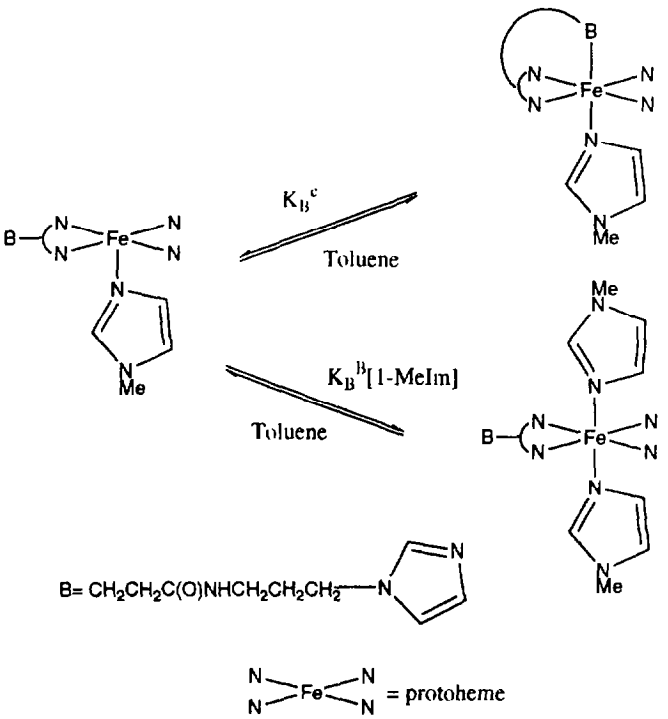
B
N
Fe
N
N
N
N
Me
K_B^C
Toluene
K_B^B[1-MeIm]
Toluene
B= $CH_2CH_2C(O)NHCH_2CH_2CH_2$
= protoheme

Scheme 3.

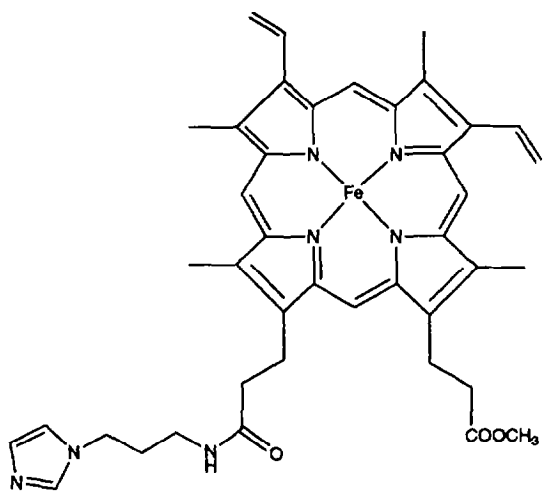
N
Fe
N
N
N
N
$COOCH_3$
O
H

(113)

N-alkylhaemin (**115**) and that this species inhibits the catalytic activity of cytochrome P-450.

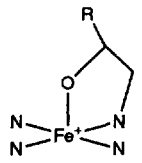

(114)

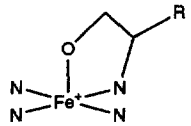

(115)

A peptide-sandwiched mesohaem has been synthesized using a 13 residue peptide and iron(III) mesoporphyrin IX (**116**) [66]. The peptide was chosen so that helix formation would be induced by coordination of a histidine residue to the haem metal. Circular dichroism experiments showed that the complex is 52% α-helical in aqueous solution, but addition of 2,2,2-trifluoroethanol increases this to a maximum of 97%. Two diastereomeric monopeptide adducts have also been isolated and have been found to aggregate owing to the fact that one face of the haem is exposed to the solvent.

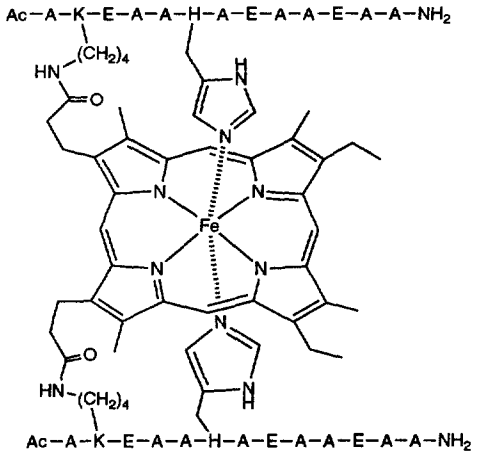

(116)

6.2.2. Complexes with oxygen, peroxides and superoxides

In the catalytic epoxidation of norbornylene and α-methylstyrene by peracids in methylene chloride in the presence of [(TMP)Fe(III)(RCO_2), the selectivity between the different reactants was almost constant while varying the peracids [67]. This is because the π-cation radical $[O{=}Fe(IV)TMP]^{+\cdot}$ (**117**) was the predominant oxidant. If [(**118**)Fe(III)(X)] was used instead, the predominant oxidant changes over to the peracid–Fe(III) complex (**119**), which has been confirmed spectroscopically, and a dependency on the peracid was seen. In toluene the peracid dependency was seen for both catalyst types. Whether (**117**) or (**119**) participate as the active oxidant

was proposed to be controlled either by the electronic structure of the catalyst (push–pull effect) or by alternation of the solvent.

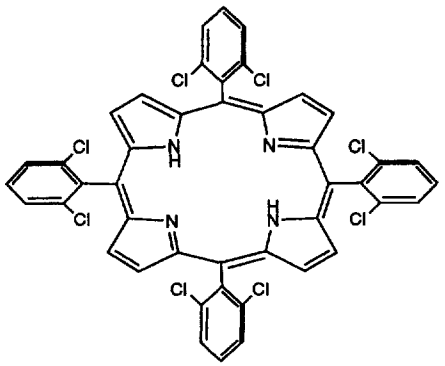

(118)

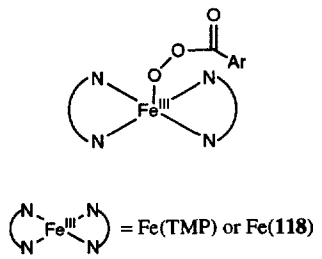

(119)

The reaction, in hydroxylic solvents, of iodosylbenzenes, peracids, hydroperoxides and hydrogen peroxide with iron(III) porphyrin chlorides ([(TPP)FeCl], [(TPFPP)FeCl], [(TMP)FeCl], and (**120–126**)FeCl]) carrying electronegative substituents leads to a high-valent oxene. Previously, the mechanism was proposed to change from heterolysis with peracids to homolysis with hydroperoxides, but the suggestion from structure–reactivity studies is that there is a continual change in the transition state structure instead of a change in mechanism [68].

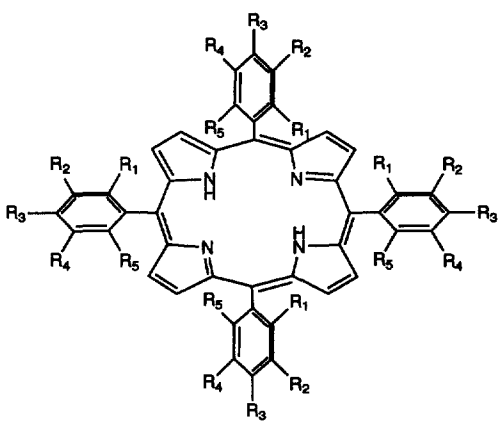

(120) $R_1=R_2=R_3=R_4=R_5=Cl$
(121) $R_3=CN$, $R_1=R_2=R_4=R_5=H$
(122) $R_3=Br$, $R_1=R_2=R_4=R_5=H$
(123) $R_3=OCH_3$, $R_1=R_2=R_4=R_5=H$
(124) $R_3=N(CH_3)_2$, $R_1=R_2=R_4=R_5=H$
(125) $R_1=R_5=Cl$, $R_2=R_3=R_4=H$
(126) $R_1=R_3=CF_3$, $R_2=R_4=R_5=H$

When styrene and other olefins were added to $[(TMP^{+\cdot})Fe(IV)(O)(ClO_4)]^+$, generated by ozonolysis of $[(TMP)Fe(ClO_4)]$ at -80 °C in $CDCl_3$, a new complex was formed [69]. The complex was stable at temperatures up to -30 °C and was then converted into the Fe(III)porphyrin and mainly styrene oxide. The new complex was interpreted as a trapped intermediate in the reaction of oxoiron(IV) porphyrin cation radical complexes and olefins and identified as an ET complex through EPR measurements.

Three iron porphyrin complexes of the type [Fe(III)(X)(OH)(OOH)] (X=TMP (**127**), TPP (**128**), OEP (**129**)) have been prepared by low temperature reaction of the iron porphyrin chloride with KOH and hydrogen peroxide [70]. The formation of [Fe(III)(X)(OH)(OOH)] was shown by optical absorption and X-band EPR spectroscopy. Reaction of (**127**) with imidazole in a large excess gave a new complex (**130**). Based on the low separation of g_1-g_3 in the EPR spectrum of (**130**), compared with other six-coordinate iron(III) hydroxide complexes, it was suggested to be [Fe(III)(TMP)(ImH)(OOH)]. Complexes (**128**) and (**129**) gave no similar products.

A kinetic study of the reaction of hydrogen peroxide with protohaemin has been undertaken in aqueous solution (pH 5–10) with potassium ferrocyanide as a substrate and in the presence and absence of imidazole bases [71]. 1 equiv. of protons showed the reaction to be inhibited in the absence of bases and hydroxide coordination to the ferric haemin was suggested to be essential for peroxidase activity. Monoligation of imidazole bases showed enhancement in the reaction rate, whereas inhibition strongly correlated with biscoordination, which prevents access of H_2O_2 to the iron.

Nuclear magnetic resonance studies on the complex [Fe(III)(**131**)] provide evidence for the slow interconversion between the aquo and hydroxy forms of the complex [72]. It has been reported previously that proton transfer to some μ-oxo ligands can be slow, but these recent results suggest that the phenomenon may not be restricted to μ-oxo dimers.

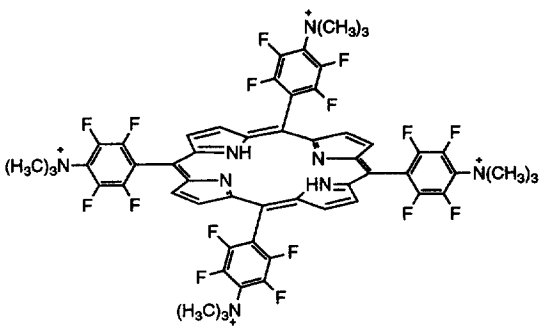

(131)

The new polycationic, water-soluble Fe(III) complex, ([(**132**)Fe(III)(X)$_2$] (**133**), where X=H_2O and/or OH^-) has been synthesized and characterized by mass, UV–VIS, ^1H NMR and ^{13}C NMR spectroscopy [73]. The ligand H_2(**132**) was

synthesized by a selective bromomethylation reaction of $TMPH_2$ with formaldehyde and HBr–acetic acid.

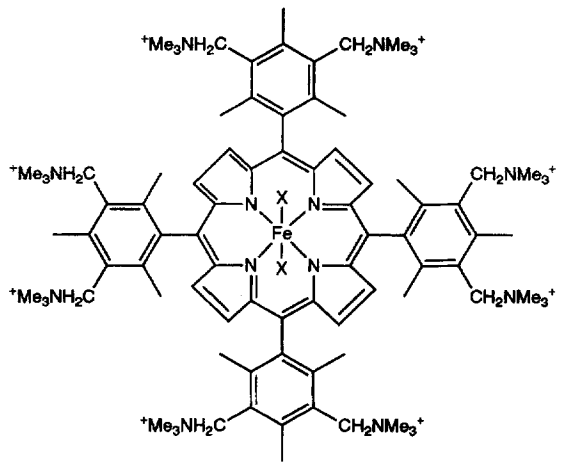

(133)

Reaction between ^{t}BuOOH and (**133**) ($X = H_2O$ and/or OH^-) in buffered aqueous solution has been studied in the range pH 0.9–12.1 [74]. The reaction is found to be first-order with respect to both ^{t}BuOOH and (**133**) concentrations and no general acid or general base catalysis is observed at any pH. The products from the reaction are discussed in terms of four mechanisms: (i) heterolysis of ^{t}BuOOH with a contribution from radical chain reactions; (ii) a radical chain mechanism initiated by [(**132**)Fe(IV)(X)(O)]; (iii) Fenton chemistry involving (**132**)Fe(II) and (**132**)Fe(III) states; (iv) rate-limiting homolysis of the O–O bond in ^{t}BuOOH. The monoligation of acetate has been studied by spectrophotometric titration and a pH-independent binding constant $K_B = 42\ M^{-1}$ has been determined for this process. There is no evidence for μ-oxo dimer formation for the complex. The two halogenated porphyrin complexes [Fe(III)(**134**)Cl] (**135**) and [Fe(III)(**134**)$(py)_2$] (**136**) have been prepared and characterized by X-ray crystallography and show saddle distortions [75]. The facts that the Fe(II) analogue of (**135**) was rapidly oxidized by ^{t}BuOOH, but reacted slowly with dioxygen and that (135) was readily reduced by ^{t}BuOOH strongly support the proposal that Fe(III)(134)Cl/O_2-catalysed alkane oxygenations occur via a radical chain mechanism.

Two polymorphs of $[Fe(OEP)]_2O$ have been structurally investigated by X-ray crystallography. The two forms, one triclinic (**137**) and one monoclinic, have strong structural similarities and parameters typical for five-coordinate high-spin iron(III) [76]. Mössbauer spectra also show parameters consistent with a high-spin iron(III) complex. The largest difference in structure between the two forms is the orientation of the peripheral ethyl groups. The triclinic form has ten ethyl groups pointing outwards and six inward, whereas the monoclinic form has eight pointing in each

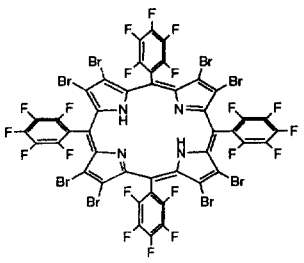

H_2-(134)

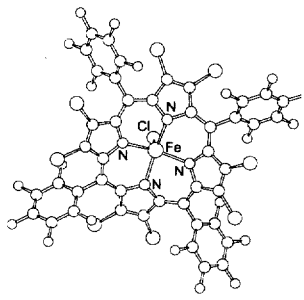

(135)

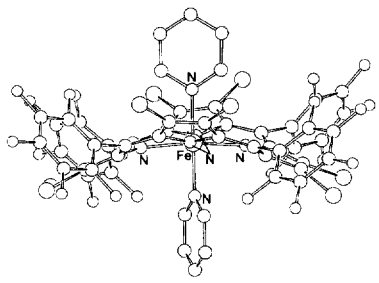

(136)

direction. This also gives a difference in the interplanar angle (7.3° and 2.7° respectively). A common feature for the two forms is the unusually small dihedral angle in the intramolecular porphyrin ring orientation, 17.0(10)° in the triclinic form and 16.8(6)° in the monoclinic form. The role of the orientation of the peripheral ethyl groups was investigated using MM calculations of structural features. Calculations reproduced the small dihedral angle, but when a calculation was performed putting all ethyl groups pointing outwards, the dihedral angle increased to 31.6°. It thus appears that the intramolecular inter-ring ethyl group interactions are important in defining the orientations of the rings.

The crystal structure of the complex μ-oxo-bis[Fe(III)(5,15-dinitro-OEP)] (**138**), an active catalyst for the oxidation of alkanes, a μ-oxo-bis[iron(III)porphyrin], has been determined [77]. Complex (**138**) was made by partial nitration of [Fe(III)(OEP)Cl]. The porphyrin planes are not perfectly parallel (169(2)°) and the Fe–O–Fe angle is 167.9(3)°. The Fe atoms are displaced towards the bridging oxygen atom, 0.46 Å and 0.49 Å. The porphyrin rings are eclipsed with respect to each other, but the nitro-groups are in a staggered position.

Oligomerization of monomeric [(2-OH–TPP)Fe(III)Cl] has been shown to give a cyclic trimeric complex $[(2\text{-O–TPP})\text{Fe(III)}]_3$ with a head-to-tail structure with bridges from the 2-O in one macrocycle to the iron in an adjacent [78]. The ^{1}H NMR spectrum for the compound was studied and the large distinguishable contri-

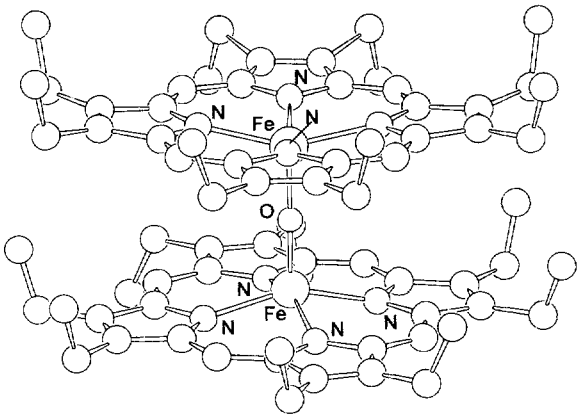

(137)

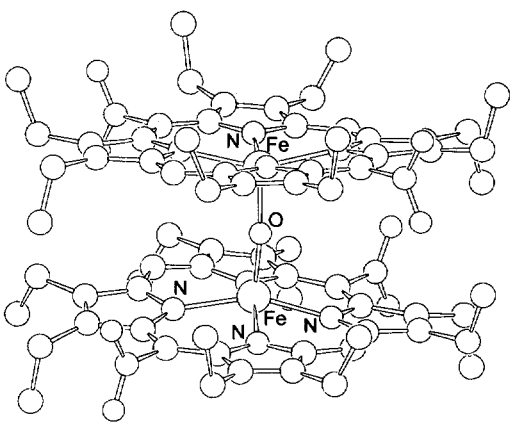

(138)

butions of the 3-H pyrrole contact shift were accounted for by the donation from the external Fe(III) ion. The trimer was cleaved in HX to give monomers [(2-OH–TPP)Fe(III)X], whereas addition of oxygen base (MeO^-, OH^- in MeOH) gave $[(2\text{-O–TPP})Fe(III)X]^-$ ($X=CH_3O^-$, OH^-), for which tautomerism was observed for the (3-H) hydrogen.

Three different $TPivPPH_2$ derivatives bearing a proximal imidazole (**139–141**) have been synthesized and the O_2 binding properties of their iron(II) complexes have been studied [79]. The iron complexes were five-coordinate with the imidazole coordinating at the fifth position and reversibly formed a stable dioxygen adduct in toluene at 25 °C under O_2 pressure.

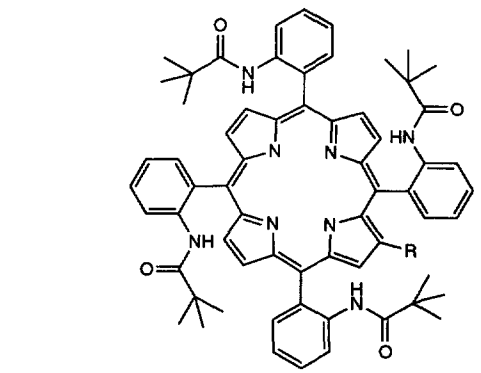

R =

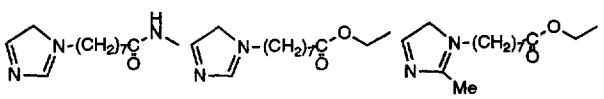

(139) (140) (141)

6.2.3. Other porphyrin complexes

To investigate the influence of peptide-like superstructure on iron porphyrin redox potentials, first- and second-generation dendrimers have been synthesized containing the iron porphyrin core unit [80]. The redox behaviour of the two compounds was studied in methylene chloride and aqueous solution and it was found that the redox potential in water for the Fe(III)/Fe(II) couple shifted 420 mV to more positive potential when going from the relatively open, first-generation, to the densely packed, second-generation dendrimer. The effect, which is also apparent when comparing cytochrome C and more open model compounds thereof, was attributed to the more hydrophobic microenvironment created in the solvent-shielded second generation.

Several iron porphyrins (Fe(TPP), Fe(TMP), Fe(OEP), Fe(4-OCH_3–TPP), and Fe(TPFPP)) have been shown to be useful as active catalysts for the cyclopropanation of alkenes by ethyl diazoacetate [81]. In contrast to many other catalysts for the system, a considerable diastereoselectivity was seen.

The oxidation of the dimeric octaethyloxophlorin (OEPO) complex (**142**) occurred more readily than oxidation of both the μ-oxo dimer [(OEP)Fe(III)–O–Fe(III)(OEP)] and the monomeric [ClFe(III)(OEPOMe)] complex [82]. This effect was at least to some extent attributed to the direct overlap of the tetrapyrrole plane in (**142**). Spectroscopic studies of the oxidized form $(\mathbf{142})^+$ indicate that a ligand-based oxidation has occurred and that the unpaired electron is delocalized over both macrocycles. The oxidation product was reacted with potential axial ligands—an example is its reaction with bromide to form (**142**) and [Fe(III)(OEPO)Br].

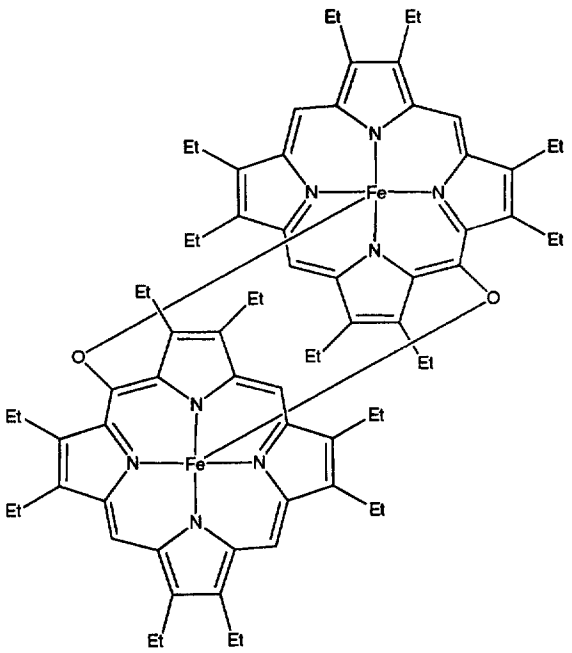

(142)

As a model of the dinuclear Fe/Cu site of haem–copper oxidases, a hydroxo-bridged iron/copper complex has been synthesized [83]. By reacting $[Cu(Me_5dien)(OH_2)](ClO_4)_2$ with $Li(OC_6H_2$-4-Me-2,6-t-$Bu_2)$ the copper compound $[Cu(Me_5dien)(OH)]_2(ClO_4)_2$ was made. This compound was reacted with [Fe(OEP)($OClO_3$)] to give [(OEP)Fe–OH)–Cu(Me_5dien)($OClO_3$)](ClO_4) (**143**). The X-ray structure of (**143**) has been determined. The copper atom has a distorted square pyramidal coordination. The iron atom has a five-coordinate haem stereochemistry, indicative of high-spin iron(III), with the iron atom displaced towards the bridge by 0.44 Å. The Fe(III)–OH–Cu(II) bridge in (**143**) is bent (157.0(2)°) as usual for hydroxo bridges. The GNXAS MS method was used to analyse EXAFS data of (**143**), but the method showed to be less reliable when bridging angles deviated from linearity. Treatment of (**143**) with more $Li(OC_6H_2$-4-Me-2,6-t-$Bu_2)$ probably gives [(OEP)Fe–O–Cu(Me_5dien)($OClO_3$)], as indicated by diastereotropic methylene signals in the ^{1}H NMR spectrum, but no pure sample could be isolated.

The reaction of $[\{(tpa)Cu\}_2O_2]^{2+}$ (**144**) and [Fe(III)(**145**)Cl] or [Fe(III)(TPP)Cl] has been investigated [84]. When equal amounts of (**144**) and [Fe(**145**)Cl] are used (Cu:Fe = 2:1) the product is $[(\mathbf{145})Fe(III)–O–Cu(II)(tpa)]^+$ (**146**). A stoichiometric Cu:Fe ratio of 1:1 leads to the formation of [Fe(**145**)–OH] or [(TPP)Fe–O–Fe(TPP)] as products. This is explained by noting that complete reduction of [Fe(**145**)Cl] or [Fe(TPP)Cl] when the Cu:Fe ratio is 1:1 leaves copper(II) products insensitive to O_2. In order to be able to prepare (**146**),

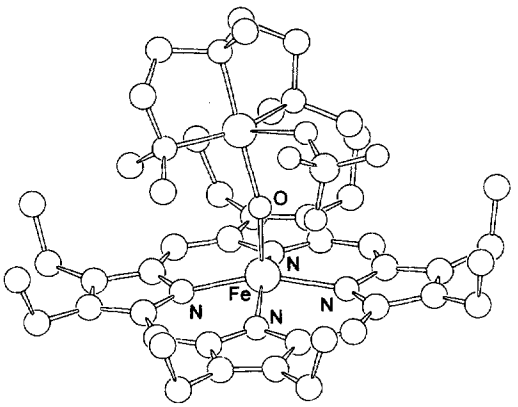

(143)

[(tpa)Cu(I)], its O_2-adduct and/or their decomposition products must be present. In another experiment, highly reactive [Fe(II)(**145**)]·C_7H_8 (**147**) was synthesized by the reaction of [{(tpa)Cu(I)}(MeCN)]$^+$ and [Fe(**145**)Cl] in toluene. Here, reaction of (**144**) and (**147**) in a 1:2 ratio (Cu:Fe = 1:1) gives (**146**) as the product. [Fe(II)(TPP)]·C_7H_8 can be obtained in a similar way starting from [Fe(TPP)Cl].

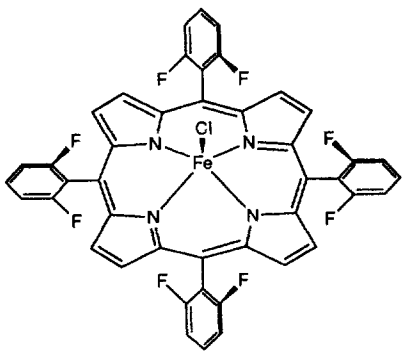

[Fe(**145**)Cl]

Some porphyrinatoiron(III)–Mo(V) complexes with different axial ligands ((**148**) L = NMeIm; (**149**) L = ImH; (**150**) L = 4-(dimethylamino)pyridine) have been thoroughly studied with ^{1}H NMR [85]. One of the axial ligands has a hindered rotation due to the oxomolybdenum substituent. This is shown by the split of the eight pyrrole proton resonances. The exchange rate of the axial ligands L in (**148**) and (**150**) were determined by line broadening measurements showing a decrease in exchange rate for the ligand on the same side of the plane as the oxomolybdenum group.

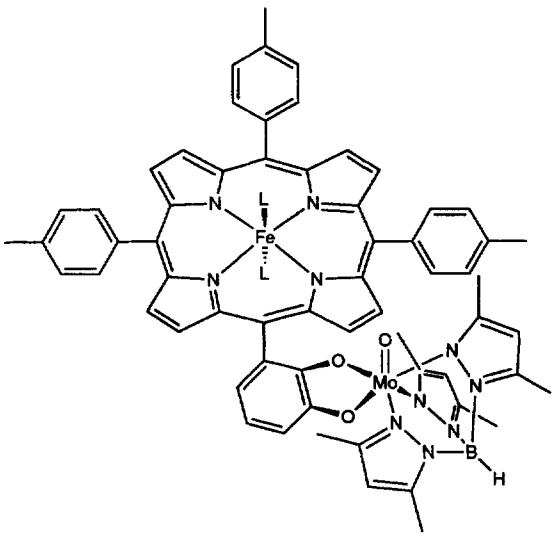

(148) L=N-MeIm
(149) L=ImH
(150) L=4-(dimethylamino)pyridine

6.3. Complexes with chlorins

The iron chlorin complex ([Fe(III)(**151**)]$^+$) has been synthesized to model compound I and II of chlorin-containing catalases [86]. The complex is protected for aromatization by the gem substitution at both pyrroline β-carbon atoms. Cyclic voltammetry shows a reversible ligand-based one-electron oxidation. The compound I analogue, [Fe(IV)=O(**151**)]$^+$, has been prepared by treatment of [Fe(III)(**151**)]$^+$ with *m*-CPBA at −80 °C and has been characterized by UV–VIS, resonance Raman, Mössbauer, and ^{1}H NMR spectroscopy. An analogue of compound II, [Fe(IV)=O(**151**)], can be generated from [Fe(IV)= O(**151**)]$^+$ by reduction of the chlorin radical in butyronitrile. The compound II analogue has also been characterized by UV–VIS, Mössbauer and resonance Raman spectroscopy.

6.4. Miscellaneous tetrapyrrole complexes

The cationic ferrous complex protoverdohaem (**152**) has been investigated electrochemically and shown to have a reduction potential estimated to −903 mV (vs Ag/Ag$^+$). The reduction gives a C-neutral radical (**153**) [87]. The radical has an isotropic EPR signal (g=1.985) at −30 °C, whereas the frozen solution EPR spectrum (−110 °C) shows anisotropic g signals (g=2.002, g=1.937). Further reduction of the radical (−950 mV) gives an iron biliverdin complex (**154**). A reaction mechanism for the decomposition of protoverdohaem to biliverdin was suggested.

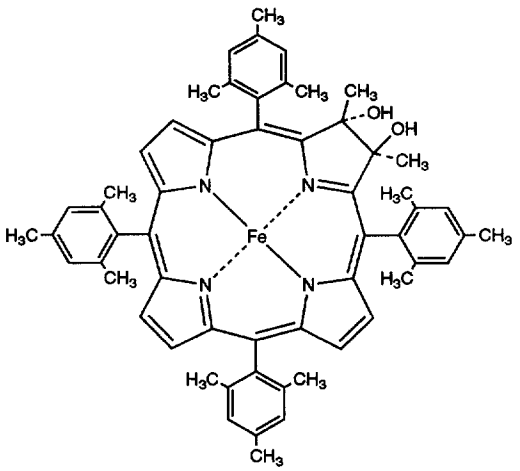

[Fe(III)(**151**)]$^+$

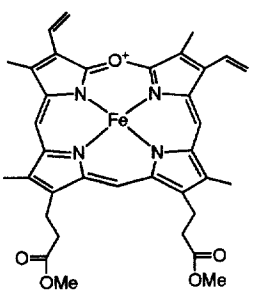

(**152**)

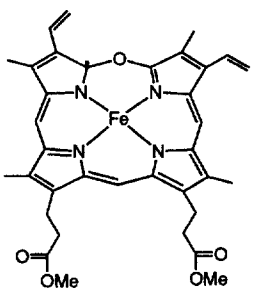

(**153**)

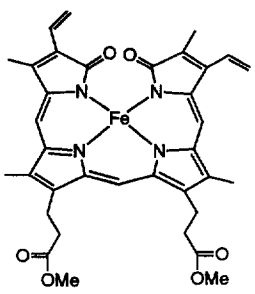

(**154**)

Reaction of the μ-oxo dimer [O{Fe(III)(**155**)}$_2$] or [(OH)$_2$Fe(III)OPTAP]$^-$ with HX (X=F, Cl, Br, I, HSO_4) leads to the five-coordinate iron(III) complexes [XFe(**155**)], in which X acts as an axial ligand [88]. These new complexes have been characterized by UV–VIS, IR, ^{1}H NMR and ^{57}Fe Mössbauer spectroscopy and also by magnetic susceptibility measurements. The magnetic data and the results from the NMR and Mössbauer experiments are consistent with an intermediate spin-state ($S=\frac{3}{2}$) in these complexes.

7. Complexes with *O*-donor ligands

7.1. Complexes with carboxylic acids and derivatives

Complexation of transition metals with pyridone carboxylic acids used as antimicrobial drugs is of interest since such complexes lower the effect of the drugs. A

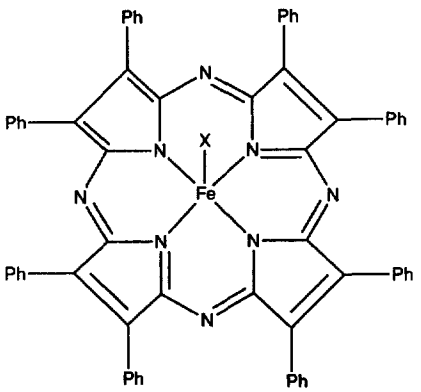

[(X)Fe(**155**)]

complex of iron(III), nitrilotriacetate (**156**) and the antimicrobial ciprofloxacin (**157**) has been studied [89]. The X-ray structure reveals that the complex [Fe(**156**)(**157**)]·$5H_2O$ (**158**) has an octahedrally coordinated ferric ion forming a six-membered ring with (**156**) through the keto and the carboxylic acid oxygen.

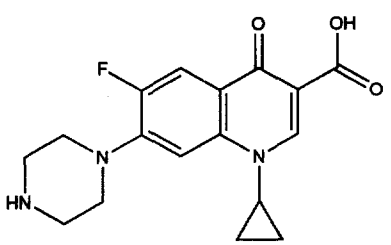

(**157**)

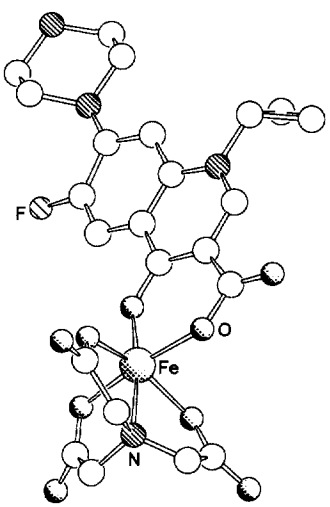

(**158**)

The crystal structure of [Fe(**159**)] (**160**) has been reported as the first hexadentate 3-hydroxypyridinone ligand complex, which is interesting as a potential drug for treatment of diseases related to iron-overload [90]. Previous binding experiments have shown that didentate analogues of (**159**) bind stronger to Fe(III). The apparent unfavourable conformational changes of (**159**) have been investigated through MM studies, which have indicated that the conformation with N1 directed towards the iron is the most stable, both in vacuo and in aqueous media.

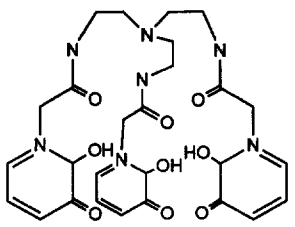

H_3-(159)

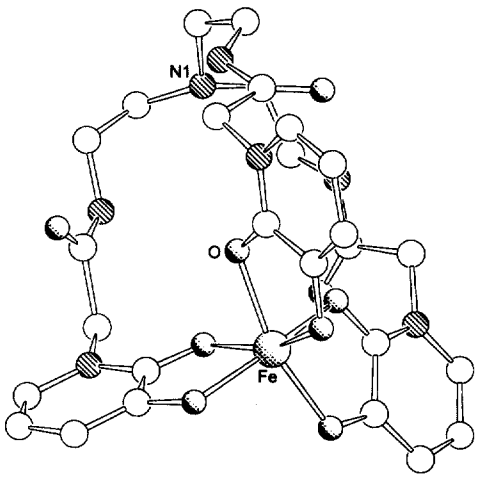

(160)

Several linear trinuclear iron complexes with the general formula $[Fe_3(O_2CR)_6L_2]$ have been synthesized and structurally characterized. Two of the complexes, $[Fe_3(OAc)_6(\mathbf{161})_2]\cdot 2MeOH$ (**165**) and $[Fe_3(OAc)_6(\mathbf{162})_2]$ (**166**) contain iron atoms linked by two didentate and one monodentate bridging carboxylate ligands [91]. The terminal iron atoms in (**165**) and (**166**) also have a didentate nitrogen ligand coordinated ((**161**) and (**162**) respectively). The two complexes $[Fe_3(O_2CPh)_6(\mathbf{163})_2]$ (**167**) and $[Fe_3(O_2CPh)_6(\mathbf{164})_2]$ (**168**) have similar coordination spheres but also a coordination from the second oxygen atoms of the monodentately bridging carboxylates to the terminal iron atoms. Magnetic measurements on (**165–168**) reveal that there is ferromagnetic exchange coupling with resultant high-spin $S=6$ ground states in (**165**) and (**166**), whereas (**167**) and (**168**) show antiferromagnetic coupling with $S=2$ ground states.

Four carboxylate-bridged diiron(II) complexes having the dicarboxylate (**169**) as a ligand have been reported [92]. The complexes are $[Fe_2(\mu\text{-OBz})(\mathbf{169})(ImH)_2(OBz)(MeOH)]$ (**170**), $[Fe_2(\mu\text{-F})(\mathbf{169})(N\text{-MeIm})_2(MeOH)_3](BF_4)$ (**171**), $[Fe_2(\mu\text{-}O_3SCF_3)(\mathbf{169})(N\text{-MeIm})_3(MeOH)(H_2O)](CF_3SO_3)$ (**172**), and $[Fe_2(\mu\text{-Cl})(\mathbf{169})(N\text{-MeIm})_2(MeOH)_3](BF_4)$ (**173**). The crystal structure of (**170**) shows that it consists of four- and six-coordinate iron(II) atoms bridged by the two carboxylate groups of (**169**) and a benzoate ion. An imidazole is coordinated for one of the iron atoms and the other iron atom is coordinated to an imidazole nitrogen, a monodentate benzoate ion and a hydroxyl oxygen atom of a methanol. This gives the complex the same ligand composition (four carboxylates, two imidazoles, and a solvent molecule) as the active site of the reduced soluble methane monoxygense hydroxylase. With fluoride, triflate, or chloride ions present, complexes (**171**)–(**173**) were formed. All three complexes have an unsymmetrical arrangement of the ligands, with one five- and one six-coordinated iron atom bridged by the two carboxylate groups of (**169**) and F^-, $CF_3SO_3^-$ and Cl^- respectively.

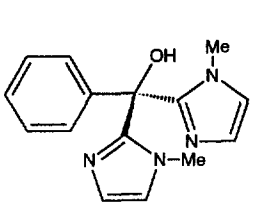

(161)

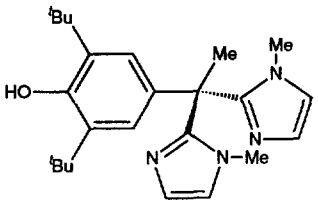

(162)

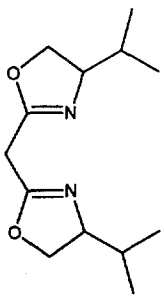

(163)

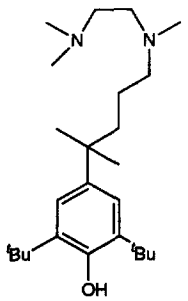

(164)

Stability constants have been determined and the bonding modes and effects caused by the side-chain NH_3^+ moiety in aminohydroxamic acids evaluated for complexes formed in aqueous solution between iron(III) with α-alaninehydroxamic acid (**174**), β-alaninehydroxamic acid (**175**), aspartic acid–β-hydroxamic acid (**176**) and glutamic acid–γ-hydroxamic acid (**177**) [93]. The metal(III)–acetohydroxamic acid (**178**) systems were studied as models. Coordination of hydroxamate oxygen atoms occurs in the case of (**174**), (**175**), and (**178**), whereas (**176**) and (**177**) are coordinated via their hydroxamate and carboxylate oxygen atoms. The OH^- ion was found to be an effective ligand in these systems, causing the formation of both binary and ternary hydroxo complexes. The presence of NH_3^+ in the hydroxamic acids favours the hydrolysis to an extent which depends on the distance between the hydroxamate moiety and NH_3^+, and can be explained by the electron-withdrawing effect of NH_3^+ and electrostatic repulsion between it and the coordinating M^{3+} ion.

Iron(III) complexes of the dihydroxamic acid ligands (**179–181**) have been prepared as models for rhodotorulic acid, a dihydroxamate siderophore secreted by some yeast [94]. For the 1:1 complexes, where $n=2$ or 4, a dimeric product, $[Fe_2L_2(H_2O)_4]^{2+}$ (**182**) (L=(**179**) or (**180**)), is obtained. For the $n=8$ ligand the complex is monomeric, $[Fe(\mathbf{181})(H_2O)_2]^+$. Equilibrium constants for hydrolysis of coordinated water for both the monomeric and the dimeric complexes have been determined spectrophotometrically. For the dimeric complexes, in which deprotonation of all four coordinated water molecules occurs, the value of $\log K_2$ is unexpectedly large, (−5.77 and −5.07 for $n=2$ and 4 respectively), larger in fact than the

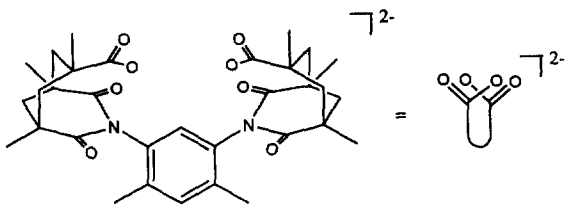

(169)

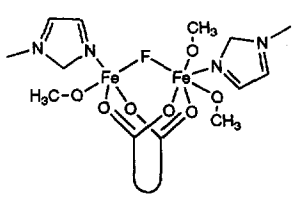

(171)

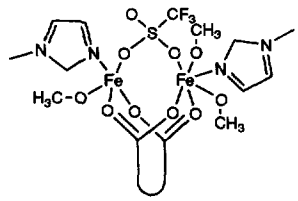

(172)

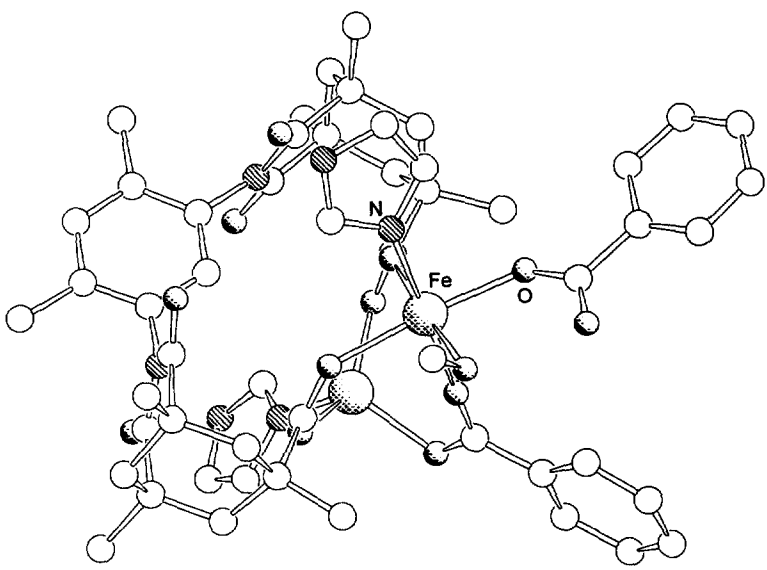

(170)

value measured for $\log K_1$ (-6.37 and -5.54 for $n=2$ and 4 respectively). This observation is inconsistent with the formation of simple ternary hydroxo complexes and implies that intermolecular μ-oxo species may be formed.

The complex Fe(**183**)$_3$ is afforded when H–(**183**) and NaOH are added to $Fe(NO_3)_3 \cdot 9H_2O$ in ethanol [95]. The presence of the $Fe(III)O_6$ chromophore has been verified by elemental analysis, UV–VIS spectroscopy and a magnetic moment

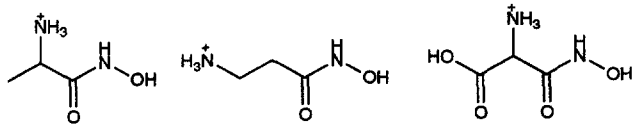

(174) (175) (176)

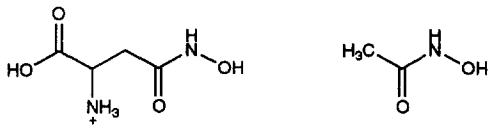

(177) (178)

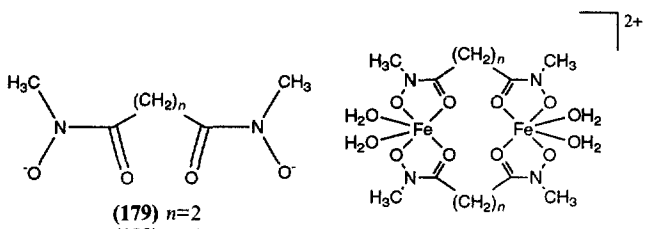

(179) n=2
(180) n=4
(181) n=8

(182)

of 5.58 μ_B. It is proposed that Fe(**183**)$_3$ is monomeric with an octahedrally coordinated iron. Cyclic voltammetry studies on Fe(**183**)$_3$ determine that $E_a^c = +80$ mV and that $E_c^c = -960$ mV (vs Ag/AgCl). Thus this is characterized as an irreversible electrode process, and since the cathodic peak area is larger than the anodic peak area, it has been suggested that the reduction product evolves into a species which is no longer electroactive.

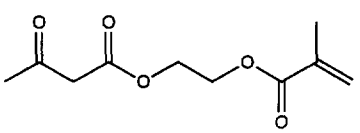

(183)

The crystal structures and physical properties of three charge transfer salts of (**184**), (**184**)$_4$A[Fe(C_2O_4)$_3$]C_6H_5CN (A = H_2O, K, NH_4) have been reported [96]. The structures consist of layers of approximately hexagonal geometry with alternating A and $Fe(C_2O_4)_3^{3-}$ and successive layers of (**184**). When A = K or NH_4, the salts are semiconductors ($\sigma \approx 10^{-4}$ S cm^{-1}, $E_A = 0.14$ eV). The magnetic susceptibilities and EPR spectra of these salts are dominated by contributions from Fe(III). When A = H_2O, the salt is a superconductor ($T_c = 7.0(3)$ K). The EPR spectrum of this salt has two resonances: one coming from the conducting electrons on the organic cations and one coming from the 3d electrons of Fe(III).

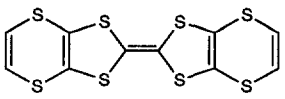

(184)

7.2. Complexes with other O-donor ligands

The iron–catecholate complexes [Fe(bpy)(3,6-dbsq)(3,6-dbcat)] (**185**), [Fe(tmeda)(3,6-dbsq)(3,6-dbcat)] (**186**) and [Fe(tmeda)(3,5-dbsq)(3,5-dbcat)] have been synthesized and their molecular structures have been determined by X-ray crystallography [97]. Unlike analogous cobalt complexes, these Fe(II) species do not exhibit redox isomerism. Magnetic measurements on (**185**) show that the magnetic moment drops to 0.81 μ_B at 5 K. This observation is consistent with the formation of an [Fe(II)(3,6-dbsq)$_2$] species that is either high-spin with a strongly antiferromagnetic metal–ligand coupling or diamagnetic low-spin, but Mössbauer measurements do not show evidence for the existence of ferrous species. It is more likely that the low magnetic moment is due to intermolecular exchange through the stacked bpy ligands. All complexes exhibit solvatochromism.

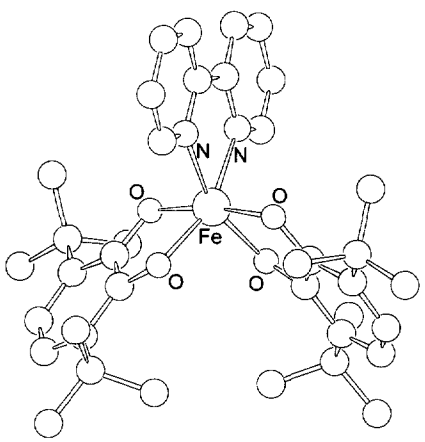

(185)

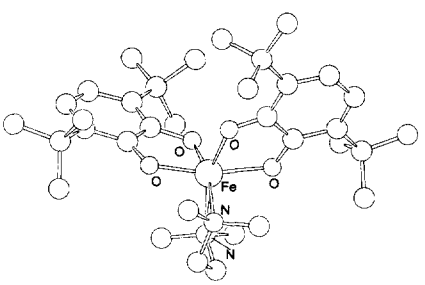

(186)

The polymer-supported ligands (**187**), (**188**) and (**189**) have been used to extract Fe(III) ions selectively from aqueous solutions at low pH [98]. The complexes formed are proposed to correspond to structures (**190**), (**191**) and (**192**). The order of the rate of removal of Fe(III) from a pH 2.1 solution is (**188**)>(**187**)>(**189**).

Second-sphere coordination of ferrioxamine B $[Fe(HL)]^+$ (**193**) by dicyclohexano-18-crown-6 (**194**) occurs through host–guest complex formation with the protonated amine side chain $(CH_2)_5NH_3^+$ [99]. The influence of steric factors on the association constants K_a for both nitrate and perchlorate salts of ferrioxamine B with *cis–syn–cis* and *cis–anti–cis* isomers of (**193**) in $CHCl_3$ has been investigated.

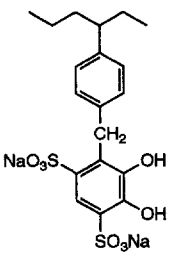

(187)

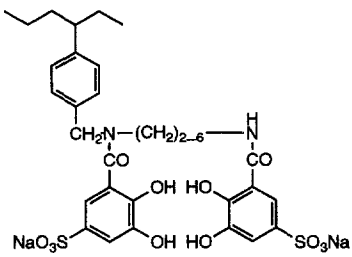

(188)

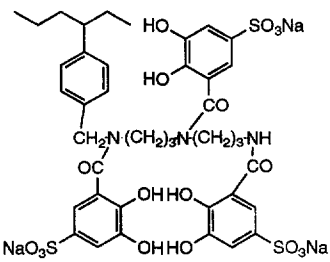

(189)

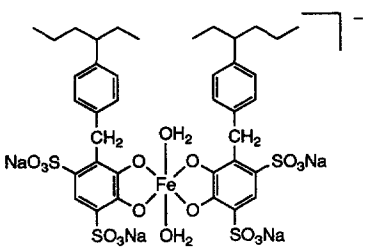

(190)

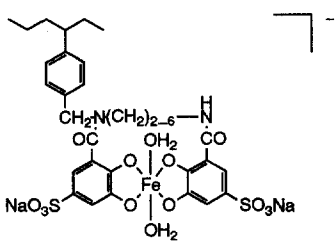

(191)

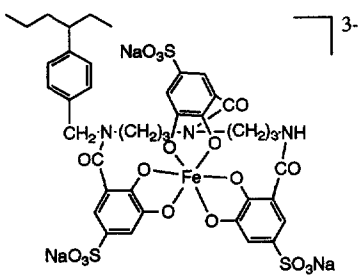

(192)

The absolute values of K_a for (**193**)X association with (**194**) are strongly dependent on the identity of the anion (X). The selectivity ratio expressed for the *syn* crown ether is 3:1 and is independent of anion variations. Discrimination between the *syn* and *anti* isomers of (**193**) in $CHCl_3$ is greater than expected based on comparison with the parent NH_4^+ ion. This is likely due to the significant steric requirements of the bulky metal complex molecule (**193**) giving a selectivity for the less hindered *syn* isomer.

For the process $Fe^{3+} + H(\mathbf{195}) \leftrightarrow Fe(\mathbf{195})^{2+} + H^+$ the reaction volume ΔV°_{FeL} has been determined to be $+7.8 \pm 0.1$ cm^3 mol^{-1} by spectrophotometry in aqueous acid media under pressures up to 250 MPa [100]. From this value and the reported

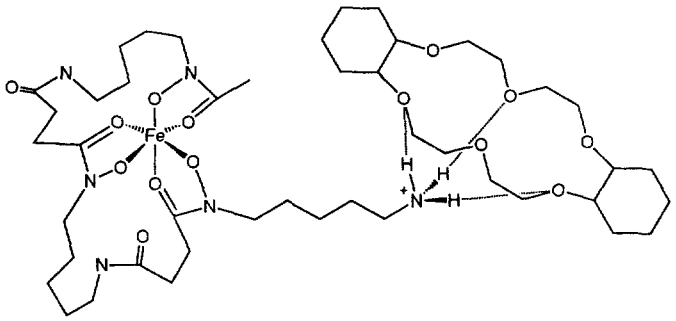

[(193)(194)]

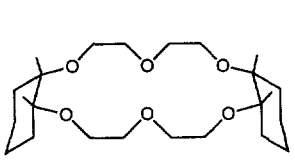

cis-syn-cis **(194)**

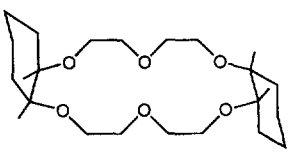

cis-anti-cis **(194)**

activation volume for formation of Fe(**195**)$^{2+}$, the activation volume for dissociation of Fe(**195**)$^{2+}$ has been calculated to be -16.5 ± 0.9 cm^3 mol^{-1}. This negative value for the dissociation reaction confirms associative activation for reaction of Fe^{3+} ions.

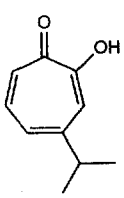

H-(**195**)

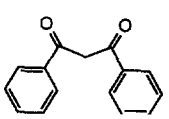

(**196**)

The trinuclear complex K[$Fe_3(OMe)_7$(**196**)$_3$]·4MeOH (**197**) has been synthesized and its crystal structure has been determined [101]. Variable-temperature magnetic susceptibility measurements indicate that the high-spin iron(III) ions are antiferromagnetically coupled. The exchange integrals may be estimated by assuming a C_{2v} point-group symmetry for the complex.

A complex with a [12]metallacrown-6 structure has been reported [102]. The complex is [$NaFe_6(OCH_3)_{12}$(**196**)$_6$]Cl·12MeOH·$CHCl_3$ (**198**). The crystal structure shows that (**198**) has a flat structure with an [$Fe_6(OH)_{12}$]$^{6+}$ ring-like core that hosts a sodium ion, and a peripheral hydrophobic shell. The distance of two opposing iron atoms in the ring is 6.39(2) Å. Each iron atom has a distorted octahedral coordination having a didentate (**196**) ligand and four methoxo bridges forming two Fe_2O_2 rhombi with adjacent iron atoms. Adjacent Fe_2O_2 planes are twisted

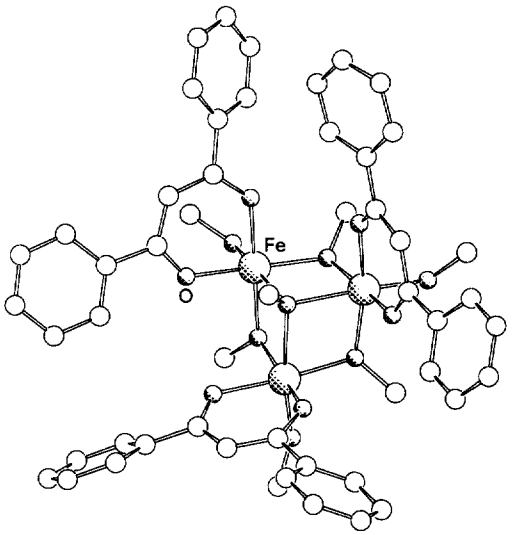

(197)

with respect to each other. The complex is EPR silent at low temperatures, suggesting an $S=0$ ground state.

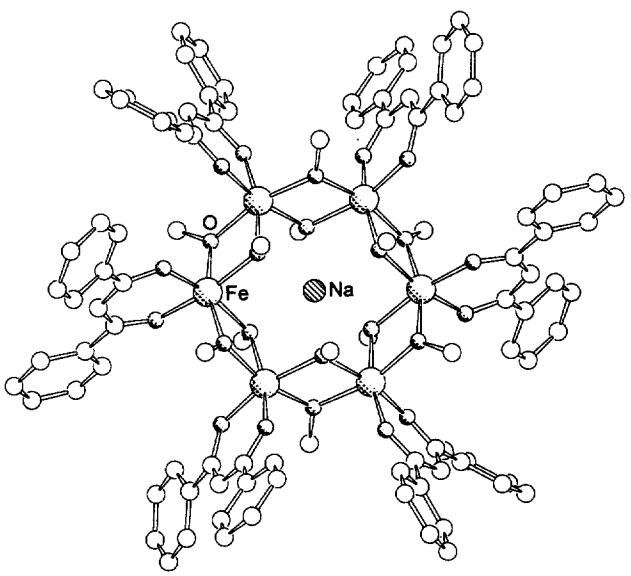

(198)

The crystal structure of $[Fe(DMSO)_6](NO_3)_3$ (**199**) has been determined [103]. The iron(III) atom has approximately octahedral coordination and is on a site of

$\bar{3}$ symmetry. The Fe–O bond length is 2.020 Å, which is comparable with Fe–O distances in $[Fe(DMSO)_xCl_{6-x}]^{3-x}$ ($_x$=1,2) and, as expected, shorter than in $[Fe(DMSO)_6]^{2+}$.

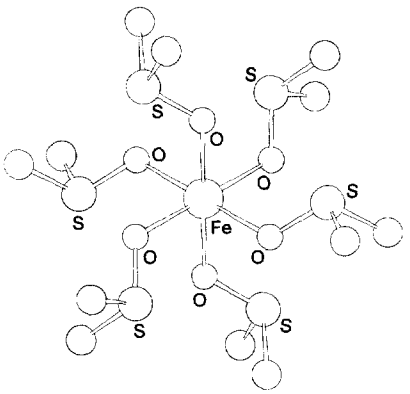

(199)

The iron(II) complex $[Fe(CH_3CN)_2(OPPh_3)_4](I_3)_2$ (**200**) has been synthesized by several methods starting from FeI_2, $Fe_2(SO_4)_3$, $FeSO_4$, and Fe (powder) [104]. The single-crystal X-ray structure showed that (**200**) has an octahedral coordination around the iron atom with the two N atoms cis coordinated and a pseudo-twofold rotation axis bisecting the N–Fe–N angle. Magnetic susceptibility measurements indicate that (**200**) is a high-spin complex with a quartet ground state and a weak antiferromagnetic coupling. Complex (**200**) catalyses the oxidation of PPh_3 into $OPPh_3$ in the presence of O_2.

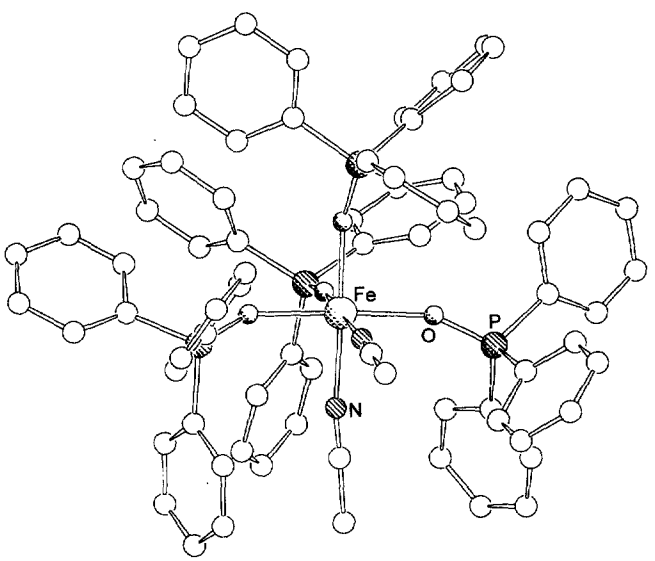

(200)

The crystal structure of $[Fe(NCS)_3(OPPh_3)_3]$ (**201**) has been determined [105]. There are two crystallographically unique molecules of (**201**) in the structure. The iron atom is similarly coordinated in the two molecules; three NCS^- and three $OPPh_3$ ligands at facial sites, but with opposite chirality. This is possibly due to crystal packing. Deviation from the octahedral symmetry includes twisting of O_3 and N_3 faces by 55° in the same direction in both types of molecule.

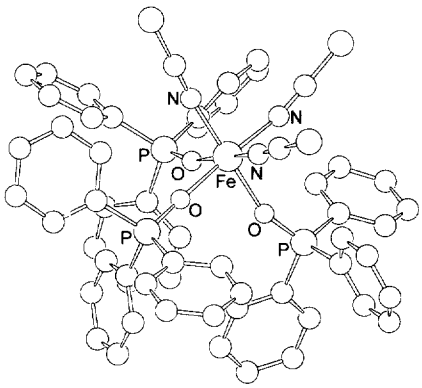

(201)

8. Complexes with *S*-donor ligands

The high-spin ferrous complexes $[FeI_2(\mathbf{202})]$ and $[FeBr_2(\mathbf{202})]$ may be described as either octahedral or square-planar coordinate complexes [106]. Mössbauer measurements and molecular orbital calculations indicate that the octahedral description is correct. Furthermore, the MO calculations indicate that the large iron–sulfur bond distances in $[FeI_2(\mathbf{202})]$ and $[FeBr_2(\mathbf{202})]$ are due to the size of the macrocycle.

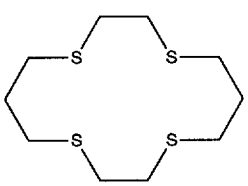

(202)

9. Complexes with *P*-donor ligands

The reaction of $[FeH_2(dmpe)_2]$ with sodium azide affords initially the mono-azide complex $FeH(N_3)(dmpe)_2$ and then in a subsequent step the bis-azide complex $[Fe(N_3)_2(dmpe)_2]$ (**203**) [107]. The crystal structure of (**203**) shows that the azide

groups are trans coordinated and linear. The N_3 ligands are tilted by approximately 132° with respect to the Fe–P_4 plane and positioned anti with respect to each other in the crystal. Complex (**203**) reacts further with terminal alkynes by replacing the N_3 ligands to form his acetylide iron complexes.

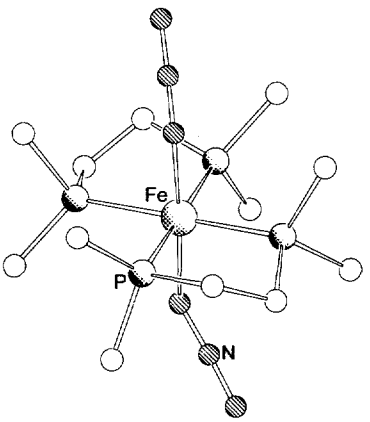

(203)

Two iron(II) complexes with the tripod P-donor ligand (**204**) have been synthesized [108]. The first, $[Fe(\mathbf{204})_2](BF_4)_2 \cdot 2H_2O$ (**205**), has been structurally characterized by X-ray crystallography and has an unusual $[Fe(P)_6]^{2+}$ core. The iron atom has a slightly distorted coordination geometry with the two ligands facially coordinated. The Fe–P bonds are between 2.277 and 2.351 Å. Reaction of (**205**) with $FeCl_2$ gave a red–violet complex isolated as a BPh_4 salt and identified with elemental analysis as $[(\mathbf{204})Fe(\mu\text{-}Cl)_3Fe(\mathbf{204})]BPh_4 \cdot H_2O$.

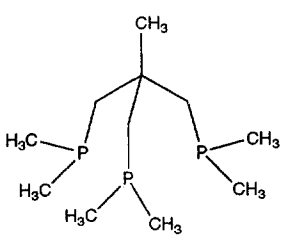

(204)

10. Complexes with mixed-donor ligands

10.1. Complexes with mixed N,O-donor sets

The reaction of [Fe(salen)Cl] with an excess of L (L=ImH, *N*-MeIm, 2- or 4-MeImH) in acetone resulted in the isolation of hetero-bisadducts, [Fe(salen)(L)Cl]

(L=ImH, *N*-MeIm or 2-MeImH) and a homo-bisadduct, [Fe(salen)L_2]Cl (L=4-MeImH) [109]. The structures of [Fe(salen)(*N*-MeIm)Cl] and [Fe(salen)(4-MeImH)$_2$]Cl were determined by single-crystal X-ray crystallography. A significant difference between the two structures is that the dihedral angle between the two phenyl rings of the salen ligand is 17.5° for [Fe(salen)(*N*-MeIm)Cl] and 4.4° for[Fe(salen)(4-MeImH)$_2$]Cl. The complexes were characterized by variable-temperature magnetic susceptibility and Mössbauer spectroscopy. The hetero-bisadducts exhibit an admixed electronic ground state, whereas the homo-bisadduct is high spin.

The complex [Fe(III)(**205**)$_2$]Cl·H_2O has been prepared [110]. Infrared spectroscopy shows that (**205**) acts as a tridentate ONO ligand where the nitrogen atom of the azomethine is ligating. Magnetic susceptibility measurements show that the iron(III) atom is in a high-spin configuration and octahedrally coordinated. The electronic spectra confirms the octahedral geometry showing a spin allowed $^5T_{2g} \rightarrow {}^5E_g$ transition.

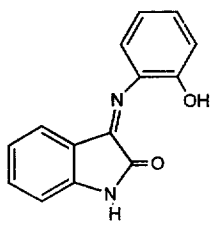

(**205**)

1,3,5-Tris(5-substituted salicylamino) cyclohexanes (H_3–(**206**), H_3–(**207**) and H_3–(**208**)) have been synthesized by Schiff-base condensation between *cis*-1,3,5-triaminocyclohexane and a substituted salicylaldehyde, followed by reduction with KBH_4 [111]. Reaction with iron(III) salts gave neutral six-coordinate Fe–N_3O_3 complexes. The distribution coefficients between octan-1-ol and water indicate that the complexes show ligand-to-metal charge-transfer (LMCT) bands in the 450–500 nm range. The structures of all three complexes have been confirmed by single-crystal X-ray crystallography.

An attempt to synthesize Fe(**209**)NO_3 by a published procedure gave instead Fe(**210**)O_2NO (**211**) as determined by X-ray crystallography [112]. In this instance, the crystals were prepared by recrystallization from dichloromethane and diethyl ether with one drop of 8 M HNO_3 added. The structural analysis reveals a complex with a distorted octahedral iron(III) centre.

Iron(III) salts have been reacted with a boiling mixture of 2,6-diaminopyridine and acetylacetone to give dimeric iron complexes [113]. Magnetic measurements suggested some antiferromagnetic exchange via the diaminopyridines, so the structure was suggested to be (**212**) (X=Cl, Br, NO_3, or NCS) with square-pyramidal coordinated iron atoms bridged by the 2,6-diaminopyridine residues.

A series of iron(III) complexes of the type [$FeLCl_2$]·H_2O (L=H(**213**) to H(**219**)) and [Fe(**220**)Cl_3]·H_2O have been prepared and fully characterized by spectral and

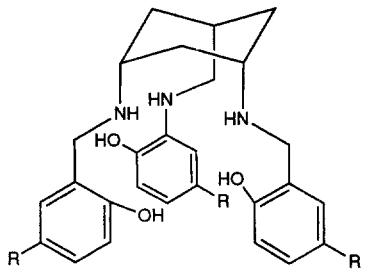

(206) R=H
(207) R=NO_2
(208) R=OMe

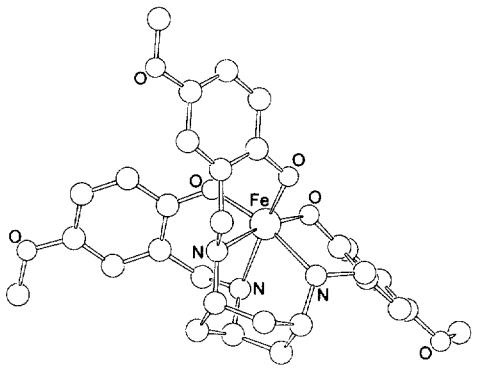

[Fe(208)]

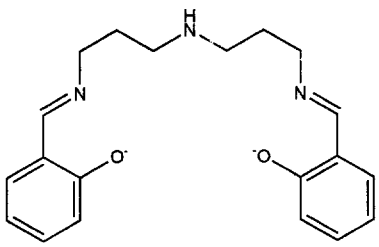

(209)

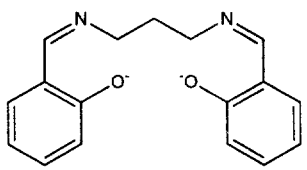

(210)

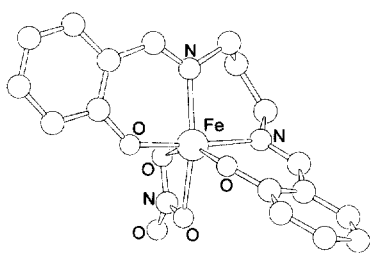

(211)

electrochemical techniques [114]. Their interactions with a variety of mono- and di-dentate heterocyclic bases, as well as phenols, have been investigated using electronic and EPR spectroscopy. The redox behaviour of the iron(III) complexes and their 1:1 adducts with 3,5-dbcat anions generated in situ has been investigated. There is a linear correlation between Fe(III)–Fe(II) redox potential and the charge-transfer band energy of the complexes. All the complexes catalyse the oxidation cleavage of 3,5-dbcatH_2 by molecular oxygen to yield *cis,cis*-muconic anhydride.

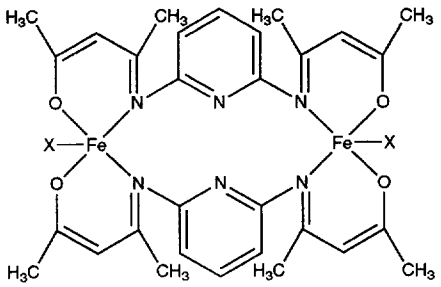

(212)

The catalytic activity has been correlated with the Fe(III)–Fe(II) as well as (3,5-dbsq°)–(3,5-dbcatH_2) redox potentials of the 3,5-dbcat adducts.

Complexes of iron(III) and 2,6-pyridinedicarboxylic acid (**221**) have been studied

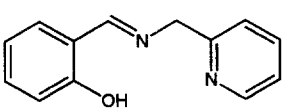

H(213)

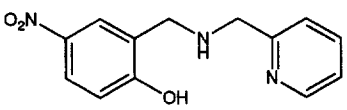

H(214)

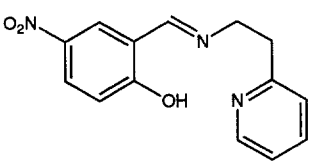

H(215)

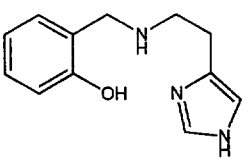

H(216)

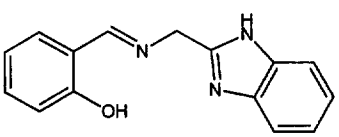

H(217)

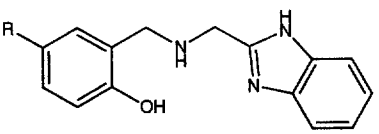

H(218): R=H
H(219): R=NO_2

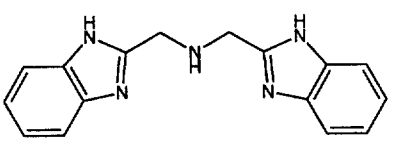

(220)

[115]. The reaction of [(**221**)Fe(II)$(OH_2)_3$] with bromine water gives [(**221**)(H_2O)Fe(III)(μ-OH)Fe(III)(OH_2)(**221**)] which on further reaction with HX gives [(**221**)(X)Fe(III)$(OH_2)_2$] (X=Br, Cl (**222**)). Reaction of (**222**) with acacH or phen affords [(**221**)(H_2O)Fe(III)(acac)] (**223**) and [(**221**)(Cl)Fe(III)(phen)] (**224**) respectively. The terdentate ligand tpy gives instead [Fe(II)$(tpy)_2$][Fe(III)$(\mathbf{221})_2]_2$ (**225**). The crystal structures of (**222–225**) have been determined.

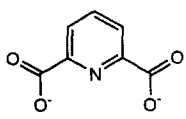

(222)

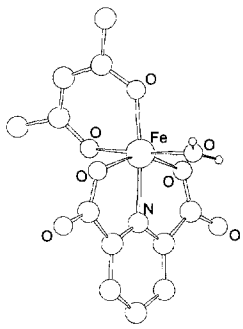

(223)

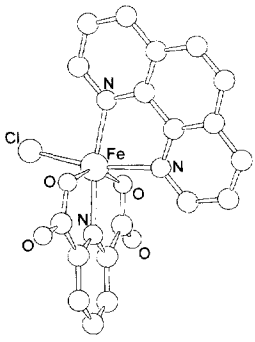

(224)

The complex [(**221**)$Fe(OH_2)_3$] (**226**) has been prepared by the reaction of H_2–**221** with Mohr's salt (ammonium Fe(II) sulfate hexahydrate) [116]. Reaction of (**226**) with NaOH or NPr_4OH leads to the formation of X_2[Fe(**221**)$_2$] (**227**) (X=Na^+ or NPr_4^+). Complex (**227**) is very solvatochromic; this effect is attributed to interaction of the lone pairs of the dipic oxygen atoms with solvent. Slow air oxidation of (**227**) leads to the corresponding ferric complex [Fe(**221**)$_2$]$^-$ (**228**). The crystal structures of (**226**), (**227**) and (**228**) have been determined. The Fe–O bond lengths in (**228**) are considerably shorter (by 0.1–0.15 Å) than the corresponding bond distances in (**227**).

Reaction of (**226**) with Mohr's salt at pH 5.65 affords a purplish–blue compound of overall formula [(**221**)$_{10}$(H–**221**)$_6Fe_{13}(OH_2)_{24}]\cdot 13H_2O$ [117]. This compound decomposes slowly to form the heptacoordinated mononuclear complex [(H–**221**)$_2$Fe(OH_2)] (**229**). Acidification of Na_2[(**221**)$_2$Fe]$\cdot 2H_2O$ yields [(**221**)$_2$(H–**221**)$_2Fe_3(OH_2)_6$], which decomposes to form the heptacoordinated dinuclear complex [(H–**221**)$_2Fe_2(OH_2)_6$] (**230**). The crystal structures of (**229**) and (**230**) have been determined. Complex (**230**) consists of dimers of heptacoordinated iron atoms which are linked via two carboxylate oxygen atoms of two dipic ligands. The dimers are, in turn, linked into a network structure via hydrogen bonding. Analysis of the thermal variation of the magnetic susceptibility of (**230**) indicates weak antiferromagnetic interactions ($J=-3.4\ cm^{-1}$, $H=-2J\cdot S1\cdot S2$).

The crystal structure of Na[Fe(**221**)$_2$]$\cdot 2H_2O$ has also been reported [118]. The complex consists of a pseudo-octahedrally coordinated Fe atom with an N_2O_4 coordination sphere. The two nitrogen donor atoms are trans to each other with an N–Fe–N angle of 168.3°. In the crystal the Na^+ ions bridge the [Fe(**221**)$_2$]$^-$ units, each Na^+

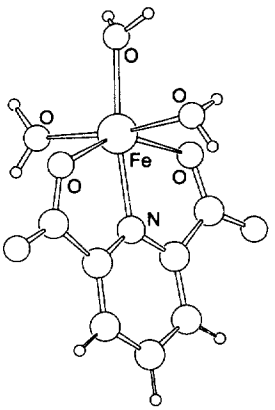

(226)

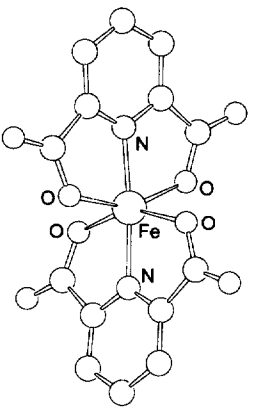

(228)

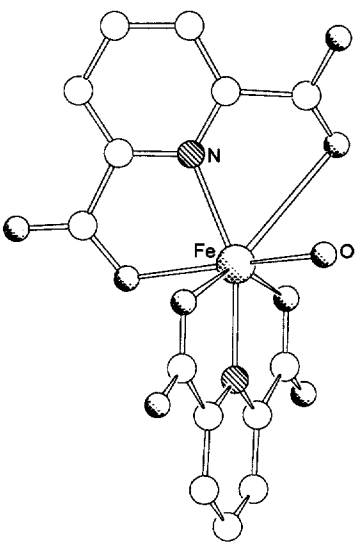

(229)

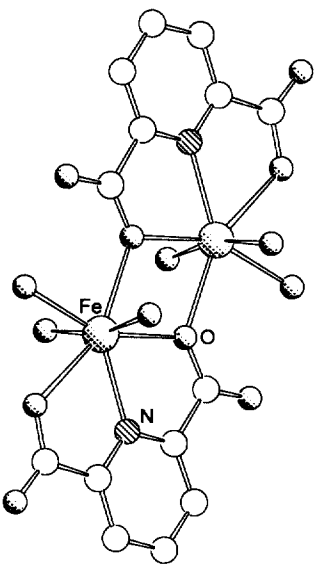

(230)

ion being coordinated by four carboxylate oxygen atoms (one of them is used in Fe chelation) and two water molecules. The complexes $[(\mathbf{221})_2(\text{H}\text{–}\mathbf{221})_2\text{Fe}_3(\text{OH}_2)_4]\cdot 2\text{H}_2\text{O}$ (**231**), $[(\mathbf{221})_2\text{Fe}_2(\text{OH}_2)_5]$ (**232**), $(\text{NH}_4)_2[(\mathbf{221})_4(\text{H}_2\text{–}\mathbf{221})_2\text{Fe}_3(\text{OH}_2)_6]\cdot 4\text{H}_2\text{O}$ (**233**) and $[(\mathbf{221})_{10}(\text{H}\text{–}\mathbf{221})_6\text{Fe}_{13}(\text{OH}_2)_{24}]\cdot 13\text{H}_2\text{O}$ (**234**) have been prepared by reacting $\text{Na}_2[\text{Fe}(\mathbf{221})_2]\cdot 2\text{H}_2\text{O}$ or Mohr's salt with (H_2–**221**) [119]. The crystal structures of (**231**–**234**) have been determined. A scheme for interconversions between species (**231**–**234**) (Scheme 4) has been proposed.

Four complexes, Fe(II)$(\mathbf{235})_2$, $[\text{Fe(II)}(\mathbf{235})\text{Cl}(\text{MeOH})_2]_2$ (**238**),

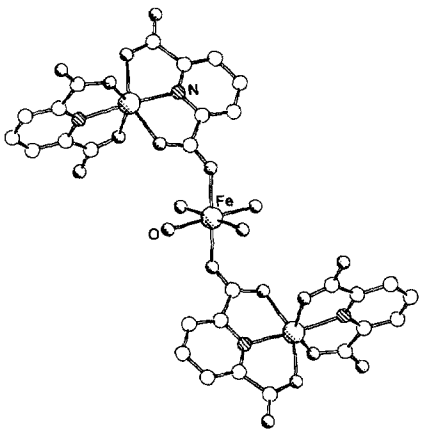

(231)

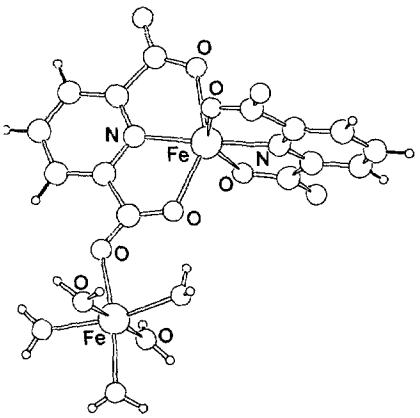

(232)

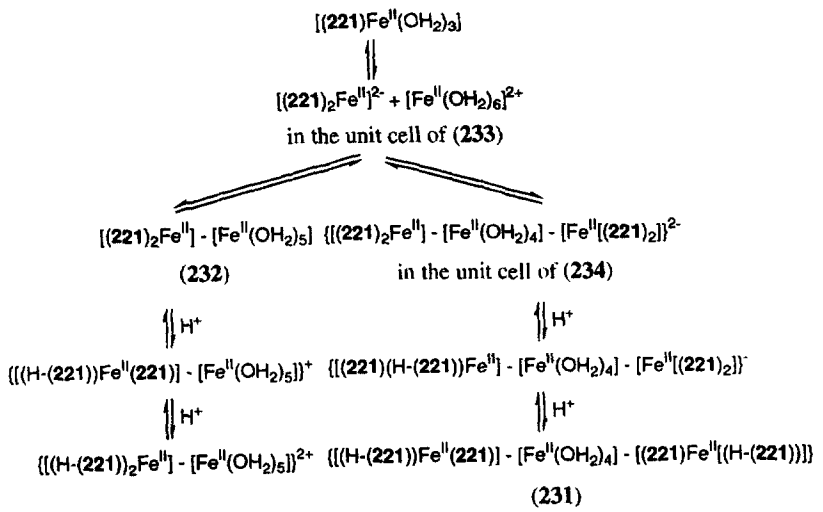

Scheme 4.

Fe(II){H_2–(**236**)}$_2$ and [Fe(III)(**237**)$_2$Cl]·2(Et_3N·HCl)·0.5CH_3CN, where H–(**235**), H_3–(**236**) and H–(**237**) are analogues of pyrroloquinolinequinone or methoxatin (PQQ), have been synthesized and spectroscopically characterized [120]. The structure of (**238**) has been determined by X-ray crystallography and revealed as a dimeric configuration linked through the carboxylate function of (**235**). The differences in spectroscopic properties of the complexes exemplify the variety of structural types and nuclearities obtained for iron complexes of PQQ analogues, synthesized under different stoichiometric conditions and pH.

An iron(III) complex of the new terdentate ligand (**239**) has been investigated thermodynamically and kinetically [121]. The complex formed, [Fe(**239**)$_2$]$^+$ (**240**),

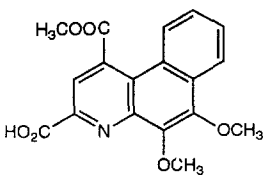

H-(**235**)

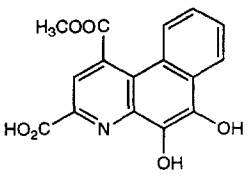

H_3-(**236**)

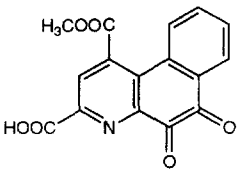

H-(**237**)

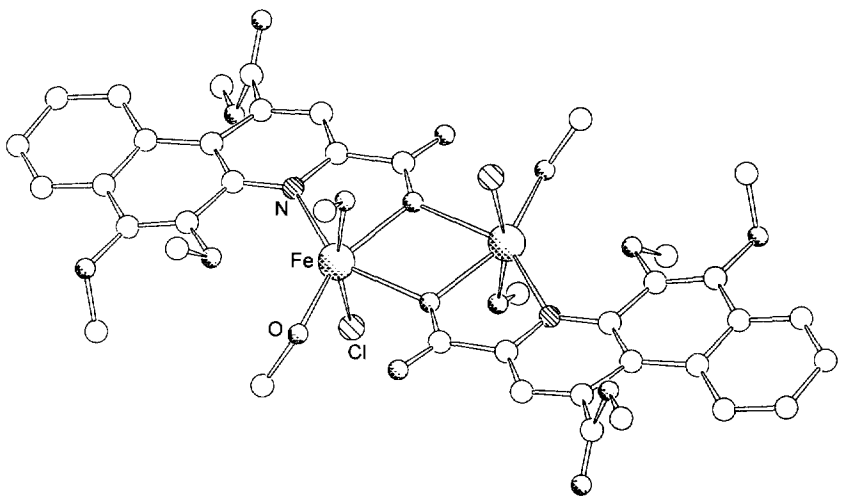

(**238**)

is very stable ($\log \beta_{12} = 45.8 \pm 0.2$ dm^6 mol^{-2}). There are several parallel pathways for the formation of (**240**) in 0.10 mol dm^{-3} $NaClO_4$, starting from Fe^{3+} or $FeOH^{2+}$ and H_2(**239**)$^+$ or H_3(**239**)$^{2+}$. The rate constants for these reactions have been determined. A mechanism has been proposed and it is suggested that the coordination of the phenolato oxygen of the pyridoxyl moiety to the iron(III) is the rate-determining step in the formation of (**240**).

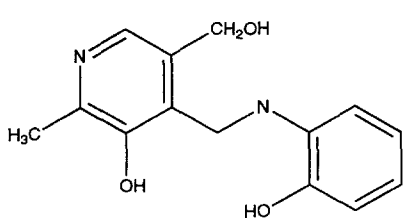

H-(**239**)

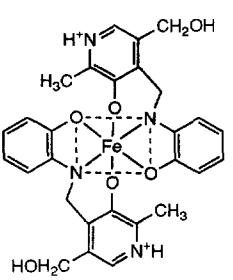

(**240**) estimated structure

The coordination of the bifunctional multidentate ligand H_4–(**241**) to iron(III) appears to proceed via a kinetic linkage isomerism in aqueous solution [122]. Initially the ligand binds through two parallel pathways with the didentate quinolinoato(N–O) moiety to form $Fe\{H_2(\mathbf{241}\text{-}N,O)\}^+$. This intermediate transforms to $Fe\{H_2\text{–}(\mathbf{241}\text{-}O,N,O)\}^+$, where the terdentate dihydroxyazo moiety coordinates with a rate constant of $k_{isom} = (1.3 \pm 0.1) \times 10^{-1}\ s^{-1}$. The stability constant for the final complex is $\log(\beta_{11}) = 18.32 \pm 0.11\ dm^3\ mol^{-1}$.

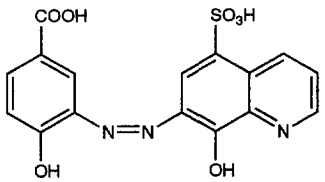

H_4-(**241**)

The formation of a complex between iron(II) and (**242**) in aqueous solution has been studied to determine the reaction mechanism [123]. The first step involves coordination of one of the carboxylate oxygen atoms to Fe(II). The next step is the rate-determining coordination of the phenolate oxygen, which is followed by the rapid binding of the last oxygen and the nitrogen atom. The resulting complex, $[Fe(\mathbf{242})(H_2O)_2]^-$, has a formation constant of $\log \beta_{11} = 14.42 \pm 0.20\ mol\ dm^{-3}$.

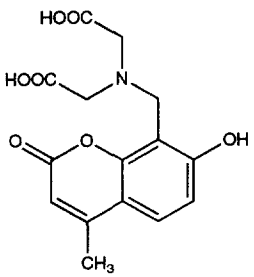

(**242**)

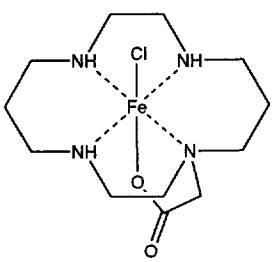

(**243**)

Complex (**243**) has been characterized by microanalysis and IR, UV–VIS and ESR spectroscopies [124]. It undergoes a reversible one-electron reduction ($E_{1/2} = -0.19 \pm 0.01$ V) to an Fe(II) complex which reacts rapidly with dioxygen. Under aerobic conditions, the electrochemical response of (**243**) indicates the production of an Fe(III)–(μ-peroxo) dimer. Further kinetic analysis by stopped-flow spectrophotometry demonstrates that the complex accelerates dismutation of the superoxide radical in aqueous solution. ESR studies on DMSO solutions of potassium superoxide demonstrate that the radical is rapidly removed by (**243**). A new low spin form of the iron(III) complex, characterized by a lower g anisotropy, is formed during the course of the reaction.

The interactions between iron(III) and two ligands with either two or three acid–base centres have been studied [125]. With ligand (**244**) iron(III) forms either

$[Fe(\mathbf{244})_2]NMe_4$ (**246**), $[Fe\{H(\mathbf{244})\}_2]ClO_4$ or $[Fe(\mathbf{244})_2][Fe\{H(\mathbf{244})\}_2]$, depending on the conditions. Complex (**246**) has been structurally characterized and shows that the iron atom is pseudo-octahedrally coordinated by four oxygen atoms and two nitrogen atoms. Iron(III) forms similar complexes with ligand (**245**), $[Fe(\mathbf{245})_2]NMe_4$ (**247**) was identified with ESI-MS. Cyclic voltammetry measurements of (**246**) and (**247**) show a single quasi-reversible one-electron step for both complexes with a ΔE of 0.300 V. This difference might be explained by some participation of the phenolic function of (**247**) in the complexation process. Under different conditions $[Fe(\mathbf{245})_2][Fe\{H(\mathbf{245})\}_2]$ was formed.

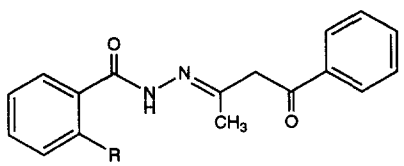

(**244**) R=H
(**245**) R=OH

Reaction of $Fe(NO_3)_3 \cdot 9H_2O$ with ligand (**248**) results in the formation of $[Fe(\mathbf{248})_2](NO_3)_3 \cdot 3H_2O$ (**249**) and $[Fe\{H_{-1}\text{–}(\mathbf{248})\}(\mathbf{248})](NO_3)_2 \cdot 2H_2O$ (**250**) [126]. The related complex $[Fe\{H_{-3}\text{–}(\mathbf{251})_2\}] \cdot 12H_2O$ (**252**) has also been prepared. The crystal structures of (**248**), (**249**) and (**252**) have been determined. In complexes (**249**) and (**250**) the iron atom is coordinated by three amines of one ligand and three alkoxo moieties of the second ligand. They differ only in the degree of coordination of one of the non-coordination amino moieties. In ligand (**251**), coordination via the three amine groups is sterically unfavourable and electron-withdrawing groups on the amine nitrogen atoms deactivate the amine moieties. Therefore, the ligand coordinates to iron through alkoxo (alcohol) groups (the ligand is partially deprotonated).

The metal binding properties of (**253**) have been investigated [127]. The ligand forms a complex of the form $[Fe(\mathbf{253})]^{3+}$ (**254**) with iron(III) and the single crystal X-ray structure of $(\mathbf{254})Cl^3 \cdot 15H_2O$ has been determined. The iron is approximately octahedrally coordinated by the six alkoxo groups. The intraligand O–M–O angles are all $<90°$ and the interligand O–M–O angles are $>90°$. Twelve water molecules are coordinated to (**254**) in a hydrophilic pocket formed by the six coordinated oxygen atoms and the six N–H protons. In solution, NMR spectroscopy shows that the complex has a D_{3d} symmetry.

Studies of the promotion of hydrolysis of 4-nitrophenyl phosphate (NPP) by an iron(III) complex have been performed [128]. A 1:1 mixture of Fe^{3+} and (**255**) was used and the active complex at a low ratio $R_0 = [Fe(III)]_0:[NPP]_0$ was suggested to be (**256**). A marked change in the slope of the initial rate of NPP hydrolysis as a function of R_0 at $R_0 = 2$ suggests a third iron to be coordinated to the complex (**257**) activating the hydrolysis by providing a coordinated hydroxide positioned to attack the phosphorus (Scheme 5). At pH > 6 the rate of hydrolysis lowers, probably due to the formation of dihydroxo and dimeric complexes of Fe(**255**).

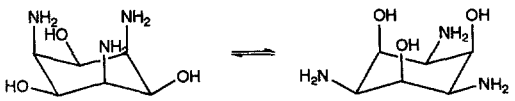

(248)

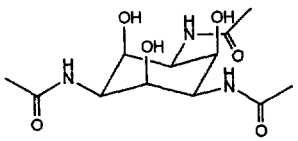

(251)

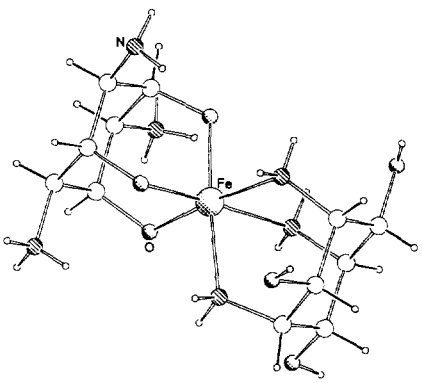

(250)

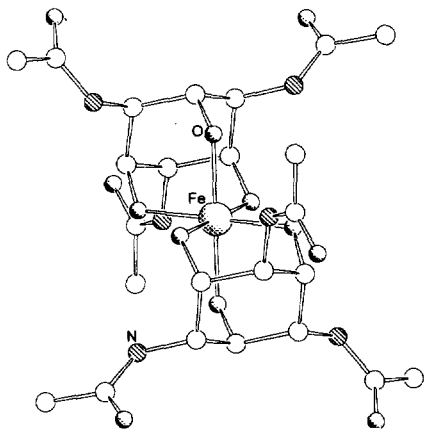

(252)

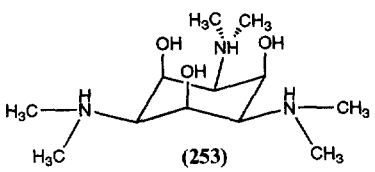

(253)

The synthesis of a new water-soluble iron chelator for both Fe(III) and Fe(II) has been reported [129]. The tripodal ligand (**258**) has been prepared from 8-hydroxyquinoline and tris(2-aminoethyl)amine and characterized by mass spectral data and ^{1}H NMR and ^{13}C NMR spectroscopy. The UV–VIS spectra of Fe(III)–(**258**) and Fe(II)–(**258**) was measured. Cyclic voltammetry measurements on the ferric complex showed a quasi-reversible reduction at +0.087 V (vs NHE). The stability constants β_{110} were determined for the two complexes and showed that

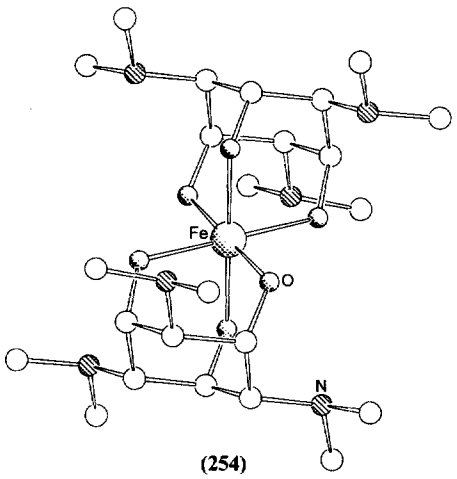

(254)

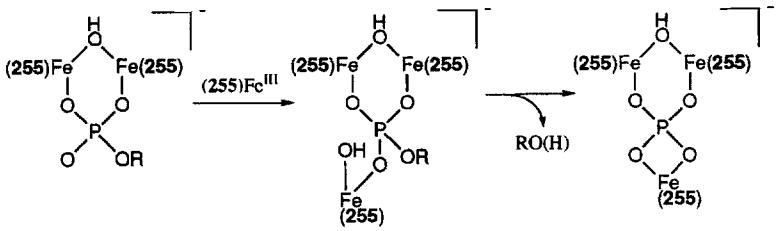

(256) (257)

Scheme 5.

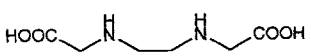

(255)

both were stable but that the iron(III) complex was more stabilized than the iron(II) complex ($\log(\beta_{110}) = 30.9$ and 19.3 respectively). The Fe(III) complex is not photoreducible and does not induce radical damage in the presence of hydrogen peroxide, which suggests that it may have interesting biological properties.

The crystal structure of an iron(III) complex with two *N,N,O*-donor ligands has been reported [130]. The complex [Fe(**259**)$_2$][PF_6] (**260**) has a distorted octahedral structure around the iron atom with sections of the aromatic ligands forming an interleaved stack in the solid state. The magnetic susceptibility (83–299 K) of (**260**) and its EPR spectrum in a frozen glass at 77 K is consistent with a high-spin state. Cyclic voltammetry measurements of (**260**) showed one reversible Fe(II)/Fe(III) couple at −0.67 V (vs Fc/Fc^+) and a reversible ligand-based reduction at −2.12 V.

In a study of the influence of geometric factors on the preference of redox

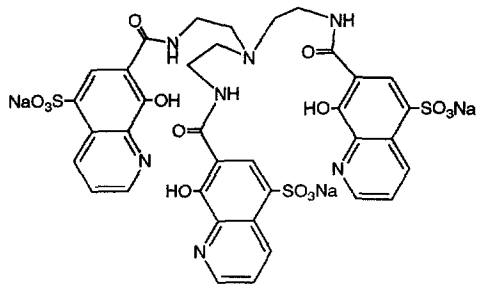

(258)

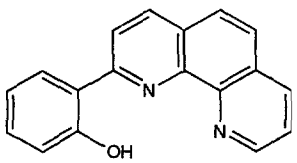

H-(259)

state for a metal, two iron(III) complexes with cryptand ligands have been reported [131]. The compounds, [Fe(III)(**261**)][ClO_4]$_3$ · 0.5MeCN (**263**) and [Fe(III)(**262**)][ClO_4]$_3$ (**264**) could be obtained both from iron(II) and iron(III) salts. Magnetic and spectroscopic measurements show that both complexes have a distorted octahedral geometry, enough to give a spin-quartet ground state in (**263**) and a more complex low-spin magnetic behaviour in (**264**). Compound (**263**) has also been characterized by X-ray crystallography, which confirms the distortion of octahedral coordination geometry towards a trigonal prism with the twist angle $\varphi = 40.3°$.

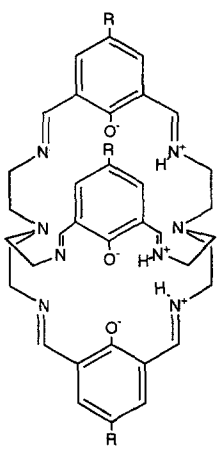

(**261**) R=Me
(**262**) R='Bu

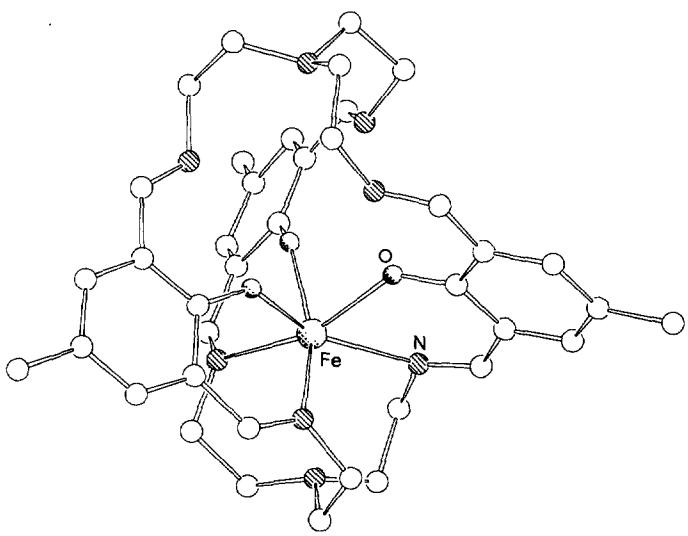

(**263**)

The ligand H_3–(**265**) forms a very stable complex with iron(III) at pH 7–10 [132]. The crystal structure of the complex Fe(**265**) · C_6H_6 · $2H_2O$ has been determined and reveals a ferric ion in a slightly disordered octahedral environment with the three

tertiary amines and the three hydroxypyridine oxygen atoms forming six-membered chelate rings to give an N_3O_3 donor set. The twist angle (O–Fe–N) is 54°, close to the octahedral angle (60°). The octahedral arrangement, together with the low pK values for H_3–(**265**), is thought to give the high stability of Fe(**265**).

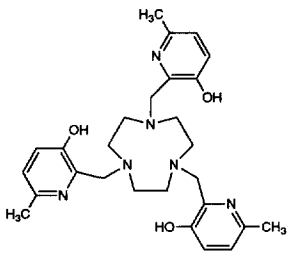

H_3-(**265**)

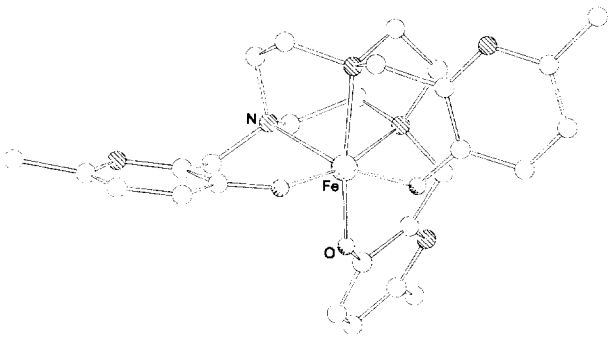

[Fe(**265**)]

The new iron(III)-specific ligand H_3–(**266**), containing three hydroxamic acid groups as pendant arms on a macrocyclic triamine backbone, has been synthesized. Its chelating properties with iron(III) have been studied by potentiometric and spectroscopic techniques [133]. The mechanism of electron transfer, the kinetics of dissociation and the stability constants of the reduced species, which are thought to be important in the biological activity of this siderophore analogue, have been studied by voltammetric methods ($E_{1/2} = -530$ mV for [Fe(H–(**266**))]$^+$, $E_p^c = -630$ mV). This ligand complex has proved to be biologically active, and its properties were compared with ferrichrome and ferrioxamine B.

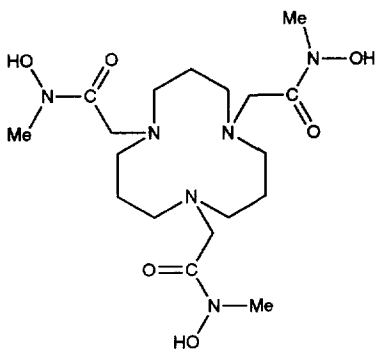

H_3-(**266**)

The design and synthesis of chelating agents which are effective in coordination and removal of Fe^{3+} is of considerable interest in treating cases of iron overload [134]. Stoichiometric 1:1 complexes of Fe^{3+} with (**267**) have been prepared. Potentiometric measurements were made of pH and of ligand–ligand competition. Stability constants were found to be lower than for the analogous complexes with

(**268**), which may be attributed to the fact that the metal is more strongly coordinated by the two phenolate groups of (**268**) than by the single phenolate group of (**267**).

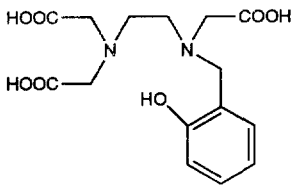

(267)

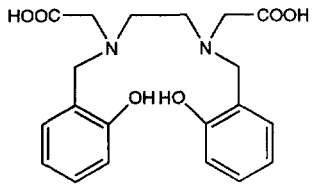

(268)

A diiron complex with a bridging ligand that mimics the unsymmetrical histidine coordination in the active site of semimet haemrythrin has been reported [135]. The ligand (**269**) gives, together with $Fe(NO_3)_3$ and Na_2(**270**), the complex [Fe(II)Fe(III)(**269**)(H_2O)(**270**)]$(BPh_4)_2 \cdot 2H_2O$ (**271**). X-ray structure determination and Mössbauer spectra (30–300 K range) of (**271**) show that the valences of the Fe atoms are localized in the solid state. The iron atoms in (**271**) are bridged by the phenolate O-atom of (**269**) and the two carboxylate groups of (**270**). The coordination of the iron(III) atom is completed by two pyridine N atoms and an amine from (**269**) giving an N_3O_3 coordination, whereas the iron(II) atom has an N_2O_4 coordination sphere with one pyridine N atom, one amine N atom and one water molecule. The Fe–O–Fe unit is highly unsymmetric, with the Fe(III)–O distance being 0.16 Å shorter than the Fe(II)–O distance; the Fe...Fe distance is 3.409 Å. A variable-temperature ^1H NMR experiment shows that the localization of valences is kept in solution. Preliminary studies also show that the terminal aqua ligand can be replaced easily.

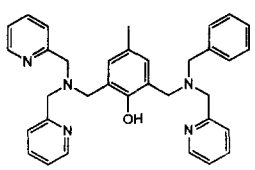

(269)

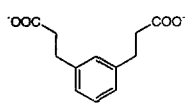

(270)

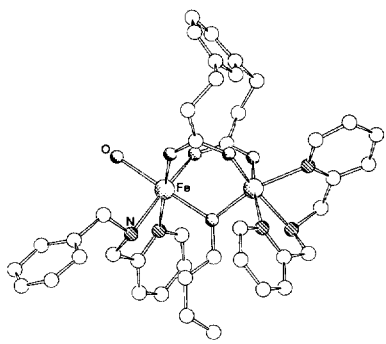

(271)

Dinuclear iron(II,III) complexes [Fe_2(**272**)(O_2CMe)][O_2CMe]X_2 with a nonadentate ligand H(**272**) ($X = PF_6^-$ (**273**) or BF_4^-) have been prepared [136]. Their Mössbauer spectra consist of two quadrupole doublets due to high-spin iron(II) and low-spin iron(III) and magnetic susceptibilities corroborate this formulation of the electronic structure. Cyclic voltammograms showed a quasi-reversible redox

couple with $E_1 = -0.07$ V and an irreversible redox couple with $E_2 = 0.58$ V (vs SCE) for (**273**), corresponding to a comproportionation constant of 1.0×10^{12}. No visible or near-IR bands due to intervalence electron transitions between iron(II) and iron(III) were observed.

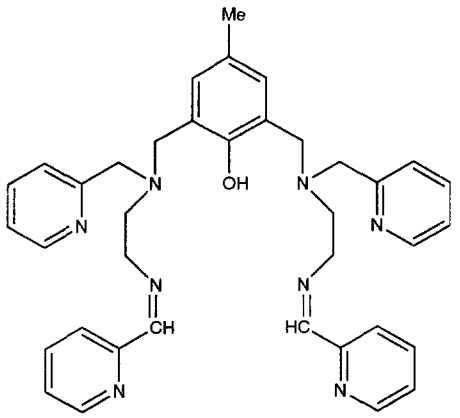

H-(**272**)

The complexes $[Fe_2(\mathbf{273})(O_2CR)(H_2O)_2]$ (R = C_6H_4OH (**274**), $CH_2CH{=}CH_2$ (**275**), $C_6H_4NH_2$ (**276**), CH_2CH_2Br (**277**), CH=CHMe (**278**)) have been synthesized and the crystal structures of (**274**) and (**275**) have been determined [137]. EXAFS, XANES, and IR measurements indicate that the structures of (**276**)–(**278**) are very similar to those of (**274**) and (**275**). Variable-temperature magnetic susceptibility measurements have been performed on complexes (**274**)–(**278**). In all cases, the magnetic behaviour is consistent with antiferromagnetic coupling between Fe(III) ions. The coupling constants derived for (**274**)–(**278**) are very similar ($J = -14$–$16\ cm^{-1}$) and a small but significant decrease in the J value with shorter Fe–(μ-O) distance may be noted.

Reaction of ligand (**279**) with $Fe(ClO_4)_2 \cdot 6H_2O$ under inert atmosphere leads to a red–purple product that is postulated to be a dinuclear mixed-valent Fe(II)/Fe(III) species [138]. Exposure of this product to air affords the dinuclear Fe(III) complex $[Fe_2(\mathbf{279})(\mu\text{-}OAc)_2](ClO_4) \cdot H_2O$ (**280**) whose crystal structure has been determined. Complex (**280**) displays an intense phenolate–iron LMCT band at 586 nm. Magnetic measurements indicate that the iron atoms are antiferromagnetically coupled with $J \approx -6\ cm^{-1}$. Mössbauer spectra of (**280**) are consistent with a high-spin octahedral diferric complex. The complex undergoes two quasi-reversible one-electron redox processes at −0.78 V [$Fe(II)_2/Fe(II)$, Fe(III)] and −0.225 V vs Ag/AgCl [Fe(II), $Fe(III)/Fe(III)_2$].

Two new dinucleating ligands, the symmetric (**281**) and the unsymmetric (**282**), and their μ-alkoxo diiron(II) complexes, $[Fe_2(\mathbf{281})(C_6H_5COO)(H_2O)](BF_4)_2$ (**283**), $[Fe_2(\mathbf{281})(CF_3CO_2)(H_2O)_2](BF_4)_2$ (**284**), and $[Fe_2(\mathbf{282})(CF_3CO_2)](BF_4)_2 \cdot nH_2O$ (**285**) have been synthesized [139]. Complex (**283**) has been structurally characterized; the complex consists of one five- and one six-coordinate iron atom that are

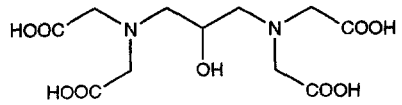

(273)

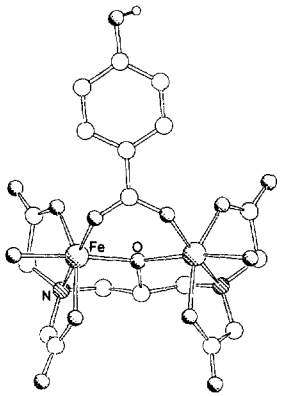

(274)

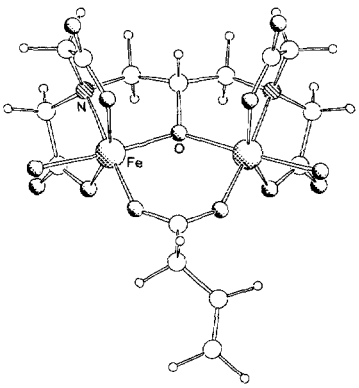

(275)

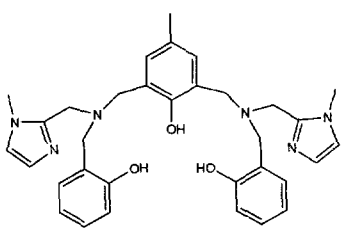

(279)

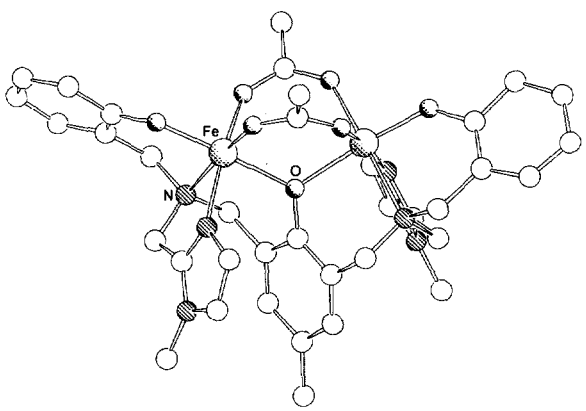

(280)

doubly bridged by the benzoate oxygen atoms and the alkoxide oxygen of (**281**). The five-coordinate iron has a distorted trigonal bipyramidal structure. The six-coordinate iron has an additional water molecule to make the iron atom distorted octahedrally coordinated. The Mössbauer spectrum of (**283**) also shows two distinct iron centres, whereas the spectrum of (**284**) indicates two six-coordinate centres. The electronic spectrum of (**283**) in CH_2Cl_2 reveals a dissociation of the coordinated water molecule to give two five-coordinate iron atoms, whereas the spectrum in DMSO corresponds to two six-coordinate iron atoms due to coordination of DMSO.

Complex (**283**) and (**284**) are reversibly oxygenated at temperatures below −35 °C, whereas complex (**285**) is irreversibly oxygenated to form an oxy-(**283**) species. The resonance Raman spectra of oxy-(**283–285**) are interpreted as μ-peroxo (Fe–O–O–Fe) species.

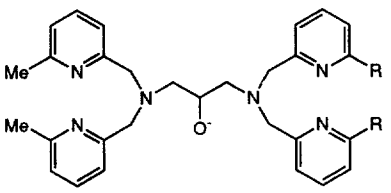

(**281**) R=Me
(**282**) R=H

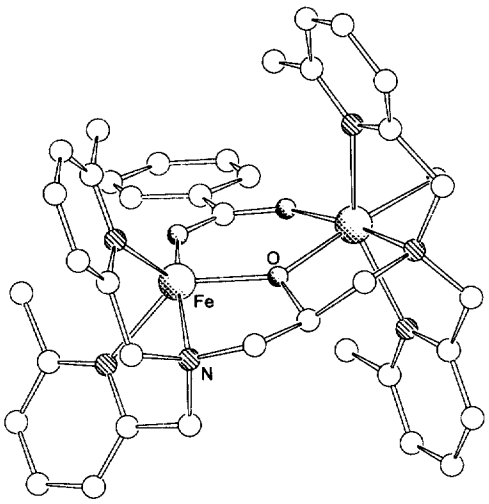

(**283**)

In order to provide synthetic analogues for the coordination environment of the active site of purple acid phosphatases, the diiron complex, $[Fe(II)Fe(III)(\mathbf{284})(OAc)_2]ClO_4 \cdot CH_3OH$ (**285**) has been synthesized by reaction of $Fe(ClO_4)_2 \cdot 6H_2O$, H_2(**284**) and sodium acetate trihydrate in methanol [140]. The product has been characterized by IR, ^{57}Fe Mössbauer and electron-absorption spectroscopy, microanalysis, magnetic susceptibility, molar conductivity and electrochemistry. The redox potentials of (**285**) are very similar to those of uteroferrin. On the other hand, the potentials differ from those observed for diiron complexes of ligands with four pyridine arms or two pyridine arms and two phenolate arms. This suggests that the ratio of tyrosines to histidines might be 2:3 in the dinuclear iron centre of uteroferrin, as in (**285**).

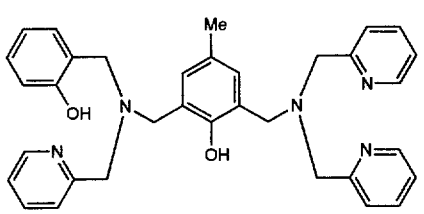

H_2-(**284**)

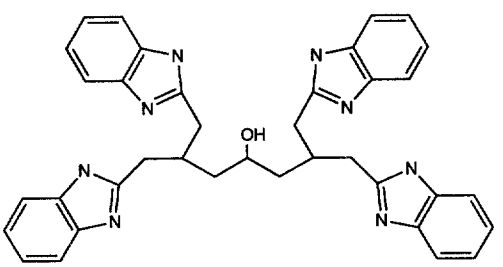

H(**286**)

A diferric model for a uteroferrin–arsenato complex has been reported [141]. The X-ray crystal structure shows that the complex $[Fe_2(\mathbf{286})(O_2AsMe_2)(Cl)(H_2O)](ClO_4)\cdot 5MeOH\cdot H_2O$ (**287**) has a (μ-alkoxo)(μ-dimethylarsinato)diiron(III) core. The coordination sphere around each of the iron atoms consists of three nitrogen atoms and one alkoxo oxygen from the heptadentate ligand (**286**) and one oxygen from the dimethylarsinato bridge. The sixth position is occupied by a Cl atom for one of the iron atoms and a water molecule for the other. Data from EXAFS and Mössbauer experiments are in agreement with the crystal structure showing two non-equivalent iron centres. Electrochemical measurements showed two quasi-reversible one-electron reductions at +210 mV and −40 mV (vs Ag/AgCl/3 M NaCl) assigned as the Fe(III)–Fe(III)/Fe(III)–Fe(II) transition and the Fe(III)–Fe(II)/Fe(II)–Fe(II) transition respectively.

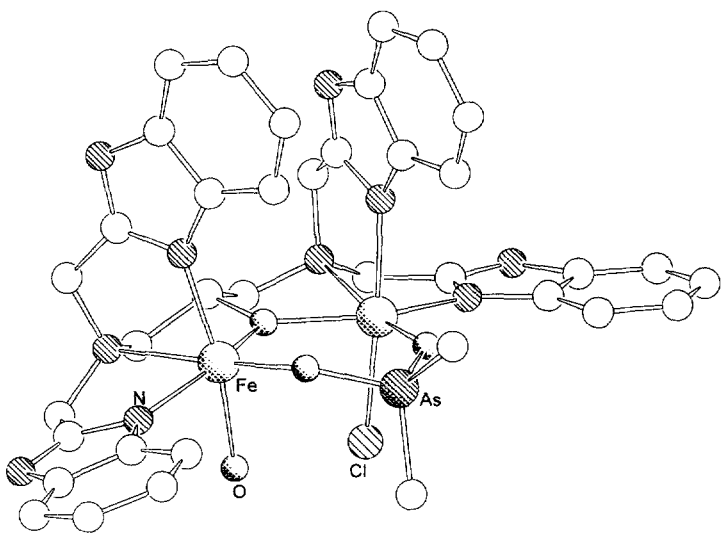

(287)

10.2. Complexes with mixed N,S-donor sets

Three iron(II) complexes with thiolate bridges have been reported [142]. The complexes $[Fe\{Fe(\mathbf{288})_2\}_2](ClO_4)_2\cdot CH_3OH$ and $[Fe\{Fe(\mathbf{289})_2\}_2]Cl_2\cdot 2CH_3OH$ (**291**) both have a linear triiron core with octahedrally coordinated terminal iron atoms and a tetrahedrally coordinated central atom. The central atom is only coordinated through thiolate bridges to the two other iron atoms. The last complex, $[Fe_2(\mathbf{290})_2(NO_3)_2]$, is a diiron complex with two thiolate bridges. The octahedral coordination of the iron atoms is completed by the two nitrogen atoms on the ligand and a didentate nitrate ion on each iron atom. Magnetic susceptibility measurements shows antiferromagnetic coupling through the thiolate bridges for all the complexes, strong for the two trinuclear complexes and weaker for the dinuclear.

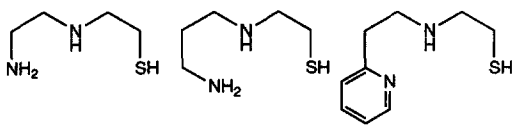

(288) (289) (290)

Reaction of Fe(II) and Fe(III) halides with the nitrogen–sulfur ligands (**291**) and H_2–(**292**) generates the new complexes $FeCl_2$(**291**)$_2$, $FeCl_4$(H–(**293**)) and Fe(H–(**292**))$_2$. These have been characterized by IR and ^{57}Fe Mössbauer spectroscopy [143]. X-ray crystal structure determination shows that $FeCl_4$(H–(**293**)) consists of discrete [H–(**293**)]$^+$ and $FeCl_4^-$ ions. Mössbauer experiments on $FeCl_2$(**291**)$_2$ and Fe(H–(**292**))$_2$ indicate iron(II) atoms with S-donor ligands in a tetrahedral symmetry in both complexes.

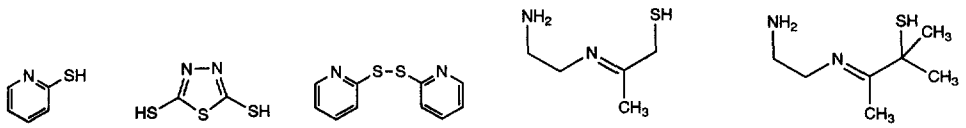

(291) H_2-(292) (293) H-(294) H-(295)

The low-spin ferric complexes [Fe(**294**)$_2$]Cl and [Fe(**295**)$_2$]Cl (**296**) have been synthesized as models for the active site of nitrite hydratase [144]. Magnetic measurements and EPR spectroscopy are consistent with $S=\frac{1}{2}$ ground states for both compounds. The crystal structure of (**296**) has been determined; it shows that the Fe–S and Fe–N_{ave} distances are relatively short.

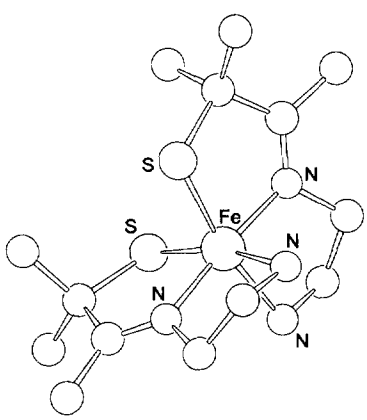

(296)

A new tripodal ligand, tris(2-mercaptobenzyl)amine (**297**), has been synthesized and its complex with Fe(II) has been made and structurally characterized [145].

The single crystal structure of $[Ph_4P][Fe(II)(\mathbf{297})_3)]$ (**298**) shows that the iron atoms have a distorted tetrahedral geometry, with the iron atom 0.37 Å out of the plane of the three S donor atoms. The overall structure has an idealized C_3 symmetry and is therefore chiral. Cyclic voltammetry of (**298**) shows a quasi-reversible Fe^{3+}/Fe^{2+} couple at -0.13 V (DMF; vs SCE). Oxidation of (**298**) in air with *N*-methylimidazole present gives [Fe(III)(297)(*N*-MeIm] (**299**), which has also been characterized by X-ray crystallography. The imidazole adds opposite to the amine nitrogen and gives a trigonal bipyramidal coordination geometry where the iron atom has moved into the plane of the S atoms; the ligand maintains its chirality. Room-temperature magnetic measurements of (**299**) show a high-spin iron(III) atom, with an $S=\frac{5}{2}$ ground state.

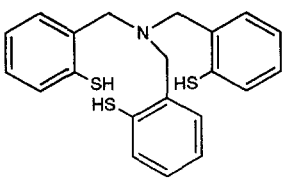

(297)

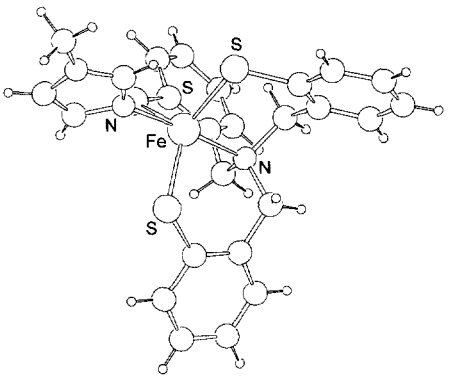

(299)

10.3. Complexes with other mixed-donor ligands

Reaction of $[\{Fe(NO)_2Cl\}_2]$ (**300**) and 2-(diphenylphosphino)pyridine yields $[Fe(NO)_2Cl(PPh_2Py)]$ (**301**) in which PPh_2Py acts as a monodentate ligand, donating to iron through phosphorus [146]. Complex (**301**) is unstable, rapidly converting to $[Fe(NO)Cl(OPPh_2Py)]$ (**302**). This process involves the substitution of one NO ligand by the pyridine nitrogen atom and also oxygenation of the ligand to form the didentate $OPPh_2Py$. Reaction of (**300**) with $OPPh_2Py$ gives (**302**) directly. Oxidation of either (**301**) or (**302**) by O_2 (1 atm) affords the nitrate complex $[Fe(NO_3)_2Cl(OPPH_2Py)]$ (**303**). Two iron nitrate complexes with 2-(diphenylphosphineoxide)pyridine ligands have been reported [147]. The complexes were $[FeCl_4][Fe(NO_3)_2(OPPh_2py)_2]$ (**304**) and (**303**); the latter was also structurally characterized. Both complexes (**304**) and (**303**) catalyse the auto-oxidation of cyclohexene, probably by decomposing cyclohexenyl hydroperoxide to give 2-cyclohexene-1-one and 2-cyclohexene-1-ol, but neither of the complexes oxidizes cyclohexene under anaerobic conditions. The geometry of (**303**) is a distorted pentagonal bipyramid around the iron atom. The oxygen atom of the phosphine oxide and the chlorine atom occupy axial positions with an O–Fe–Cl angle of 176.0(2)°.

The pyridine nitrogen atom and two symmetrically didentate nitrate ligands are in the equatorial positions.

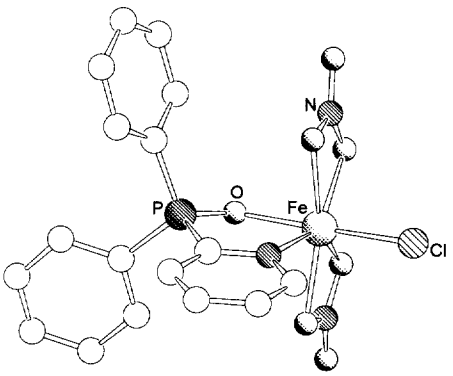

(303)

The coordination of two tetradentate phosphines, $P(CH_2CH_2PPh_2)_3$ (**305**) and $N(CH_2CH_2PPh_2)_3$ (**306**), to iron(II) have been studied in a (60:40) acetonitrile–toluene mixture [148]. Spectrophotometric determination of the formation constants gave $\log \beta_{11} = 6.00$ and $\log \beta_{11} = 5.37$ for ligands (**305**) and (**306**) respectively. The kinetics of the complex formation were also studied using the stopped-flow technique and were found to be first-order both in Fe(II) and incoming ligand. Second-order rate constants for the formations of $[FeL(MeCN)_2]_2^+$ (L=(**305**) or (**306**)) from $[Fe(MeCN)_6]^{2+}$ were determined to be 10.1×10^4 dm^3 mol^{-1} s^{-1} for ligand (**305**) and 8.6×10^4 dm^3 mol^{-1} s^{-1} for ligand (**306**). It is assumed that the rate-determining step is the coordination of the central ligand atom.

The crystal structure of $[FeH(N_2)(\mathbf{306})](BPh_4)$ (**307**) has been determined [149]. Reaction of (**307**) with HBr yields hydrazine. It is suggested that this reaction proceeds via the initial formation of an Fe(II) diazene complex.

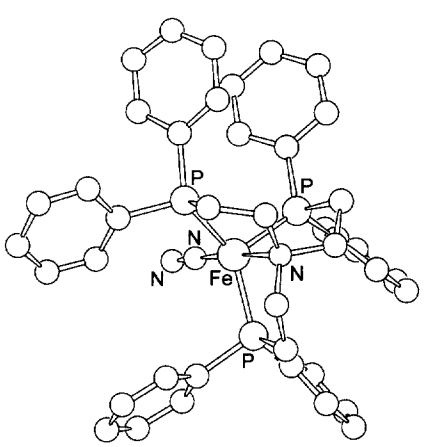

(307)

11. Iron–oxo clusters

11.1. Di- and tri-nuclear iron–oxo and hydroxo clusters

Single-crystal EPR spectra of $Na_4\{[Fe(edta)]_2O\}\cdot 3H_2O$ (**308**) and $\{[Fe(phen)_2O]O\}(NO_3)_4\cdot 7H_2O$ (**309**) in the $S=2$ and $S=3$ states have been measured [150]. The crystal structure of (**308**) has been determined by X-ray diffraction. The reported zero-field-splitting parameters are D_2, E_2, D_3, $E_3 = 0.248(1)$, $0.060(1)$, $0.604(1)$, $-0.016(1)\,cm^{-1}$ for (**308**) and $0.256(1)$, $0.037(1)$, $0.686(1)$ and $-0.008(1)\,cm^{-1}$ for (**309**); $|D_{exchange}|$, $|E_{exchange}| = 1.25$, $0.03\,cm^{-1}$ for (**308**) and 1.41, $0.02\,cm^{-1}$ for (**309**). In both cases, the z axis is parallel to the Fe–Fe vector. Predicted values for $|D1||E1|$ are 3.00, $0.62\,cm^{-1}$ for (**308**) and 2.33, $0.31\,cm^{-1}$ for (**309**).

Several iron complexes of 2,2′:6′,2″:6″,2‴-quaterpyridine (**310**) in di- and tri-valent oxidation states have been prepared, and the structures of $[Fe(\mathbf{310})(OH_2)_2][ClO_4]_2$ (**311**), $[\{Fe(\mathbf{310})(ClO_4)\}_2(\mu\text{-}O)]\cdot 8.5H_2O$ (**312**) and $[\{Fe(\mathbf{310})(Cl)\}_2(\mu\text{-}O)][ClO_4]_2\cdot 2H_2O$ (**313**) have been determined by X-ray crystal analyses [151]. In each complex, the quaterpyridine ligand is planar. In (**311**) the Fe(II) is seven-coordinate with the perchlorate ion acting as a didentate ligand; the resultant Fe–O–Fe angle is 155.2°. In (**313**) the Fe–O–Fe unit is linear and the Fe–O distance of 1.779 Å is considerably shorter than the Fe–O(OH_2) distance of 2.141 Å in (**311**). The results of molecular orbital calculations revealed that the unoccupied molecular orbitals of (**312**) and (**313**) mainly comprise the π^* orbital of (**310**). In (**312**), bending of the Fe–O–Fe unit gives rise to a decrease in the antibonding interaction between Fe(d_{yz}) and O(p_y) orbitals. Complex (**313**) is less stable in the spin-paired ($S=0$) than in open-shell ($S=1$) state by 49.3 kcal mol^{-1}. This coincides with paramagnetic susceptibility measurements, which show that (**313**) is paramagnetic with $\mu_{eff} = 1.75\mu_B$ per iron atom.

Two complexes containing Fe(μ-O)$_2$Fe cores with a formal Fe(III)Fe(IV) oxidation state and ligands derived from tpa have been reported. The first, $[(\mathbf{314})Fe(\mu\text{-}O)_2Fe(\mathbf{314})](ClO_4)_3$ (**316**), was obtained by treating $[(\mathbf{314})_2Fe_2(\mu\text{-}O)(OH)(H_2O)](ClO_4)_3$ with H_2O_2 [152]. The magnetic moment and the EPR spectrum (anisotropic g values at 4.45, 3.90, and 2.01) of (**316**) shows an $S=\frac{3}{2}$ ground state and the EXAFS indicates the presence of an Fe(μ-O)$_2$Fe core. The formula was confirmed by electrospray mass spectrometry and elemental analysis. Mössbauer spectroscopy indicates two equivalent iron centres. These observations suggest a valence-delocalized low-spin Fe(III) ($S=\frac{1}{2}$–low-spin Fe(IV) ($S=1$) pair. The other complex, $[(\mathbf{315})Fe(\mu\text{-}O)_2Fe(\mathbf{315})]^{3+}$ (**317**), was similarly obtained by treating $[(\mathbf{315})_2Fe_2(\mu\text{-}O)(OH)(H_2O)]^{3+}$ with H_2O_2 and was characterized by electrospray mass spectrometry [153]. The X-band EPR spectrum of (**317**) shows an almost isotropic $S=\frac{1}{2}$ signal at $g=2.00$. Low temperature Mössbauer spectra suggested that one site is a high-spin Fe(III) ion ($S=\frac{5}{2}$) and the other a high-spin Fe(IV) ($S=2$) antiferromagnetically coupled. This system differs only little from (**316**), but, when (**316**) is valence delocalized, (**317**) is better described as a localized

system; this difference is suggested to come from steric effects of the 6-methyl group preventing the short metal–ligand bond required for a low-spin configuration.

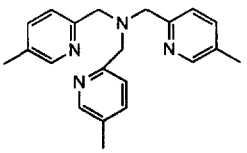

(314)

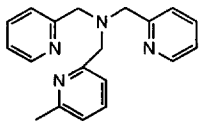

(315)

The nature of an alkylperoxoiron(III) intermediate formed from $[Fe_2O(tpa)_2(H_2O)_2](CF_3SO_3)_4$ (**318**) has been studied by EPR, resonance Raman, and electrospray ionization mass spectroscopy [154]. Reaction of (**318**) with benzyl alcohol and an excess of ^{t}BuOOH gives the intermediate (**319**) with an EPR spectrum consistent with a low-spin Fe(III) atom ($S=\frac{1}{2}$, $g=2.19$, 2.14 and 1.98). Resonance Raman spectra show that (**319**) is sensitive to the use of $[D_9]^t$BuOOH but not to the use of $H_2{}^{18}O$, suggesting that (**319**) is an alkylperoxoiron(III) species rather than an oxoiron(III) species. Electrospray ionization mass spectra of (**319**) suggest that the intermediate can be formulated as $[Fe(tpa)(OO^tBu)(HOCH_2Ph)]^{2+}$. Intermediate (**319**) decomposes in a pseudo first-order process and the rate constant increases as the benzyl alcohol concentration is increased, but it can be regenerated by addition of ^{t}BuOOH. The rate of decomposition decreases if $C_6D_5CD_2OH$ is used; this indicates that the decomposition is accompanied by the breaking of the benzylic C–H bond.

The first complex with a bis(μ-oxo)diiron(III) core, $[Fe_2(O)_2(\mathbf{320})_2](ClO_4)_2$ (**321**), has been prepared by reaction of $[Fe_2(O)(OH)(\mathbf{320})_2](ClO_4)_3$ with Et_3N [155]. The crystal structure of (**321**) shows that the complex has an $Fe_2(\mu\text{-}O)_2$ core with asymmetric oxo bridges. The Fe–O bonds are the longest and the Fe–O–Fe angle the smallest observed (92.5(2)°) for μ-oxo–diiron(III) complexes. This may reflect the repulsion between the oxo bridges. Mössbauer spectra of (**321**) are similar to those observed for antiferromagnetically coupled diiron sites in iron–oxo proteins. The temperature dependence of the magnetic susceptibility in (**321**) gives $J=+54(8)\,cm^{-1}$. This value is lower than in other μ-oxo diiron(III) complexes, reflecting the long Fe–O bonds.

Dinuclear iron complexes containing the tetradentate N_4 ligand (**322**) have been prepared [156]. The diiron(II) complex $[(\mathbf{322})Fe(O_2CMe)_2Fe(\mathbf{322})][ClO_4]_2$ (**323**) has been characterized by X-ray crystallography. The complex contains two iron(II) ions bridged by two acetate groups; the Fe–Fe distance is 4.382(2) Å. Each acetate bridges the iron atoms in an O,O′ mode using the *syn* lone pair of one carboxylate oxygen atom and the anti lone pair of the other. The ligand shows a *cis*-α conformation about the iron(II) centres. Complex (**323**) is readily oxidized in solution by air. A diiron(III) complex containing a μ-oxo–μ-acetato core, $[(\mathbf{322})FeO(O_2CMe)Fe(\mathbf{322})][ClO_4]_3$, was recovered from oxidized solutions of (**323**). Another diiron(III) complex, prepared in the absence of other possible bridging groups, is $[(\mathbf{322})FeO(OH)Fe(\mathbf{322})][ClO_4]_3$ (**324**). The spectroscopic data for (**324**)

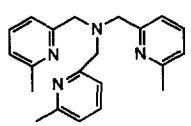

(320)

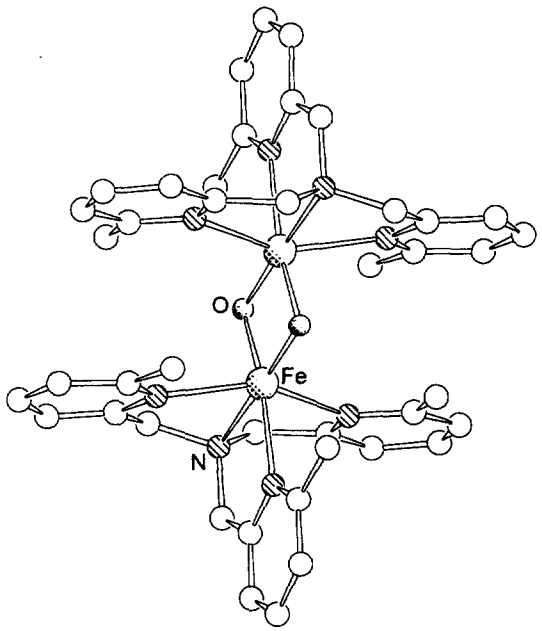

(321)

are consistent with the unusual formulation of a doubly bridged μ-oxo–μ-hydroxodiiron(III) core. In solution, (**324**) is sensitive towards carbon dioxide, reacting to give [(**322**)FeO(CO_3)Fe(**322**)][ClO_4]$_2 \cdot 2H_2O$ (**325**). The structure of (**325**) has been solved by X-ray crystallography and shows a dibridged μ-oxo–μ-carbonato-*O,O′* core. Again, (**322**) is in a *cis*-α conformation. Complex (**324**) was used to prepare other complexes containing the [(**322**)Fe(μ-O)Fe(**322**)]$^{4+}$ core: [(**322**)FeO(O_2CMe)Fe(**322**)][ClO_4]$_3$, [(**322**)FeO(O_2CH)Fe(**322**)][ClO_4]$_3$, and [(**322**)FeO(SO_4)Fe(**322**)][ClO_4]$_2$, by addition of acetic acid, formic acid and sodium hydrogen sulfate respectively, and [(**322**)(Cl)FeOFe(Cl)(**322**)][ClO_4]$_2$ by addition of chloride ions.

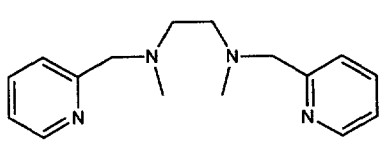

(322)

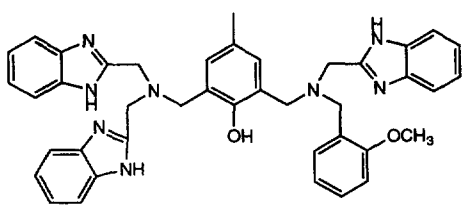

(326)

A polybenzimidazole ligand (**326**) with one tridentate and one didentate pendant arm and a methoxybenzyl spacer has been reported and its 1:1 complex with iron(III) has been synthesized [157]]. The diiron complex (327) has a μ-diphenyl–phosphato-

O,O' bridge and an unusual oxo–hydroxo bridge. The OHO^{3-} group is stabilized by hydrogen bonds to the N–H of the uncoordinated benzimidazole groups. This type of group is suggested as a possible intermediate in a stepwise deprotonation of coordinated water molecules. The FeO(oxo/hydroxo) bond length is 1.918(9) Å and is intermediate between the Fe–O distance in a μ-(aquo···hydroxo) species and a μ-oxo species. The cyclic voltammetry shows two quasi-reversible waves and the magnetic measurements show a very weak antiferromagnetic coupling.

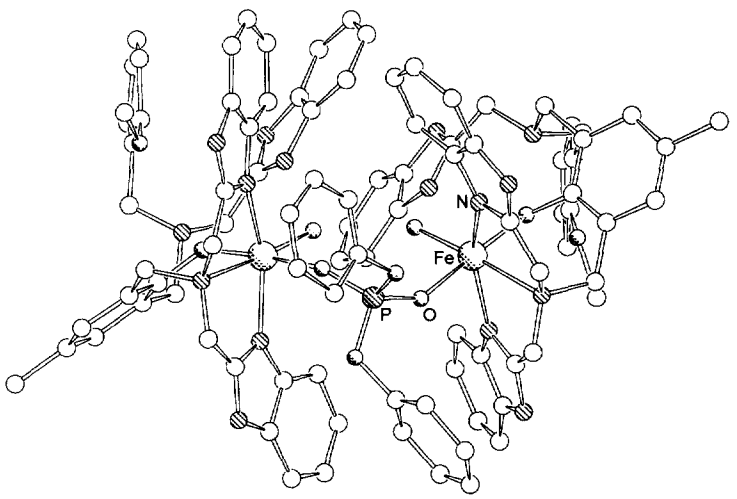

(327)

The complexes $[Fe\{H\text{–}(\mathbf{328})\}_2Cl_2]X$ ($X = Cl^-$, $FeCl_4^-$) have been synthesized [158]. The crystal structure of the latter complex has been determined. The phenoxyl radical (μ-oxo)bis(μ-carboxylato)diiron(III) complex $[Fe_2O(\mathbf{328})_2(\mathbf{329})(NO_3)_2]$ (**330**) was prepared from $[Fe_2O(\mathbf{329})(MeOH)_5(H_2O)](NO_3)_2$. Complex (**330**) is a model for the active site of the R2 protein of *E. Coli* ribonuclease reductase which contains a tyrosyl radical, and the magnetic behaviour of the model complex is found to be similar to that of the protein. The iron atoms are antiferromagnetically coupled; a theoretical fit of the magnetic susceptibility data indicates a J value of $-117\ cm^{-1}$, which is in good agreement with the coupling constant for the R2 protein of *E. Coli* ribonuclease reductase determined by pulsed saturation-recovery EPR.

Oxidation of the μ-oxo dimers $Fe(III)_2L_2O$, L = (**330–336**), gives mixed valence Fe(III)Fe(IV) dimers (e.g. (**337**)) [159]. These have been investigated over the temperature range 42–300 K by magnetic susceptibility measurements, EPR and ^{57}Fe Mössbauer spectroscopy. The Mössbauer spectra indicate that, in the complexes $[Fe_2L_2O][I_3]X$ (X = iodine or iodine chloroform solvates) and $[Fe_2L_2(OH)_2](BF_4)$, the "extra" electron appears to be delocalized between the two metal sites.

The electronic structures of the two μ-oxo diiron complexes $[Fe_2O(O_2CCH_3)_2(Me_3tacn)_2]$ and $(FeHedta)_2O$ have been studied using both theo-

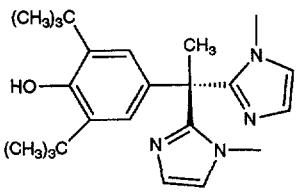

H-(328)

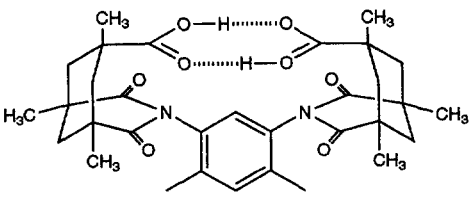

H_2-(329)

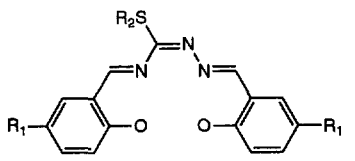

R_1=H; R_2=Et (330), ^{n}Pr (331), ^{n}Bu (332)
R_1=Me; R_2=Me (333), Et (334), ^{n}Pr (335), ^{n}Bu (336)

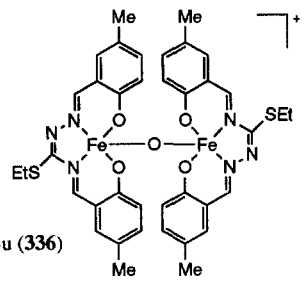

(337)

retical (SCF–Xα–SW calculations) and spectroscopic techniques (electronic absorption, MCD and RR spectroscopy) [160]. Strong σ bonding of the oxo p_σ orbital can explain the strength of the Fe–oxo bond in both complexes together with the enhancement by participation of the unoccupied Fe 4s and 4p in the bond.

Three dinuclear iron complexes with Me_3tacn and tetrachlorocatechol (Cl_4cat) as ligands have been reported [161]. The complexes [$Me_3tacn(Cl_4cat)Fe(III)$–O–$Fe(III)(Cl_4cat)Me_3tacn$] (**338**), [$Me_3tacn(Cl_4cat)Fe(III)$–N–$Fe(IV)(Cl_4cat)Me_3tacn$] (**339**), and [$Me_3tacn(Cl_4cat)Fe(IV)$=N=$Fe(IV)(Cl_4cat)Me_3tacn$]Br (**340**) were all structurally characterized by X-ray crystallography. The iron centres in all three complexes have octahedral geometries with facially coordinated Me_3tacn, a didentate tetrachlorocatechol, and the bridging atom. In (**338**) and (**340**), the bridging unit is linear and symmetrical, whereas in (**339**) the Fe=N bond is short (1.50(1) Å) and the Fe=N bond is long (1.98(1) Å). The $Fe(O,N)_{ligand}$ bonds are all longer in (**338**) than in (**340**), reflecting that the $Me_3tacn(Cl_4cat)Fe(III)$ unit has a high-spin configuration with half-filled e_g^* orbitals, whereas the $Me_3tacn(Cl_4cat)Fe(IV)$ unit has a low-spin configuration with empty e_g^* orbitals. Magnetic measurements confirmed that (**338**) has two high-spin Fe(III) atoms that are antiferromagnetically coupled, that there is a strong antiferromagnetic coupling between a high-spin Fe(III) and a low-spin Fe(IV) atom in (**339**), and that (**340**) is diamagnetic with two low-spin Fe(IV) that are very strongly antiferromagnetically coupled.

Iron powder dissolves in pivalic acid on heating to give [$Fe_3O(O_2CCMe_3)_6(Me_3CCO_2H)_3$] (**341**), a mixed-valence trinuclear iron pivalate complex–pivalic acid adduct [162]. On the (^{57}Fe) Mössbauer time scale, a valence-trapped state is exhibited below ca. 100 K, and a valence detrapped state exists

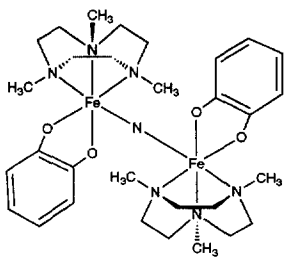

(339)

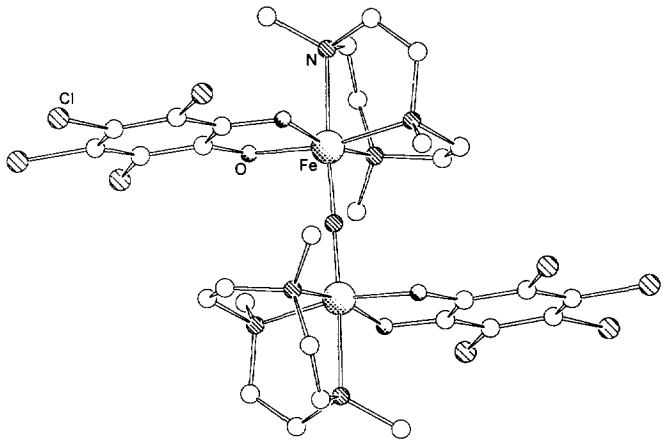

(340)

above ca. 230 K up to room temperature. Infrared studies show evidence of valence trapping at room temperature.

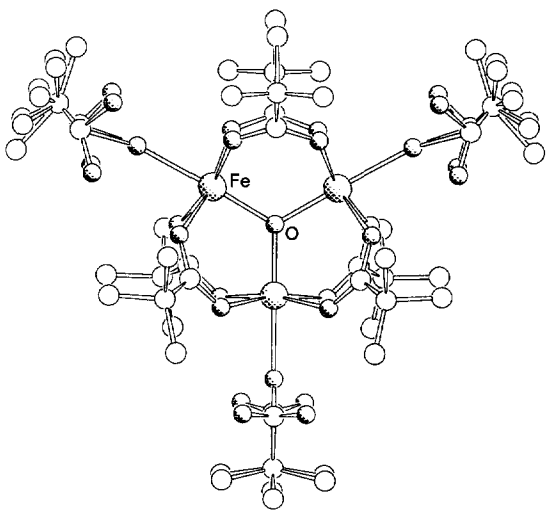

(341)

A triiron(III) complex with an Fe–(μ-oxo)–Fe–(μ-oxo)–Fe core has been synthesized and structurally characterized [163]. In the complex $[Fe_3O_2(phen)_6(OAc)_2](ClO_4)_3$ (**342**) all the iron atoms have an N_4O_2 coordination with a pseudo-octahedral symmetry. The bent triiron chain has a cis arrangement at the central iron atom; distances and angles are comparable with those in (μ-oxo)diiron(III) complexes. Magnetic susceptibility measurements and the X-band

EPR spectrum of (**342**) at 90 K are consistent with a strongly antiferromagnetically coupled $Fe(III)_3$ unit with an $S=\frac{5}{2}$ ground state.

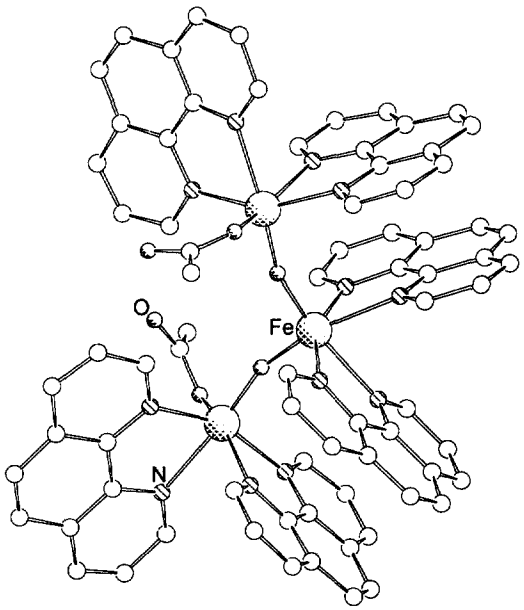

(342)

11.2. Polynuclear iron–oxo clusters

The reaction of $Fe(NO_3)_3 \cdot 9H_2O$ with $NaIO_4$ in aqueous acid solution gives brown $[Fe_4I_3O_{24}H_{15}]$ and a subsequent reaction with concentrated alkali forms $M_n[Fe_4I_3O_{24}H_{15-n}]$ (M = Li, Na, K, Rb or Cs) [164]. The crystal structure of $K_6Na_2[Fe_4I_3O_{24}H_7] \cdot 14H_2O$ has been determined; the structure contains an Anderson-type anion composed of seven edge-linked octahedra. In the crystal studied, a central FeO_6 group is surrounded by six disordered FeO_6 and IO_6 groups.

The multinuclear complex, $[OFe_6(\mathbf{343})_6]^{5+}$ (**344**) has been synthesized and has an Fe_6O_{22} core, as shown by the crystal structure of its potassium salt K_5(**344**)$\cdot 14.5H_2O$ [165]. The core is a network made of five FeO_6 octahedra and one square pyramidal pentacoordinated iron atom and dominated by edge-sharing octahedra. It has a central μ_3-oxo ligand and 11 μ_2-bridging alcohol groups from (**343**) ligands. All the (**343**) ligands are bound to more than one iron atom (2, 3 or 4) and they seem to stop further aggregation by shielding the periphery. Another polyiron complex has been prepared with sorbitol (**345**) as ligand. The complex was suggested to be $Na_6[Fe_6O_{12}(\mathbf{345})_6]$ (**346**). EXAFS and magnetic susceptibility measurements show that (**344**) and (**346**) have analogous local structures and similar magnetic properties.

The synthesis and X-ray crystal structure of a heptadecanuclear iron complex,

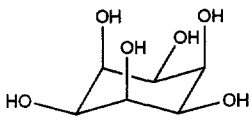

H_3-(**343**)

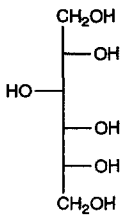

(**345**)

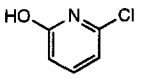

(**347**)

$[Fe_{17}O_{15}(OH)_6(\mathbf{347})_{12}(phen)_8(OMe)_3]\cdot 1.5H_2O\cdot 1.5MeCN\cdot 0.4MeCO_2Et$ has been reported [166]. The complex has an iron–oxo core surrounded by a layer of phen and (**347**) ligands. There are three kinds of iron atom in the complex, 11 octahedrally coordinated, two with trigonal-bipyramidal geometry, and four approximately tetrahedrally coordinated. The array of iron atoms is held together by μ_2-hydroxy, μ_3-oxo, and μ_4-oxo bridges. The μ_3-O atoms are all trigonal planar, and the μ_4-O atoms have trigonal-pyramidal coordination. The irregular structure of the iron core is probably caused by the packing of the strongly bound phenanthroline ligands. Preliminary magnetic studies indicate strong antiferromagnetic coupling in the complex.

Three complexes of iron(III) and the ligand $N(CH_2COOH)_2(CH_2CH_2OH)$ (H_3–(**348**)) have been reported [167]. The first is a diiron complex, $[Fe(\mathbf{348})(H_2O)]_2$, where the iron atoms are bridged by the alkoxide function of the ligand. The two others are polyiron(III) oxyhydroxide clusters, $[Fe_{19}(\mu_3\text{-}O)_6(\mu_3\text{-}OH)_6(\mu_2\text{-}OH)_8(\mathbf{348})_{10}(H_2O)_{12}]^+$ and $[Fe_{17}(\mu_3\text{-}O)_4(\mu_3\text{-}OH)_6(\mu_2\text{-}OH)_{10}(\mathbf{348})_8(H_2O)_{12}]^{3+}$, which crystallize in the same unit cell. They both contain iron hydroxide mineral portions. Magnetic susceptibility measurements, EPR and Mössbauer spectroscopy show that at least one of the clusters has a ground state spin of no less than $S=\frac{3}{2}$.

12. Iron–sulfur clusters

12.1. Di- and tri-nuclear iron–sulfur clusters

Synthetic routes to an Fe_3S_4 cluster that is not supported by a protein matrix by use of (1:3)-site-differentiated Fe_4S_4 clusters have been reported [168]. The first route (Scheme 6) uses $[Fe_4S_4(\mathbf{349})(SEt)]^{2-}$ (**350**) and starts with the reaction of $(Bu_4N)_2$(**350**) with $(Et_3NH)(CF_3SO_3)$ to give $(Bu_4N)_2$(**351**). Addition of $(Et_4N)_2$(**357**) at the unique iron site in (**351**) gives $(Et_4N)_3[Fe_4S_4(\mathbf{349})(\mathbf{357})][(Et_4N)_3(\mathbf{352})]$. The unique iron atom can now be removed by adding an excess of $(Et_4N)_2$(**357**) to give the iron–sulfur cluster $[Fe_3S_4(\mathbf{349})]^{3-}$ (**353**) (isolated as $(Et_4N)_3$(**353**)) and $[Fe(\mathbf{357})_2]^{2-}$. The Mössbauer spectrum of (**353**) is in good agreement with those of protein-bound $[Fe_3S_4]^0$ clusters. An equivalent route using $(Et_4N)_3$(citrate) in the reaction with $(Bu_4N)_2$(**351**) also

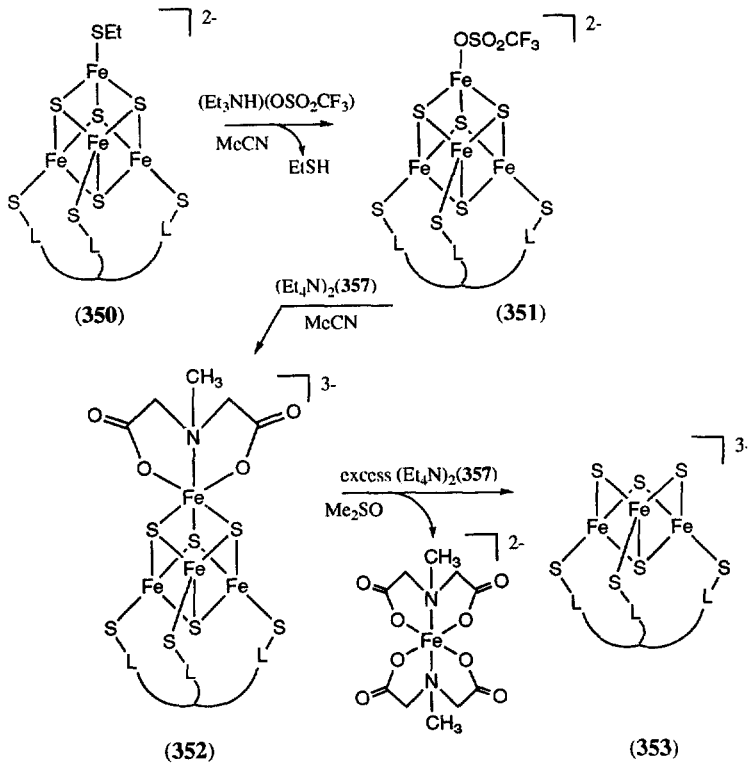

Scheme 6.

exists. Another route to get (**353**) starts with $[(OC)_3MoFe_3S_4(SEt)_3]^{3-}$ (**354**) that has a spin-isolated $[Fe_3S_4]$ fragment and long Mo–Fe/S bonds (Scheme 7). Reaction of (**354**) with H_3(**349**) gives $(Et_4N)_3$(**355**) which, together with 5 equiv. of $NaPF_6$ at −60 °C with CO passed through for 10 min, gave $[NaFe_3S_4$(**349**)$]^{3-}$ (**356**) in equilibrium with (**353**). Further reaction of $(Et_4N)_3$(**353**) with 1 equiv. each of $(Et_4N)_2$(**357**) and $Tl(CF_3SO_3)$ gave $(Et_4N)_2[TlFe_3S_4$(**349**)$]$.

12.2. Iron–sulfur cubanes

The substitution of a chloro-ligand in $[Fe_4S_4Cl_4]^{2-}$ (**358**) for 4-$RC_6H_4S^-$ (R = Cl, F, H, Me, MeO or NH_2) has been studied [169]. The associative pathway of the reaction involves binding of the thiolate to an iron atom (Fe_a) followed by a slower dissociation of a chloro-ligand (Scheme 8). The origin of the leaving group (the chloro-ligand on Fe_a or the chloro-ligand on a remote iron site (Fe_r)) changes with the electron-releasing capability of the thiolate. The binding constants (K_2^R) of 4-$RC_6H_4S^-$ to (**358**) decrease as expected from electron-releasing capabilities along the series, R = Cl > F > H > Me > MeO > NH_2, but the corresponding dissociation constants (k_3^R) decrease, R = Cl > F > H > Me and then increase,

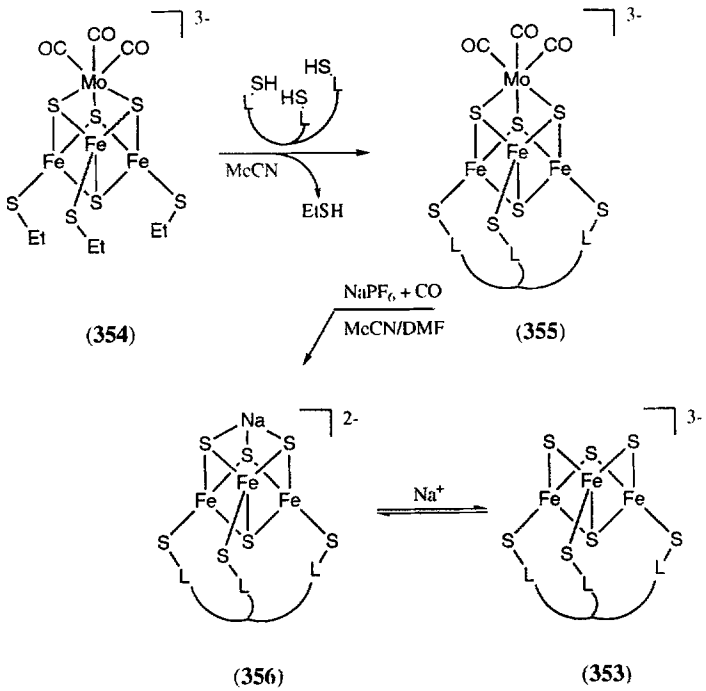

(354) (355) (356) (353)

Scheme 7.

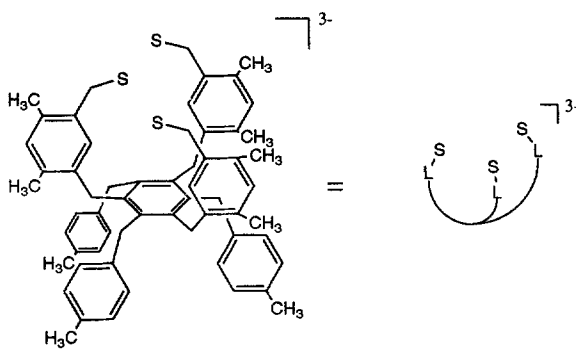

(349)

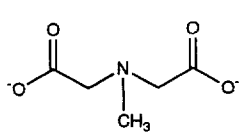

(357)

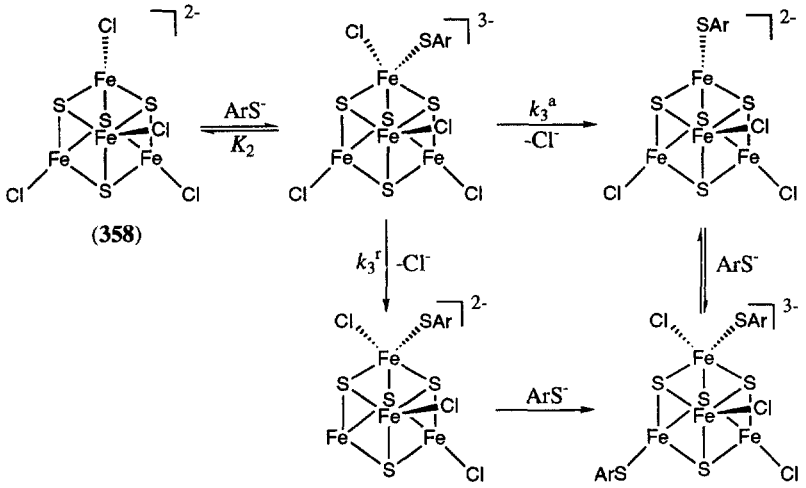

Scheme 8.

R = Me < MeO < NH_2. The more electron-releasing nucleophiles (R = Me, MeO or NH_2) are not able to labilize the chloro-ligand on Fe_a so much, but the increased electron density in the cluster instead labilizes chloro-groups on Fe_r sites. For intermediate nucleophiles (R = Me, H or F) it is probable that both pathways are working.

The compound $(Et_4N)_3[Fe_4S_4(SCH_2Ph)_4]$ has been studied by EPR spectroscopy [170]. The measurements were made at very low temperatures (around 4 K) to avoid broadening of the signals due to spin–lattice relaxation. Spin–spin interactions between the paramagnetic $[Fe_4S_4]^+$ cubanes broadened the signals, but it was still possible to study two doublets. These doublets were identified as being the fundamental and excited Kramers doublets associated with the effective spin $S=\frac{3}{2}$. A strong non-axial zero field splitting tensor ($\lambda \cong \frac{1}{3}$) is associated with the two effective g-tensors of the doublets. The real g values are around $g_{av}=1.9$.

The uncharged iron–sulfur cubane clusters $[Fe_4S_4X(P^tBu_3)_3]$ (X = Cl (**359**), Br, or I) have been prepared by reaction the appropriate $(Bu_4N)_2[Fe_4S_4X_4)$ clusters with 4 equiv. of the phosphine [171]. The EPR spectra of the clusters are consistent with $S=\frac{1}{2}$ ground states for all three clusters. In the three clusters, the $[Fe_4S_4]^{2+}/[Fe_4S_4]^+$ redox couple occurs at 600–1200 mV more positive potentials than those observed for the same redox couple in other synthetic Fe/S cubanes. Reaction of $[Fe_4S_4Cl(P^tBu_3)_3]$ with PhS^- leads to the formation of $[Fe_4S_4(SPh)_2(P^tBu_3)_2]$ (**360**) in good yield. The crystal structures of (**359**) and (**360**) have been determined.

12.3. Heterometallic iron–sulfur clusters

Various single cubanes have been made to model the reactivity of nitrogenase. The clusters possess an $[MFe_3S_4]^{n+}$ core as catalyst for reduction of

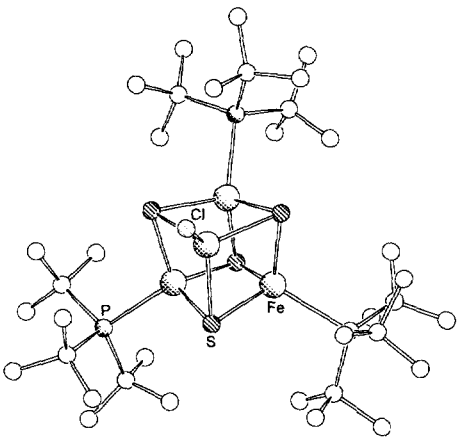

(359)

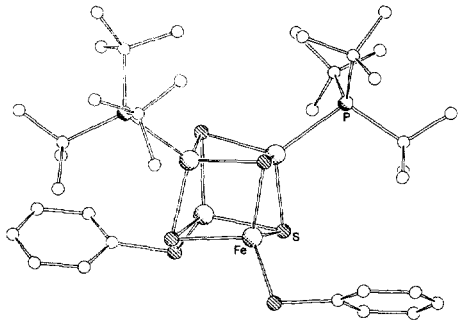

(360)

different substrates (M=Mo, $n=3$; M=V, $n=2$). The Fe/Mo/S cluster $(Net_4)_2[(Cl_4cat)(MeCN)MoFe_3S_4Cl_3]$ (**361**) was used as catalyst for the reduction of acetylene to ethanol in the presence of protons and reducing equivalents (cobaltocene) [172]. At low substrate level, K_m and V_{max} could be determined (17.9 mM and 1.1×10^{-4} M min^{-1} respectively). Several $[(L)(L')(L'')VFe_3S_4Cl_3]^{n-}$ clusters (**362–364**) have also been investigated as catalysts for the reduction of hydrazine to ammonia [173]. In all clusters (**361–364**) the reaction was found to take place at the heteroatom. The rate of the reaction was found to decrease when the labile solvent molecules at the heteroatom were exchanged for non-labile ligands for both Mo and V clusters. An Fe/V/S cluster, $[(HBpz_3)VFe_3S_4Cl_3]^{2-}$, with no labile ligands, was synthesized and structurally characterized. The cluster showed no catalytic or stoichiometric reduction of hydrazine. The iron atoms were found to reduce acetylene, but at a markedly lower rate than the molybdenum atom, whereas the iron atoms had no or very little effect on the reduction of hydrazine in the Fe/V/S clusters.

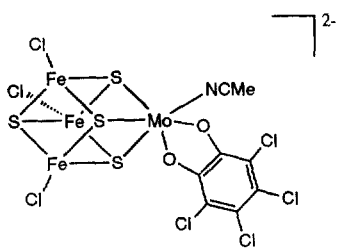

(361)

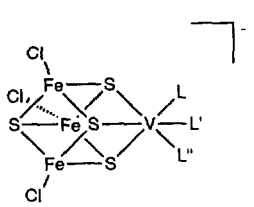

(**362**) L = L' = L" = DMF
(**363**) L = PEt_3, L' = L" = DMF
(**364**) L, L' = bpy, L" = DMF

Starting from $(Et_4N)_2[MoFe_3S_4Cl_3(Cl_4\text{-cat})(CH_3CN)]$, a number of $MoFe_3S_4$ cubanes with an Mo–polycarboxylate moiety have been synthesized by reaction of

various organic polycarboxylic acids or their salts [174]. The clusters were $(Et_4N)_4[\{MoFe_3S_4Cl_4\}_2(\mu\text{-}C_2O_4)]$ (**365**), $(Et_4N)_3[(MoFe_3S_4Cl_4)(C_2O_4)]$ (**366**), $(Et_4N)_5[\{MoFe_3S_4Cl_2(C_2O_4)\}_2(\mu\text{-}S)(\mu\text{-}CN)]$ (**367**), $(Et_4N)_x[(MoFe_3S_4Cl_3)(L)]$ ($x=3$, $L=(C_2O_4)(CN)$ (**368**) and H–citrate; $x=2$, $L=H_2$–citrate, *R*-citramalic acid, D-malic acid, and $(CH_3N(CH_2COO^-)_2$ (**369**)). Compound (**366**) was given by the reaction of (**365**) with $(Et_4N)_2(C_2O_4)$. Further reaction of (**366**) with $(Et_4N)CN$ gave (**368**), whereas reaction of (**366**) with 0.5 equiv. $(Et_4N)CN$ and $(Et_4N)SH$ gave (**367**). The single-crystal X-ray structures of the cubanes (**365–369**) were determined.

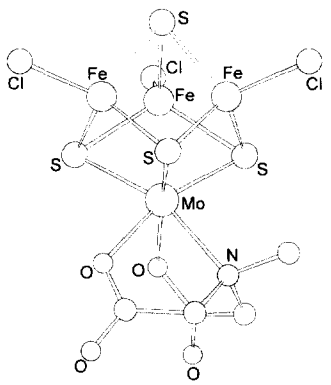

(**369**)

The double cubane clusters $[MoFe_3S_4Cl_3(SCH(R)CO_2)]_2^{4-}$ (R=H (**370**), Me (**371**), CH_2CO_2H (**372**)) and the single cubane $[MoFe_3S_4Cl_3\{O_2CCH_2)_2S\}]^{2-}$ have been synthesized [175]. The crystal structures of (**371**) and (**372**) have been determined. The fact that clusters (**370–372**) are EPR silent indicate that the double cubane structure is maintained in solution and that there is electronic coupling between the linked molecules. Cluster (**371**) is capable of acting as a catalyst for the reduction of hydrazine to ammonia in the presence of cobaltocene.

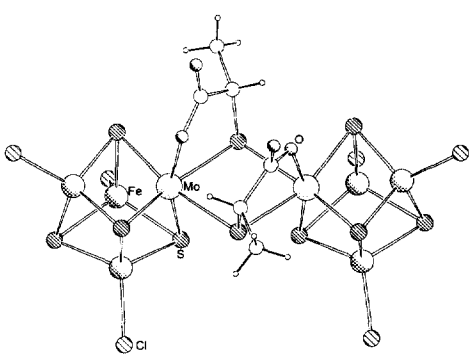

(**371**)

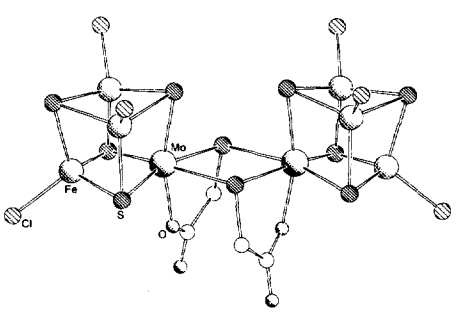

(**372**)

On deprotonation, the tridentate thiol (**373**) coordinates to the molybdenum–iron–sulfur clusters $[NEt_4][MoFe_3S_4(SEt)_4(dmpe)]$ or $[NEt_4]_2[MoFe_3S_4(SEt)_3(Cl_4cat)(solv)]$ with the elimination of ethanethiol, to give $[NEt_4][MoFe_3S_4$(**373**)$(SEt)(dmpe)]$ (**374**) and $[NEt_4]_2[MoFe_3S_4$(**373**)$(Cl_4cat)(solv)]$ (solv = DMSO (**375**) or MeCN (**376**)) respectively [176]. Cluster (**374**) reacted with 1 equiv. of trimethylacetyl chloride to give $[NEt_4][MoFe_3S_4L(Cl)(dmpe)]$ (**377**). Clusters (**374–377**) have been characterized by ^1H NMR, IR and Mössbauer spectroscopies and by elemental analysis. Reaction of (**375**) with imidazole, tetraethylammonium imidazolate, or the tetraethylammonium salt of histidine methyl ester generated clusters, isolated as black solids, in which the molybdenum NO_2S_3 coordination environment is similar to that observed for the cluster $[NEt_4]_2$ $[MoFe_3S_4(SEt)_3(Cl_4cat)(solv)]$.

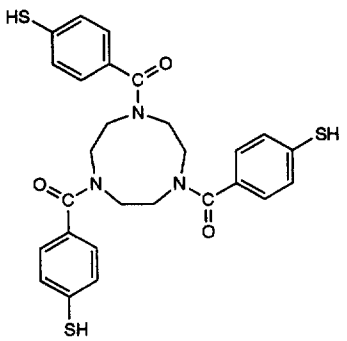

(373)

Two clusters with an Mo_3FeS_4 core have been synthesized and structurally characterized by X-ray crystallography [177]. The two clusters obtained from $[Mo_3S_4(H_2O)_9]^{4+}$ were $[Mo_3FeS_4(H_2O)_{10}](CH_3C_6H_4SO_3)_4 \cdot 7H_2O$ (**378**) and $[Mo_3FeS_4(NH_3)_9(H_2O)]Cl_4$ (**379**) The core structure is approximate C_{3v} for both (**378**) and (**379**). Mössbauer spectroscopy indicated an oxidation state of +2.39 and +2.54 for the iron atom in (**378**) and (**379**) respectively, indicating a reductive addition of iron to form the clusters. Cyclic voltammetry measurements on (**378**) show three consecutive one-electron reduction steps.

12.4. Other iron–sulfur clusters

The crystal structure of $[Fe_6(\mu_3\text{-}S)_8(PEt_3)_6][PF_6]_2$ (**380**) has been determined [178]. The electronic structures of (**380**) and $[Fe_6(\mu_3\text{-}S)_8(PEt_3)_6][PF_6]$ (**381**) have been investigated experimentally by measuring the temperature variation of the magnetic susceptibility between 300 and 4.2 K, the field dependence of the magnetization at three different temperatures in the range 2–10 K and the polycrystalline powder Mössbauer spectra at variable temperature. Complex (**381**) possesses a $S = \frac{7}{2}$ spin state well isolated from the excited states, whereas (**380**) shows a marked temperature dependence of the magnetic susceptibility.

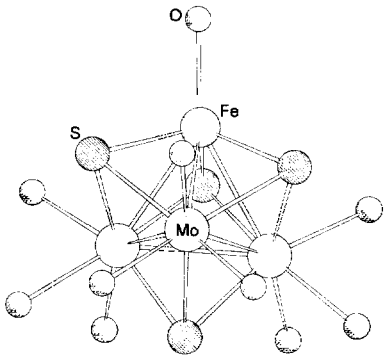

(378)

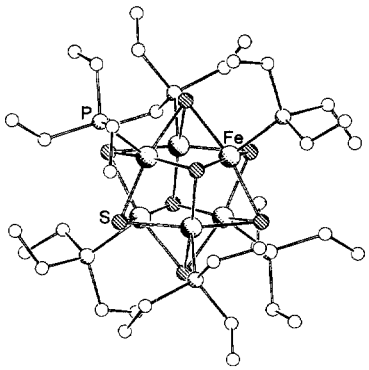

(380)

Two new clusters with direct coupling between two tetranuclear core subunits have been synthesized and structurally characterized [179]. The clusters are $[Fe_8S_8(PCy_3)_6]$ (**382**) and $[Fe_8S_{12}(CN^tBu)_{12}$ (**383**). The Mössbauer spectrum of (**382**) shows that there are three types of iron atom in a 1:1:2 ratio, as expected from the structure that consists of two Fe_4S_4 cubane cores linked via two Fe–S bonds. The intercubane Fe_2S_2 rhombus is completely planar, whereas the intracubane rhombi are not. The reaction of $[Fe_4S_4(SEt)_2(CN^tBu)_6]$, a [2:2] site-differentiated cubane, with H_2S gave compound (**383**). The single-crystal structure consists of two Fe_2S_5 components connected to each other through two bridging μ_2-S atoms. The Fe_4S_5 component consists of two octahedral and two tetrahedral iron centres with one of the μ_3-S^{2-} atoms between a tetrahedral and an octahedral iron atom replaced with a μ_3-S_2^{2-} unit. The extra S-atom induces an almost planar configuration for the Fe_2S_2 rhombus containing the two bridging tetrahedral Fe centres, minimizing the repulsive interactions of opposing S atoms in the Fe_4S_5 components.

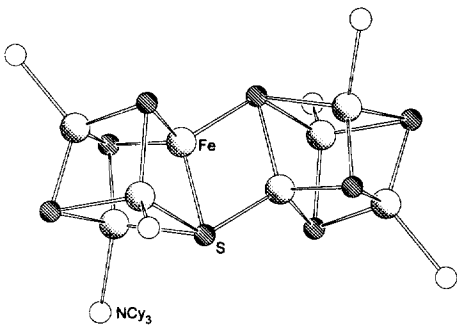

(382)

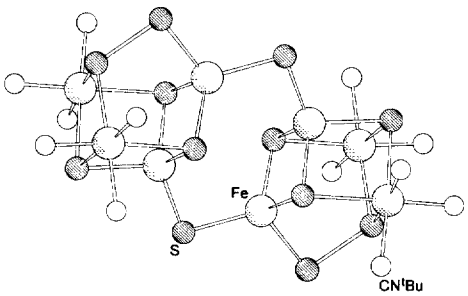

(383)

12.5. Iron–selenium clusters

A multinuclear selenato-bridged iron cluster has been reported [180]. The cluster $[Fe_{12}(SePh)_{24}]$ (**384**) was made by reaction of $FeCl_3$, PPh_3 and $PhSeSiMe_3$ in dichloroethane. Single-crystal structure determinations revealed that, depending on the conditions of crystallization of (**384**), it crystallizes as either (**384**)$\cdot 4C_2H_4Cl_2$ or (**384**)$\cdot 5C_2H_4Cl_2$. The bonding parameters in (**384**) are almost the same in the two kinds of crystal. Cluster (**384**) is cyclic with a diameter of 12 Å. Each Fe atom has a distorted tetrahedral coordination by four μ_2-SePh ligands. The edge-sharing Se_4 tetrahedra connect to form a ring, giving the cluster a $\bar{4}$ symmetry. A space-filling model of (**384**) shows that the Fe atoms are surrounded and almost completely buried in an organic layer of phenyl groups. The Mössbauer spectrum of (**384**) shows that the cluster consists entirely of iron(II) atoms and has a magnetic moment of $\mu_{eff} = 1.51\mu_B$/Fe at 293 K.

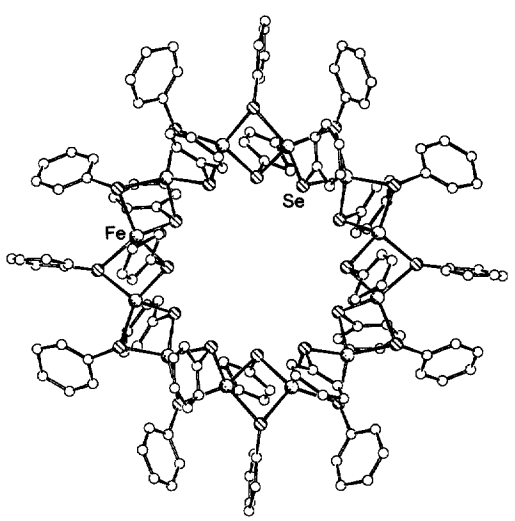

(384)

Acknowledgements

F.P. would like to thank the Foundation Blanceflor Boncompagni-Ludovisi née Bildt for financial support.

References

[1] J. Li, R.M. Dickson, T. Ziegler, J. Am. Chem. Soc. 117 (1995) 11482.
[2] U. Russo, B. Zarli, G. Favero, G. Valle, G.J. Long, Inorg. Chim. Acta 239 (1995) 67.
[3] G.N. Glavee, K.J. Klabunde, C.M. Sorensen, G.C. Hadjipanayis, Inorg. Chem. 34 (1995) 28.
[4] B. Foretic, N. Burger, V. Hankonyi, Polyhedron 14 (1995) 605.
[5] P.R. Norris, J.M. Pratt, J. Chem. Soc. Dalton Trans. (1995) 3643.
[6] P.R. Norris, J.M. Pratt, J. Chem. Soc. Dalton Trans. (1995) 3651.
[7] H. Kurosaki, S. Koga, M. Goto, Bull. Chem. Soc. Jpn. 68 (1995) 843.
[8] S. Alshehri, J. Burgess, R. van Eldik, C.D. Hubbard, Inorg. Chim. Acta 240 (1995) 305.
[9] H.F. Wu, J.S. Brodbelt, Inorg. Chem. 34 (1995) 615.
[10] G.D. Storrier, S.B. Colbran, D.B. Hibbert, Inorg. Chim. Acta 239 (1995) 1.
[11] S.L. Larson, S.M. Hendrickson, S.L. Ferrere, D.L. Derr, C.M. Elliott, J. Am. Chem. Soc. 117 (1995) 5881.
[12] S. Ferrere, C.M. Elliott, Inorg. Chem. 34 (1995) 5818.
[13] Y. Zang, L.J. Que, Inorg. Chem. 34 (1995) 1030.
[14] J. Glerup, P.A. Goodson, D.J. Hodgson, K. Michelsen, Inorg. Chem. 34 (1995) 6255.
[15] M. Lubben, A. Meetsma, E.C. Wilkinson, B. Feringa, L.J. Que, Angew. Chem. Int. Ed. Engl. 34 (1995) 1512.
[16] I. Bernal, I.M. Jensen, K.B. Jensen, C.J. McKenzie, H. Toftlund, J.-P. Tuchagues, J. Chem. Soc. Dalton Trans. (1995) 3667.
[17] Y.M. Chiou, L.J. Que, J. Am. Chem. Soc. 117 (1995) 3999.
[18] E. Vallazza, R. Schmid, J. Chem. Soc. Dalton Trans. (1995) 2473.
[19] V. Briois, M.C.C. Dit, P.H. Sainctavit, C.H. Brouder, A.M. Flank, J. Am. Chem. Soc. 117 (1995) 1019.
[20] M. Enamullah, W. Linert, J. Coord. Chem. 35 (1995) 325.
[21] L.M.A. Martinez, F. Dahan, V. Petrouleas, A. Bousseksou, J.P. Tuchagues, Inorg. Chem. 34 (1995) 5346.
[22] T.H. Buchen, P. Guetlich, Inorg. Chim. Acta 231 (1995) 221.
[23] Y. Sohrin, H. Kokusen, M. Matsui, Inorg. Chem. 34 (1995) 3928.
[24] E.H. Ha, R.Y.N. Ho, J.F. Kisiel, J.S. Valentine, Inorg. Chem. 34 (1995) 2265.
[25] S. Zaydoun, M.S. Idrissi, A. Zrineh, B. Agricole, L.C. Garrigou, Polyhedron 14 (1995) 1477.
[26] L.G. Lavrenova, N.G. Yudina, V.N. Ikorskii, V.A. Varnek, I.M. Oglezneva, S.V. Larionov, Polyhedron 14 (1995) 1333.
[27] G. Brewer, J. Jasinski, W. Mahany, L. May, S. Prytkov, Inorg. Chim. Acta 232 (1995) 183.
[28] G. Matouzenko, G. Veriot, J.P. Dutasta, A. Collet, J. Jordanov, F. Varret, M. Perrin, S. Lecocq, New J. Chem. 19 (1995) 881.
[29] F.S. Nunes, H.E. Toma, J. Coord. Chem. 36 (1995) 33.
[30] K. Boubekeur, A. Deroche, F. Lambert, B.I. Morgenstern, Acta Crystallogr. C51 (1995) 2244.
[31] O. Schlager, K. Wieghardt, B. Nuber, Inorg. Chem. 34 (1995) 6449.
[32] O. Schlager, K. Wieghardt, B. Nuber, Inorg. Chem. 34 (1995) 6456.
[33] G.C. Silver, W.C. Trogler, J. Am. Chem. Soc. 117 (1995) 3983.
[34] C.A. Brown, M.A. Pavlosky, T.E. Westre, Y. Zhang, B. Hedman, K.O. Hodgson, E.I. Solomon, J. Am. Chem. Soc. 117 (1995) 715.
[35] T. Mizuta, J. Wang, K. Miyoshi, Inorg. Chim. Acta 230 (1995) 119.
[36] M.C. Kennedy, W.E. Antholine, W. Li, Q. Mao, D.H. Petering, Inorg. Chim. Acta 240 (1995) 535.

[37] K.E. Loeb, J.M. Zaleski, T.E. Westre, R.J. Guajardo, P.K. Mascharak, B. Hedman, K.O. Hodgson, E.I. Solomon, J. Am. Chem. Soc. 117 (1995) 4545.
[38] R.J. Guajardo, F. Chavez, E.T. Farinas, P.K. Mascharak, J. Am. Chem. Soc. 117 (1995) 3883.
[39] R.J. Guajardo, P.K. Mascharak, Inorg. Chem. 34 (1995) 802.
[40] M.J. Bartos, C. Kidwell, K.E. Kauffmann, W.S.W. Gordon, T.J. Collins, G.C. Clark, E. Muenck, S.T. Weintraub, Angew. Chem. Int. Ed. Engl. 34 (1995) 1216.
[41] H. Oshio, E. Ino, T. Ito, Y. Maede, Bull. Chem. Soc. Jpn. 68 (1995) 889.
[42] E.A. Ough, M.J. Stillman, Inorg. Chem. 34 (1995) 4317.
[43] T. Nyokong, Polyhedron 14 (1995) 643.
[44] C. Ercolani, J. Jubb, G. Pennesi, U. Russo, G. Trigiante, Inorg. Chem. 34 (1995) 2535.
[45] B. Cheng, W.R. Scheidt, Acta Crystallogr. Sect. C: 51 (1995) 1271.
[46] S.A. Moy, J.A. Gonzalez, L.J. Wilson, Acta Crystallogr. C51 (1995) 1490.
[47] M.H. Rakowsky, K.M. More, A.V. Kulikov, G.R. Eaton, S.S. Eaton, J. Am. Chem. Soc. 117 (1995) 2049.
[48] M. Guillemot, G. Simonneaux, J. Chem. Soc. Chem. Commun. (1995) 2093.
[49] G.B. Yi, M.A. Khan, A.G.B. Richter, Inorg. Chem. 34 (1995) 5703.
[50] O.Q. Munro, H.M. Marques, P.G. Debrunner, K. Mohanrao, W.R. Scheidt, J. Am. Chem. Soc. 117 (1995) 935.
[51] L.M. Mink, J.R. Polam, K.A. Christensen, M.A. Bruck, F.A. Walker, J. Am. Chem. Soc. 117 (1995) 9329.
[52] K. Rachlewicz, G.L. Latos, Inorg. Chem. 34 (1995) 718.
[53] D.S. Bohle, B.J. Conklin, C.H. Hung, Inorg. Chem. 34 (1995) 2569.
[54] X.D. Jiao, J.W. Huang, J.F. Liu, L.N. Ji, Polyhedron 14 (1995) 2595.
[55] A. Balch, R. Koerner, M.M. Olmstead, J. Chem. Soc. Chem. Commun. (1995) 873.
[56] M. Mylrajan, L.A. Andersson, J. Sun, T.M. Loehr, C.S. Thomas, E.P.J. Sullivan, M.A. Thomson, K.M. Long, O.P. Anderson, S.H. Strauss, Inorg. Chem. 34 (1995) 3953.
[57] I. Morishima, H. Fujii, Y. Shiro, S. Sano, Inorg. Chem. 34 (1995) 1528.
[58] D.S. Bohle, C.-H. Hung, J. Am. Chem. Soc. 117 (1995) 9584.
[59] S. Ozawa, E. Sakamoto, T. Ichikawa, Y. Watanabe, I. Morishima, Inorg. Chem. 34 (1995) 6362.
[60] G.B. Yi, M.A. Khan, A.G.B. Richter, J. Am. Chem. Soc. 117 (1995) 7850.
[61] D. El-Kasmi, C. Tetreau, D. Lavalette, M. Momenteau, J. Am. Chem. Soc. 117 (1995) 6041.
[62] N.K. Chaudhury, G.S.S. Saini, A.L. Verma, Inorg. Chem. 34 (1995) 346.
[63] R.W. Larsen, E.W. Findsen, R.E. Nalliah, Inorg. Chim. Acta 234 (1995) 101.
[64] M.A. Lopez, C.D. Ybarra, S. Hyatt, Inorg. Chim. Acta 231 (1995) 121.
[65] Z.Q. Tian, J.L. Richards, T.G. Traylor, J. Am. Chem. Soc. 117 (1995) 21.
[66] D.R. Benson, B.R. Hart, X. Zhu, M.B. Doughty, J. Am. Chem. Soc. 117 (1995) 8502.
[67] K. Machii, Y. Watanabe, I. Morishima, J. Am. Chem. Soc. 117 (1995) 6691.
[68] T.G. Traylor, C. Kim, J.L. Richards, F. Xu, C.L. Perrin, J. Am. Chem. Soc. 117 (1995) 3468.
[69] Z. Gross, S. Nimri, J. Am. Chem. Soc. 117 (1995) 8021.
[70] K. Tajima, S. Oka, T. Edo, S. Miyake, H. Mano, K. Mukai, H. Sakurai, K. Ishizu, J. Chem. Soc. Chem. Commun. (1995) 1507.
[71] T. Uno, A. Takeda, S. Shimabayashi, Inorg. Chem. 34 (1995) 1599.
[72] T. La, G.M. Miskelly, J. Am. Chem. Soc. 117 (1995) 3613.
[73] Ö. Almarsson, H. Adalsteinsson, T.C. Bruice, J. Am. Chem. Soc. 117 (1995) 4524.
[74] Ö. Almarsson, T.C. Bruice, J. Am. Chem. Soc. 117 (1995) 4533.
[75] M.W. Grinstaff, M.G. Hill, E.R. Birnbaum, W.P. Schaefer, J.A. Labinger, H.B. Gray, Inorg. Chem. 34 (1995) 4896.
[76] B. Cheng, J.D. Hobbs, P.G. Debrunner, J. Erlebacher, J.A. Shelnutt, W.R. Scheidt, Inorg. Chem. 34 (1995) 102.
[77] W.P. Schaefer, P.E. Ellis, J.E. Lyons, S.N. Shaikh, Acta Crystallogr. C51 (1995) 2252.
[78] J. Wojaczynski, G.L. Latos, Inorg. Chem. 34 (1995) 1044.
[79] E. Tsuchida, T. Komatsu, S.-I. Kumamoto, K. Ando, H. Nishide, J. Chem. Soc. Perkin Trans. 2: (1995) 747.

[80] P.J. Dandliker, F. Diederich, J.-P. Gisselbrecht, A. Louati, M. Gross, Angew. Chem. Int. Ed. Engl. 34 (1995) 2725.
[81] J.R. Wolf, C.G. Hamaker, J.P. Djukic, T. Kodadek, L.K. Woo, J. Am. Chem. Soc. 117 (1995) 9194.
[82] A.L. Balch, G.L. Latos, T.N. St Claire, Inorg. Chem. 34 (1995) 1395.
[83] M.J. Scott, H.H. Zhang, S.C. Lee, B. Hedman, K.O. Hodgson, R.H. Holm, J. Am. Chem. Soc. 117 (1995) 568.
[84] A. Nanthakumar, S. Fox, K.D. Karlin, J. Chem. Soc. Chem. Commun. (1995) 499.
[85] P. Basu, N.V. Shokhirev, J.H. Enemark, F.A. Walker, J. Am. Chem. Soc. 117 (1995) 9042.
[86] K. Jayaraj, A. Gold, R.N. Austin, D. Mandon, R. Weiss, J. Terner, E. Bill, M. Muether, A.X. Trautwein, J. Am. Chem. Soc. 117 (1995) 9079.
[87] K. Tajima, K. Shimizu, H. Mano, K. Mukai, N. Azuma, J. Chem. Soc. Chem. Commun. (1995) 601.
[88] P.A. Stuzhin, M. Hamdush, U. Ziener, Inorg. Chim. Acta 236 (1995) 131.
[89] S.C. Wallis, L.R. Gahan, B.G. Charles, T.W. Hambley, Polyhedron 14 (1995) 2835.
[90] G. Xiao, D. van der Helm, R.C. Hider, P.S. Dobbin, Inorg. Chem. 34 (1995) 1268.
[91] D.P. Goldberg, J. Telser, C.M. Bastos, S.J. Lippard, Inorg. Chem. 34 (1995) 3011.
[92] S. Herold, L.E. Pence, S.J. Lippard, J. Am. Chem. Soc. 117 (1995) 6134.
[93] E. Farkas, E. Kozma, T. Kiss, I. Tóth, B. Kurzak, J. Chem. Soc. Dalton Trans. (1995) 477.
[94] M.T. Caudle, C.D. Caldwell, A.L. Crumbliss, Inorg. Chim. Acta 240 (1995) 519.
[95] P. Mastrorilli, C.F. Nobile, G. Marchese, Inorg. Chim. Acta 233 (1995) 65.
[96] M. Kurmoo, A.W. Graham, P. Day, S.J. Coles, M.B. Hursthouse, J.L. Caulfield, J. Singleton, F.L. Pratt, W. Hayes, L. Ducasse, P. Guionneau, J. Am. Chem. Soc. 117 (1995) 12209.
[97] A.S. Attia, S. Bhattacharya, C.G. Pierpont, Inorg. Chem. 34 (1995) 4427.
[98] S.P. Huang, W. Li, K.J. Franz, R.L. Albright, R.H. Fish, Inorg. Chem. 34 (1995) 2813.
[99] I. Batinić-Haberle, I. Spasojević, R.A. Bartsch, A.L. Crumbliss, J. Chem. Soc. Dalton Trans. (1995) 2503.
[100] M. Takagi, K. Ishihara, Inorg. Chim. Acta 232 (1995) 157.
[101] A. Caneschi, A. Cornia, A.C. Fabretti, D. Gatteschi, W. Malavasi, Inorg. Chem. 34 (1995) 4660.
[102] A. Caneschi, A. Cornia, S.J. Lippard, Angew. Chem. Int. Ed. Engl. 34 (1995) 467.
[103] J.R. Tzou, M. Mullaney, R.E. Norman, S.C. Chang, Acta Crystallogr. C51 (1995) 2249.
[104] I. Ondrejkovicová, M. Melník, K. Smolander, M. Ahlgrén, Acta Chem. Scand. 49 (1995) 475.
[105] Z. Olejnik, T. Lis, I. Ondrejkovicová, Acta Crystallogr. Sect. C: 51 (1995) 2246.
[106] H. Paulsen, M. Kroeckel, M. Grodzicki, E. Bill, A.X. Trautwein, G.J. Leigh, J. Silver, Inorg. Chem. 34 (1995) 6244.
[107] L.D. Field, A.V. George, S.R. Pike, I.E. Buys, T.W. Hambley, Polyhedron 14 (1995) 3133.
[108] K. Kashiwabara, Y. Ozeki, M. Kita, J. Fujita, K. Nakajima, Bull. Chem. Soc. Jpn. 68 (1995) 3453.
[109] C.T. Brewer, G. Brewer, G.B. Jameson, P. Kamaras, L. May, M. Rapta, J. Chem. Soc. Dalton Trans. (1995) 37.
[110] A.M. Hassaan, M.A. Khalifa, A.K. Shehata, Bull. Soc. Chim. Belg. 104 (1995) 121.
[111] J.E. Bollinger, J.T. Mague, C.J. O'Connor, W.A. Banks, D.M. Roundhill, J. Chem. Soc. Dalton Trans. (1995) 1677.
[112] J.C. Fanning, X. Wang, A.E. Koziol, G.J. Palenik, Inorg. Chim. Acta 232 (1995) 199.
[113] D.P. Singh, V.B. Rana, Polyhedron 14 (1995) 2901.
[114] R. Viswanathan, M. Palaniandavar, J. Chem. Soc. Dalton Trans. (1995) 1259.
[115] P. Laine, A. Gourdon, J.P. Launay, Inorg. Chem. 34 (1995) 5156.
[116] P. Laine, A. Gourdon, J.P. Launay, Inorg. Chem. 34 (1995) 5129.
[117] P. Laine, A. Gourdon, J.P. Launay, J.P. Tuchagues, Inorg. Chem. 34 (1995) 5150.
[118] A. Cousson, F. Nectoux, F. Robert, E.N. Rizkalla, Acta Crystallogr. C51 (1995) 838.
[119] P. Laine, A. Gourdon, J.P. Launay, Inorg. Chem. 34 (1995) 5138.
[120] L. Tommasi, B.L. Shechter, D. Varech, J.P. Battioni, B. Donnadieu, M. Verelst, A. Bousseksou, D. Mansuy, J.P. Tuchagues, Inorg. Chem. 34 (1995) 1514.
[121] T. Ozawa, K. Jitsukawa, H. Masuda, H. Einaga, Polyhedron 14 (1995) 1999.
[122] Z.P. Bai, J. Hidaka, H. Einaga, Polyhedron 14 (1995) 2071.
[123] H. Yoshida, T. Ozawa, K. Jitsukawa, H. Einaga, Polyhedron 14 (1995) 997.
[124] W.S. Szulbinski, D.H. Busch, Inorg. Chim. Acta 234 (1995) 143.

[125] M. Lamrani, G. Mousset, E. Leize, A. van Dorsselaer, New J. Chem. 19 (1995) 313.
[126] K. Hegetschweiler, M. Ghisletta, P.L. Hausherr, T. Kradolfer, H.W. Schmalle, V. Gramlich, Inorg. Chem. 34 (1995) 1950.
[127] K. Hegetschweiler, T. Kradolfer, V. Gramlich, R.D. Hancock, Chem. Eur. J. 1 (1995) 74.
[128] N.P. Sadler, C.C. Chuang, R.M. Milburn, Inorg. Chem. 34 (1995) 402.
[129] P. Baret, C.G. Beguin, H. Boukhalfa, C. Caris, J.P. Laulhere, J.L. Pierre, G. Serratrice, J. Am. Chem. Soc. 117 (1995) 9760.
[130] J.C. Jeffery, C.S.G. Moore, E. Psillakis, M.D. Ward, P. Thornton, Polyhedron 14 (1995) 599.
[131] M.G.B. Drew, C.J. Harding, V. McKee, G.G. Morgan, J. Nelson, J. Chem. Soc. Chem. Commun. (1995) 1035.
[132] Y. Sun, H.L. Hu, A.E. Martell, A. Clearfield, J. Coord. Chem. 36 (1995) 23.
[133] M.A. Esteves, M.C.T. Vaz, M.L.S.S. Gonçlaves, E. Farkas, M.A. Santos, J. Chem. Soc. Dalton Trans. (1995) 2565.
[134] R. Ma, R.J. Motekaitis, A.E. Martell, Inorg. Chim. Acta 233 (1995) 137.
[135] W. Kanda, W. Moneta, M. Bardet, E. Bernard, N. Debaecker, J. Laugier, A. Bousseksou, N.S. Chardon, J.M. Latour, Angew. Chem. Int. Ed. Engl. 34 (1995) 588.
[136] Y. Maeda, K. Kawano, T. Oniki, J. Chem. Soc. Dalton Trans. (1995) 3533.
[137] M. Kato, Y. Yamada, T. Inagaki, W. Mori, K. Sakai, T. Tsubomura, M. Sato, S. Yano, Inorg. Chem. 34 (1995) 2645.
[138] H. Nie, S. Aubin, M.S. Mashuta, J. Wu, J.F. Richardson, D.N. Hendrickson, R.M. Buchanan, Inorg. Chem. 34 (1995) 2382.
[139] Y. Hayashi, T. Kayatani, H. Sugimoto, M. Suzuki, K. Inomata, A. Uehara, Y. Mizutani, T. Kitagawa, Y. Maeda, J. Am. Chem. Soc. 117 (1995) 11220.
[140] A. Neves, M.A. de Brito, V. Drago, K. Griesar, W. Haase, Inorg. Chim. Acta 237 (1995) 131.
[141] B. Eulering, F. Ahlers, F. Zippel, M. Schmidt, H.F. Nolting, B. Krebs, J. Chem. Soc. Chem. Commun. (1995) 1305.
[142] M. Mikuriya, T. Kotera, F. Adachi, M. Handa, M. Koikawa, H. Okawa, Bull. Chem. Soc. Jpn. 68 (1995) 574.
[143] M.D. Couce, U. Russo, G. Valle, Inorg. Chim. Acta 234 (1995) 195.
[144] S.C. Shoner, D. Barnhart, J.A. Kovacs, Inorg. Chem. 34 (1995) 4517.
[145] N. Govindaswamy, D.A.J. Quarless, S.A. Koch, J. Am. Chem. Soc. 117 (1995) 8468.
[146] P. Guillaume, M. Postel, Inorg. Chim. Acta 233 (1995) 109.
[147] J.P. Damiano, V. Munyejabo, M. Postel, Polyhedron 14 (1995) 1229.
[148] M.A. Manez, T.M.J. Fernandez, M.G. Basallote, Polyhedron 14 (1995) 1865.
[149] T.A. George, D.J. Rose, Y. Chang, Q. Chen, J. Zubieta, Inorg. Chem. 34 (1995) 1295.
[150] A. Ozarowski, B.R. McGarvey, J.E. Drake, Inorg. Chem. 34 (1995) 5558.
[151] C.-M. Che, C.-W. Chan, S.-M. Yang, C.-X. Guo, C.-Y. Lee, S.-M. Peng, J. Chem. Soc. Dalton Trans. (1995) 2961.
[152] Y. Dong, H. Fujii, M.P. Hendrich, R.A. Leising, G. Pan, C.R. Randall, E.C. Wilkinson, Y. Zang, L.J. Que, B.G. Fox, K. Kauffman, E. Münck, J. Am. Chem. Soc. 117 (1995) 2778.
[153] Y. Dong, L.J. Que, K. Kauffmann, E. Muenck, J. Am. Chem. Soc. 117 (1995) 11377.
[154] J. Kim, E. Larka, E.C. Wilkinson, L.J. Que, Angew. Chem. Int. Ed. Engl. 34 (1995) 2048.
[155] Y. Zang, Y. Dong, L.J. Que, K. Kauffmann, E. Muenck, J. Am. Chem. Soc. 117 (1995) 1169.
[156] R. Hazell, K.B. Jensen, C.J. McKenzie, H. Toftlund, J. Chem. Soc. Dalton Trans. (1995) 707.
[157] M. Rapta, P. Kamaras, G.A. Brewer, G.B. Jameson, J. Am. Chem. Soc. 117 (1995) 12865.
[158] D.P. Goldberg, D. Koulougliotis, G.W. Brudvig, S.J. Lippard, J. Am. Chem.Soc. 117 (1995) 3134.
[159] V.K. Voronkova, J. Mrozinski, M.A. Yampol'skaya, Y.V. Yablokov, N.S. Evtushenko, M.S. Byrke, N.V. Gerbeleu, Inorg. Chim. Acta 238 (1995) 139.
[160] C.A. Brown, G.J. Remar, R.L. Musselman, E.I. Solomon, Inorg. Chem. 34 (1995) 688.
[161] T. Juestel, T. Weyhermueller, K. Wieghardt, E. Bill, M. Lengen, A.X. Trautwein, P. Hildebrandt, Angew. Chem. Int. Ed. Engl. 34 (1995) 669.
[162] K. Asamaki, T. Nakamoto, S. Kawata, H. Sano, M. Katada, K. Endo, Inorg. Chim. Acta 236 (1995) 155.

[163] J.M. Vincent, S. Menage, J.M. Latour, A. Bousseksou, J.P. Tuchagues, A. Decian, M. Fontecave, Angew. Chem. Int. Ed. Engl. 34 (1995) 205.
[164] E.M. Jones, W. Levason, R.D. Olroyd, M. Webster, M. Thomas, J. Hutchings, J. Chem. Soc. Dalton Trans. (1995) 3367.
[165] K. Hegetschweiler, P.L. Hausherr, W.H. Koppenol, V. Gramlich, L. Odier, W. Meyer, H. Winkler, A.X. Trautwein, Angew. Chem. Int. Ed. Engl. 34 (1995) 2242.
[166] S. Parsons, G.A. Solan, R.E.P. Winpenny, J. Chem. Soc. Chem. Commun. (1995) 1987.
[167] A.K. Powell, S.L. Heath, D. Gatteschi, L. Pardi, R. Sessoli, G. Spina, G.F. Del, F. Pieralli, J. Am. Chem. Soc. 117 (1995) 2491.
[168] J. Zhou, R.H. Holm, J. Am. Chem. Soc. 117 (1995) 11353.
[169] R.A. Henderson, J. Chem. Soc. Chem. Commun. (1995) 1905.
[170] J. Gloux, P. Gloux, J. Am. Chem. Soc. 117 (1995) 7513.
[171] M.A. Tyson, K.D. Demadis, D. Coucouvanis, Inorg. Chem. 34 (1995) 4519.
[172] L.J. Laughlin, D. Coucouvanis, J. Am. Chem. Soc. 117 (1995) 3118.
[173] S.M. Malinak, K.D. Demadis, D. Coucouvanis, J. Am. Chem. Soc. 117 (1995) 3126.
[174] K.D. Demadis, D. Coucouvanis, Inorg. Chem. 34 (1995) 436.
[175] K.D. Demadis, D. Coucouvanis, Inorg. Chem. 34 (1995) 3658.
[176] J.E. Barclay, D.J. Evans, G. Garcia, M.D. Santana, M.C. Torralba, J.M. Yago, J. Chem. Soc. Dalton Trans. (1995) 1965.
[177] T. Shibahara, G. Sakane, Y. Naruse, K. Taya, H. Akashi, A. Ichimura, H. Adachi, Bull. Chem. Soc. Jpn. 68 (1995) 2769.
[178] A. Bencini, C.A. Ghilardi, S. Midollini, A. Orlandini, U. Russo, M.G. Uytterhoeven, C. Zanchini, J. Chem. Soc. Dalton Trans., (1995) 963.
[179] L. Cal, B.M. Segal, J.R. Long, M.J. Scott, R.H. Holm, J. Am. Chem. Soc. 117 (1995) 8863.
[180] D. Fenske, A. Fischer, Angew. Chem. Int. Ed. Engl. 34 (1995) 307.